An Experimental Fatigue and Finite Element Study of a Welded Joint of a Snowplow Blade

George Ernest Selburg
Marquette University

AN EXPERIMENTAL AND FINITE ELEMENT STUDY OF A WELDED JOINT OF A SNOWPLOW BLADE

by

George E. Selburg Jr., BS, ME

A Thesis submitted to the Faculty of the Graduate School,

Marquette University,

In Partial Fulfillment of the Requirements for

The Degree of Master of Science

Milwaukee, Wisconsin

August 2014

ABSTRACT
AN EXPERIMENTAL AND FINITE ELEMENT STUDY OF A WELDED JOINT OF A SNOWPLOW BLADE

George E. Selburg Jr.

Marquette University 2014

This study describes a method to evaluate the fatigue life of a welded joint of a snowplow. Fatigue specimens were fabricated, which simulated the joint and its loading characteristics. The joint in the specimens was characterized by measuring the geometry of the weld and the hardness of the parent material, weld material, and heat affected zone. It was determined that the fatigue crack that developed in the joint was exposed to mode I fracture forces in the normal plane of the crack. The specimens were then tested in a hydraulic closed looped system to determine the mechanism of fatigue for the welded joint and the fatigue crack propagation parameters. A finite element model was then generated with a pre-crack mesh in a location determined from the experimental and field data on crack growth. The crack parameters were estimated from examining the test specimens after the test was completed. The FEA results were then compared to the experimentally determined stress intensity factors.

ACKNOWLEDGEMENTS

I could not have come this far without the help of others. First and foremost is my family, which has borne the extra burden, so that I could follow my career. Second, is Dr. Raymond Fournelle, who has been there as a mentor and a confidant for a greater portion of my career. I would also like to thank Drs. Joseph Domblesky and James Rice for taking time to assist me with this undertaking.

There are many others that have had an influence on my career in and out of the Mechanical Department at Marquette University who gave of their time to assist me in completing my education. And lastly but certainly not least, I would like to extend my gratitude to my employer, Douglas Dynamics, Inc., which has given me the opportunity and resources to complete my education.

TABLE OF CONTENTS

LIST OF TABLES

LIST OF FIGURES

1 INTRODUCTION

1.1 Background

The commercial snowplow industry is faced with designing products for an ever lighter commercial vehicle. The driving force for vehicle manufacturers is the federal mandate for higher gas mileage for vehicles. The major trend over the past 15 years is to design vehicles which are lighter and this in turn usually reduces the front axle rating of the vehicle. The lighter front end of vehicles then leads snowplow designers and engineers to reduce the weight of the snowplow. They are then limited to an overall snowplow weight that can safely attach to the front of the vehicle. This results in challenges in the design of the snowplows. The snowplows must maintain current performance and yet meet the weight restrictions of the vehicle.

Fatigue has been an increasing issue in snowplow design. The requirements for greater fuel economy and lighter suspensions of mid-size vehicles have forced snowplow designers to decrease the weight of the equipment and yet maintain or improve the overall performance. The reduction in weight inherently requires that service loading, dynamic responses, and other service parameters be well understood by designers and analysts. The more complete the analysis, the greater the chance that intelligent decisions will be made to modify the structure without compromising structural integrity. This knowledge will also aid in optimizing the strength to weight ratio of the structure, which is a major obstacle.

Fatigue crack initiation and propagation in the joint chosen for this study (Figure 1) has recently become an issue because of unexpected failures observed in the field. These failures have been occurring after approximately 150 to 200 hours of service, which has been deemed to be an unacceptable product life.

Figure 1. View of the snowplow and the fatigue failure site location.

The failure that results from the fatigue of the welded joint renders the product unusable. To date extensive lab and field-testing has been performed on the snowplow to extract service loading histories experienced by the product. Data has been collected by placing strain gauges, accelerometers, and pressure transducers at key points on the snowplow. The data has been collected and analyzed, and time history profiles have been developed to determine the forces associated with the plowing events that affect the fatigue of this particular joint.

1.2 Literature Review

The study of fatigue has been of significant interest since Wilhelm Albert published his article in 1837 that outlined a test machine for conveyor chains used in the Clausthal mines[1]. It is estimated that fatigue of metal structures cost consumers an estimated 3% of the GDP in premature or unexpected failures each year[2]. The understanding of

fatigue mechanisms and the ability to predict fatigue life accurately and consistently is a large undertaking and requires vast amounts of research. Fortunately, there is an analytical tool that provides an invaluable method of predicting fatigue in a structure. This is the finite element method (FEM), which has been used since its inception in the early 1940's.[3]

1.2.1 Definitions

While actual fatigue loading may be quite complex, fatigue testing is usually performed using sinusoidal loads at various mean stresses [Figure 2]. The quantities involved are the stress range, $\Delta\sigma$, which is the difference between the maximum stress, σ_{max}, and the minimum stress, σ_{min}. The mean stress is the sum of the σ_{max} and σ_{min} divided by two, and the stress amplitude is half the stress range, $\Delta\sigma/2$. The stress ratio, R, is the ratio of σ_{min} / σ_{max}, and A is the amplitude ratio σ_a/σ_m.

$$\Delta\boldsymbol{\sigma} = \boldsymbol{\sigma_{max}} - \boldsymbol{\sigma_{min}}, \quad \boldsymbol{\sigma_m} = \frac{\boldsymbol{\sigma_{max}} + \boldsymbol{\sigma_{min}}}{\mathbf{2}}, \qquad \boldsymbol{\sigma_a} = \frac{\Delta\boldsymbol{\sigma}}{\mathbf{2}} \quad [\mathbf{1}]$$

$$\boldsymbol{R} = \frac{\boldsymbol{\sigma_{min}}}{\boldsymbol{\sigma_{max}}}, \qquad \boldsymbol{A} = \frac{\boldsymbol{\sigma_a}}{\boldsymbol{\sigma_m}} \qquad [\mathbf{2}]$$

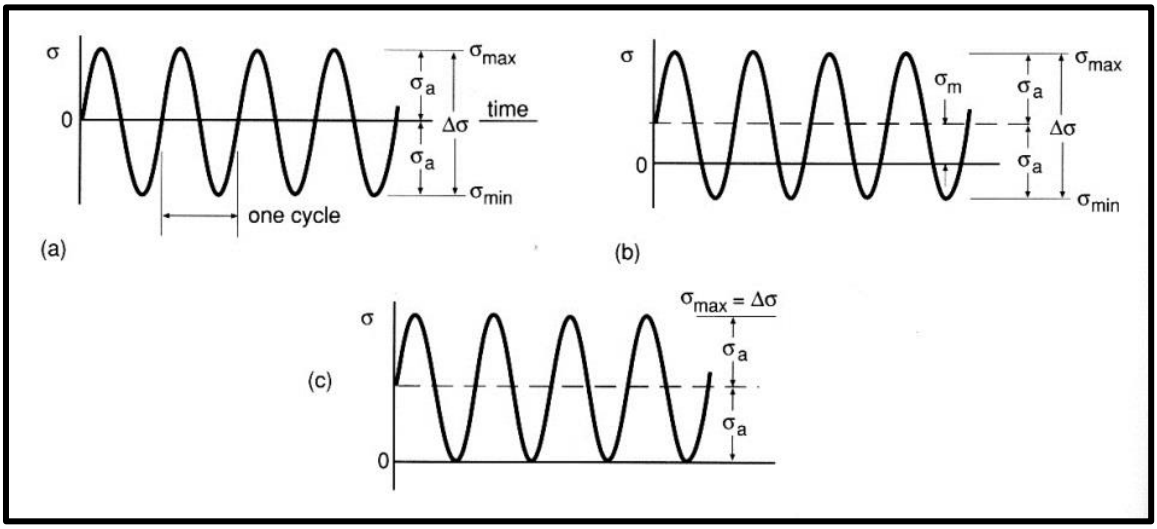

Figure 2. Constant amplitude cycling and the associated nomenclature. Case (a) is completely reversed stressing, $\sigma_m = 0$, (b) has a nonzero mean stress σ_m, and (c) is zero to tension stressing, $\sigma_{min} = 0$.[1]

1.2.2 General Observations

There are two main methods to study the fatigue of a material or engineering component. One involves stress or load controlled testing. The other involves strain or displacement controlled testing. The method used for this analysis followed the stress based approach to verify the FEM results. The stress based method involves developing a stress life (S-N) curve for the material, which is a plot of the stress amplitude versus the number of cycles to failure for a standard specimen or component. An S-N curve for A517 steel is shown in Figure 3.

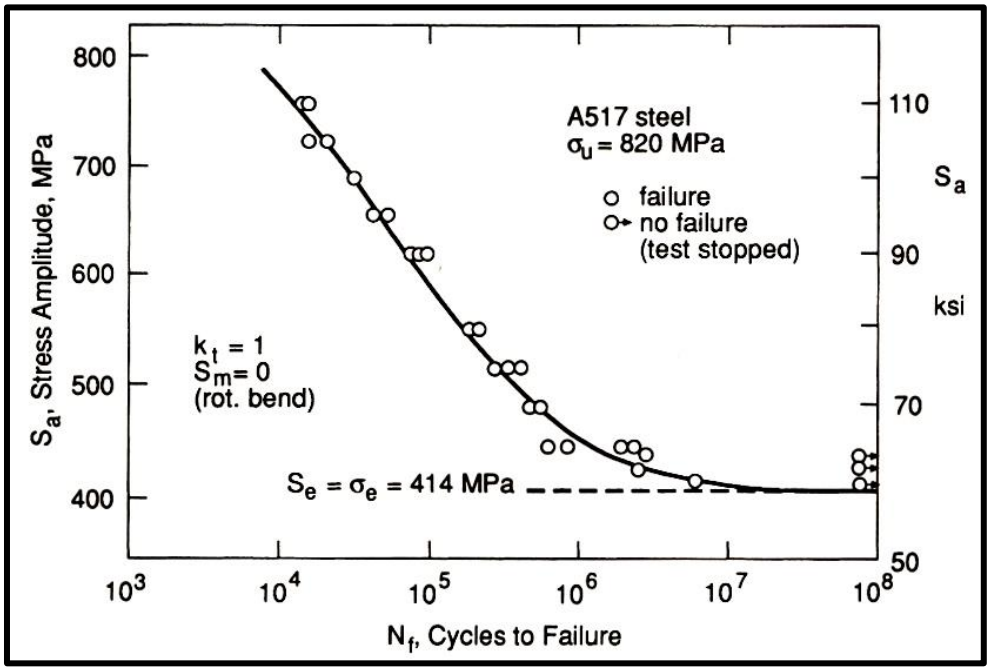

Figure 3. Rotating bending S-N curve for unnotched specimens of ASTM A517 steel with a distinct fatigue limit. [1]

The general process of fatigue in metals requires cyclic loading, tensile stresses, and plastic strain on each cycle; otherwise it will not progress to failure[1]. The process has three stages in homogenous components. Figure 4 shows the three stages of fatigue. The first stage is crack initiation, which involves the nucleation of microscopic cracks. The second stage is crack propagation (growth), which involves the slow growth of the crack with each stress cycle. This process proceeds until the third stage or final fracture stage which results in component failure. The final fracture occurs because the crack length has reached a critical length and the remaining material can no longer carry the input load. At the point where the crack has reached a critical length a brittle or ductile fracture occurs as seen in Figure 5.

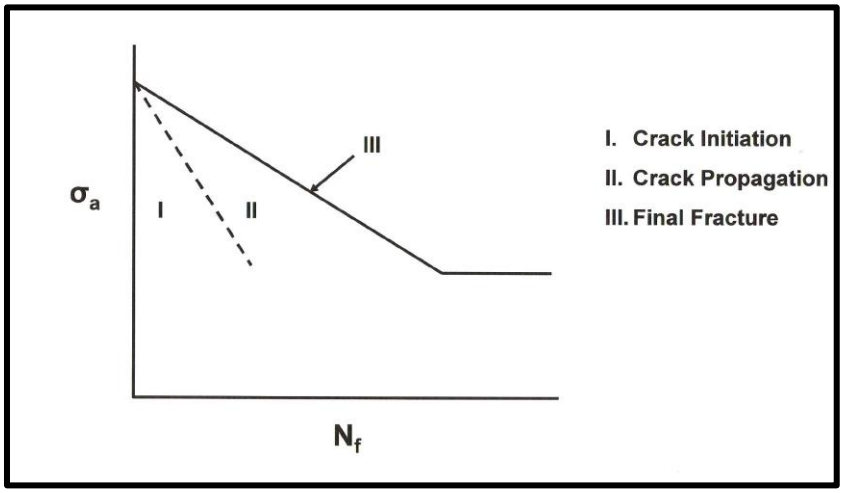

Figure 4. Schematic diagram showing the three stages of fatigue.

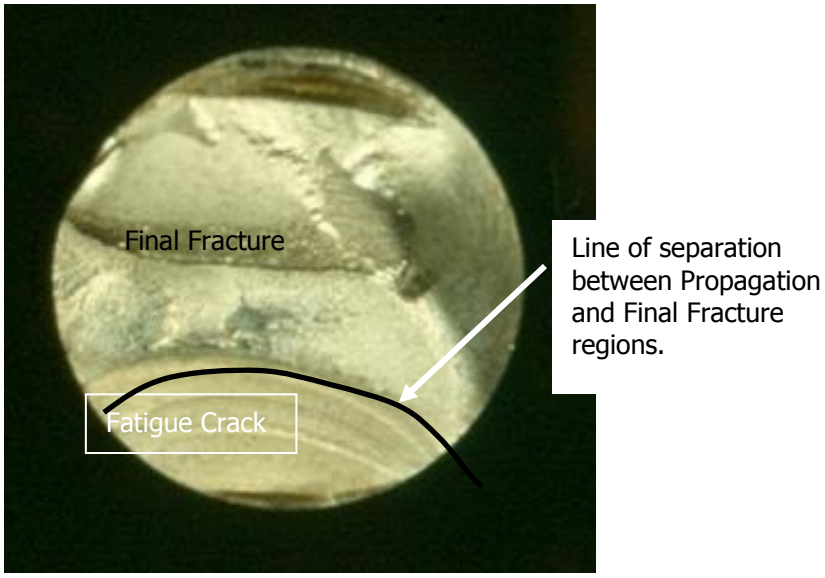

Figure 5. Fatigue fracture surface associated with the fatigue fracture of ½ inch diameter retaining pin under unidirectional bending at a high nominal stress. Note the crack initiation accounts for a negligible part of the fracture surface.

1.2.3 Fatigue Process

Fatigue is the process of cumulative damage in a benign environment that is caused by repeated fluctuating loads. The number of cycles required to initiate a fatigue crack is

the fatigue-crack-initiation life. The number of cycles required to propagate a fatigue crack to a critical size is called the fatigue-crack-propagation life. The total fatigue life is the sum of these two quantities.

The crack initiation usually takes place on the surface of the metal in the vicinity of a notch or defect that acts as a stress concentration. The mechanism is explained by a slip band mechanism at the microscopic level and is driven by the maximum shear stress parallel to the slip bands. When the load is applied, some grains will be subjected to plastic deformation involving slip on some of the slip planes. The mechanism is limited to a few grains where these slip planes have a favorable orientation for slip with respect to the local maximum shear stresses.[1] When the load is reversed, the planes will not slide back to their initial position due to the cyclic stain hardening effect. Hence, in the reversed part of the load cycle, it is the neighboring planes that will suffer yielding by sliding in the opposite direction. The final result is microscopic extrusions and intrusions on the metal surface. The intrusions act as micro-cracks for further crack extension during the subsequent loading cycles. After crack initiation has occurred within a few grains, subsequent microscopic growth will extend the crack past several grain boundaries. When the crack front extends over several grains, the crack will continue to grow in a direction perpendicular to the largest tensile principal stress. It is important to realize that while the initiation phase is related to the surface condition of the metal and governed by the cyclic shear stresses, the crack growth depends on the bulk mechanical properties of the material, and the crack growth is driven by the cyclic principal stresses.

In the growth phase, the crack growth process is explained by a mechanism involving crack front opening and front blunting followed by crack front closing and sharpening during each load cycle (Figure 6). After one complete cycle, the crack front has advanced

a small increment, which may be traced by electron microscopy of the fatigue surface. The crack advancement corresponding to one load cycle is the distance between two so called striations (Figure 7). The advancement depends on the range of the stress intensity factor (SIF). The final fracture will take place when the fatigue crack becomes so large that the remaining cross section is too small to support the peak load cycle or when the local stresses and strains at the crack front initiate a local brittle or ductile fracture. In the first case, it is the net section average stresses that are the driving force for the fracture. In the second case, it is a local failure that is driven by the maximum stress intensity factor (SIF). This factor uniquely characterizes the magnitude of the stress field at the crack front under linear elastic conditions.[2]

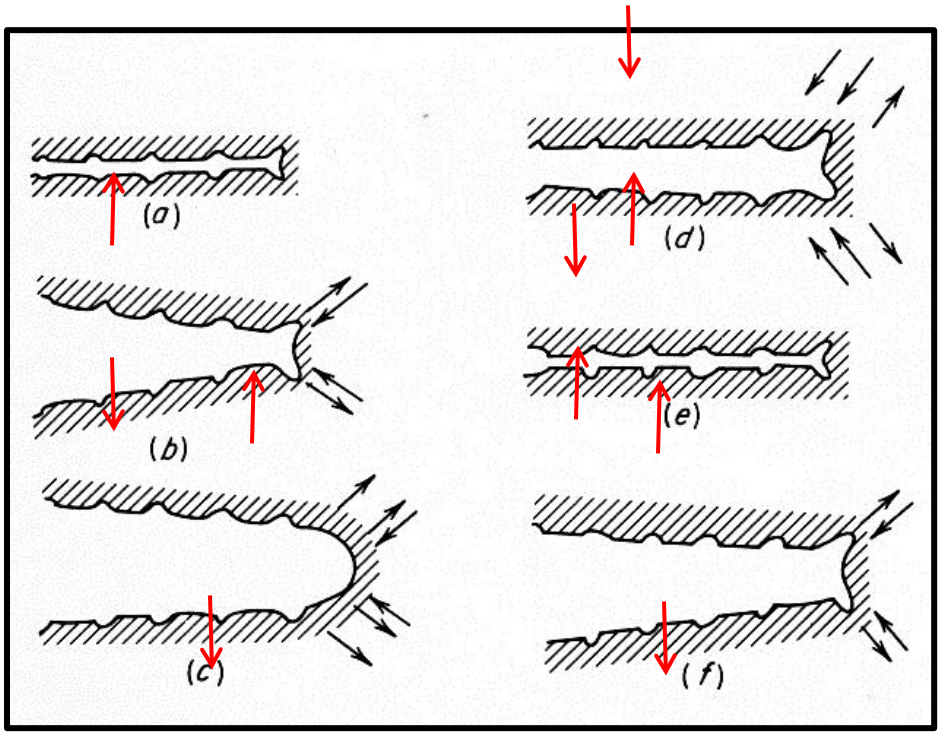

Figure 6. Schematic diagram showing the mechanism of fatigue crack growth microscopic scale.

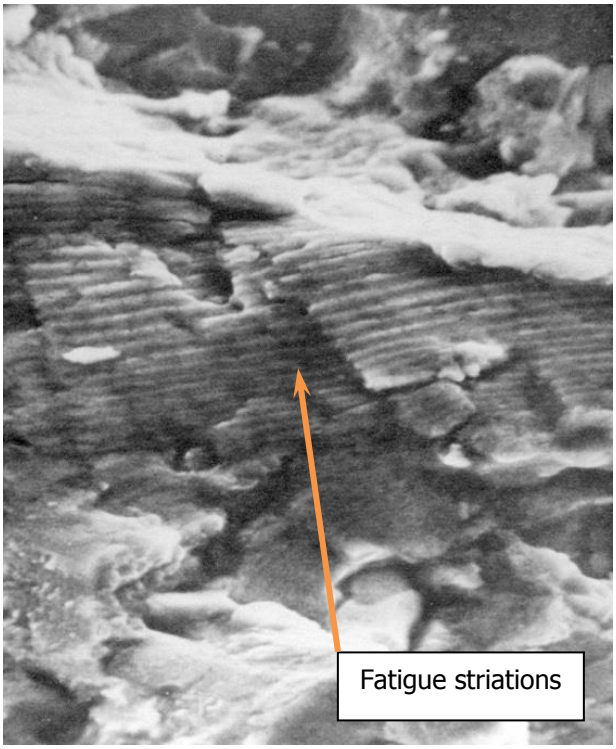

Figure 7. Scanning electron micrograph showing fatigue crack striations in an aluminum alloy (X7,600).

1.2.4 Low Cycle and High Cycle Fatigue

There are two ways to characterize the fatigue behavior of a material. One depends on the number of cycles to failure, and the other depends on the fatigue stress versus yield stress ratio. High cycle fatigue is characterized by fatigue stresses much less than a material's yield point and a total fatigue life of greater than 10,000 cycles. Low cycle fatigue is characterized by fatigue stresses close to the materials yield point and a total fatigue life of less than 10,000 cycles.[7] [8]

The determination of a high cycle fatigue S-N curve such as that in Figure 3 requires load control and keeping the stress to less than two-thirds the materials yield point. The stress is elastic on a gross scale but there will be local plasticity. The experimental

determination of a low cycle fatigue S-N curve uses displacement control to control the elastic and plastic strains.[4]

1.2.5 Fatigue Crack Propagation and Paris' Law

A great deal of experimental evidence supports the view that crack growth rate can be correlated with the cyclic variation in the stress intensity factor range (∆K) according to Paris' law,

$$\frac{da}{dN} = C(\Delta K)^n \text{ ,}$$

where a is the length of a fatigue crack, N is the number of cycles, and C and n are experimental constants. *da/dN* is the fatigue crack growth rate per cycle, $\Delta K = K_{max} - K_{min}$ is the stress intensity factor range during a cycle and $K = \sigma\sqrt{\pi a}$. a and N depend on the material, environment, frequency, temperature, and stress ratio. A typical log-log plot of the dependencies of da/dN versus ∆K is shown in Figure 8. Paris' law is valid for the linear part of the plot. The fatigue crack threshold (∆Kth) is the stress intensity range below which a crack will not grow.

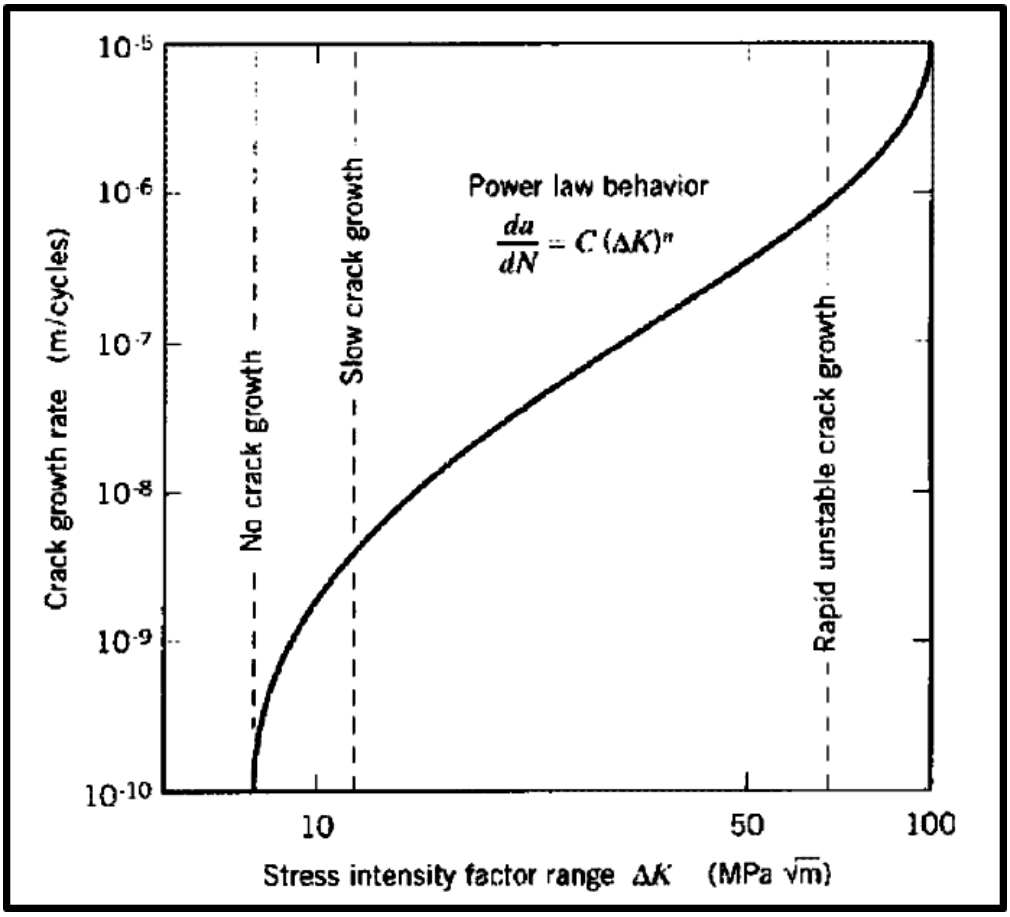

Figure 8. Typical plot of fatigue crack growth rate, (da/dN) versus stress intensity factor range (ΔK).[5]

1.2.6 Fatigue in Welded Structures

Fatigue in welded structures may be analyzed with standard stress-life, strain-life and crack growth methods. However, use of these methods is difficult because of the inherent uncertainties in a welded joint. For example, what is the local stress concentration factor for a weld (Figure 9) when the local weld toe radius is not known? Similarly, what are the material properties of the heat affected zone where the crack will eventually nucleate? One way to overcome these limitations is to test welded joints

rather than traditional material specimens and use this information for the safe design of a welded structure.[2]

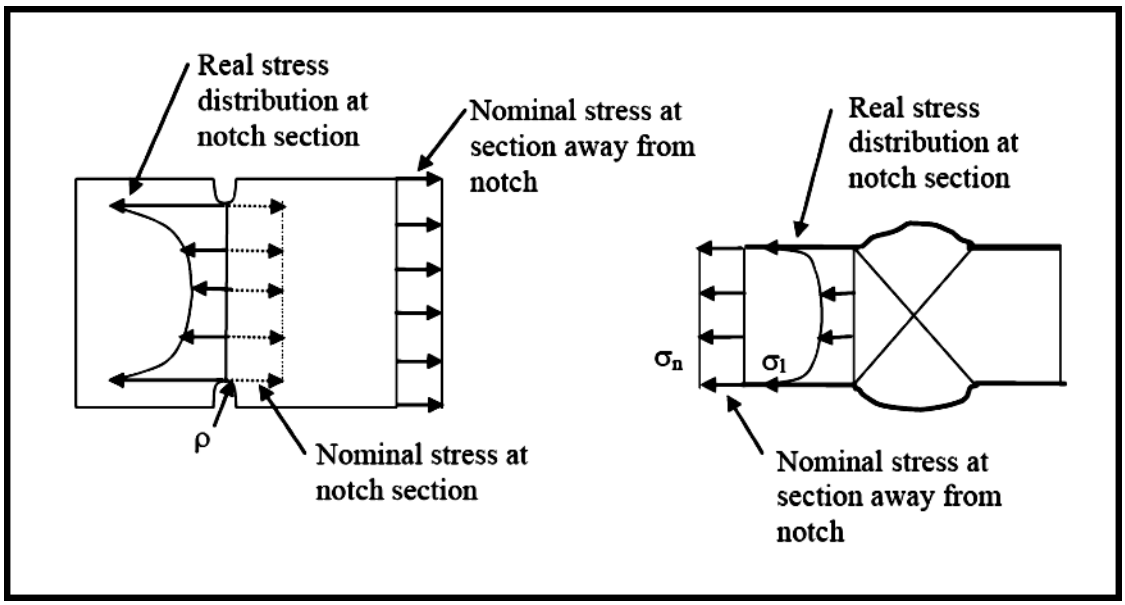

Figure 9. Stress concentrations. Left: plate with edge notches. Right: butt weld joint.[2]

The most common method of joining steel structures is the welding process. There are many types of welding processes available, with each having its benefits and drawbacks. There is MIG [Metal Inert Gas] welding, stick welding, and TIG [Tungsten Inert Gas] welding. Each process has its own parameters that must be used to produce quality joints. However, regardless of the welding process pre-cracks are inherently introduced into the joint. The vast majority of information on fatigue of welded structures concedes the initiation phase of the fatigue cycle and uses the crack propagation phase to determine fatigue life. Various stages of the crack growth in a fillet-welded joint is illustrated in Figure 10. The welding process by nature creates a defect that acts as an initiation site.[5]

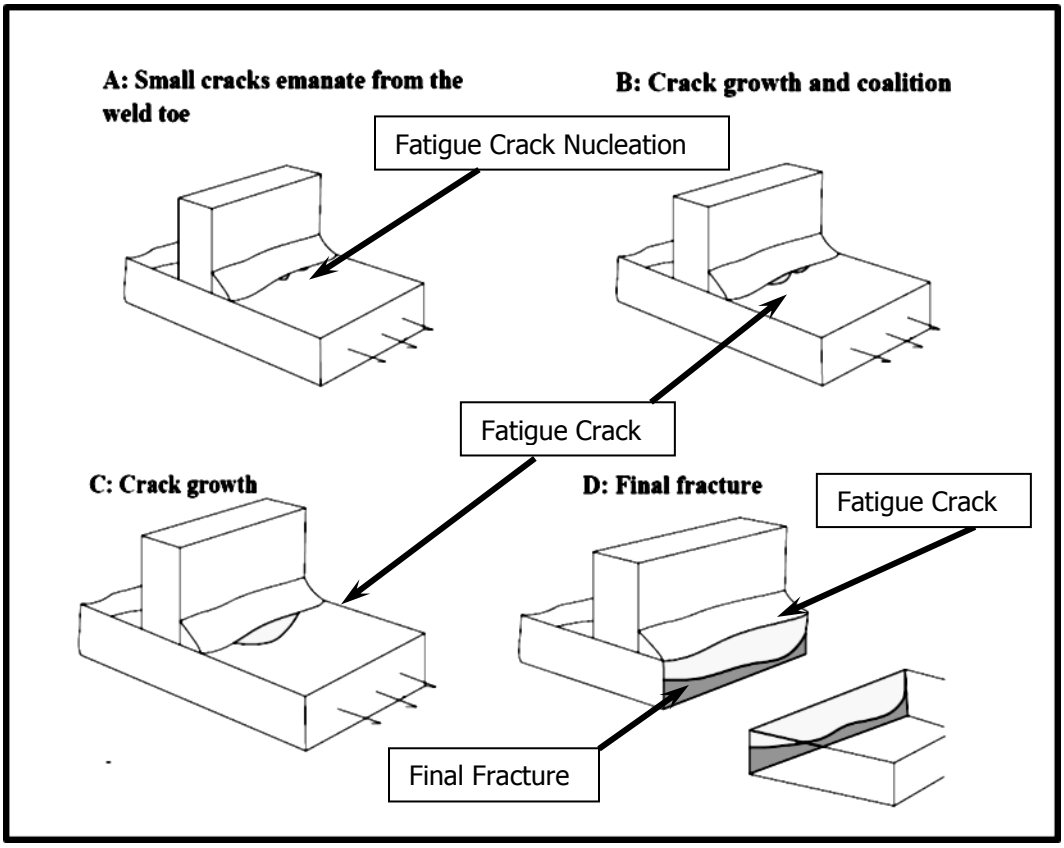

Figure 10. Various stages of crack growth in the fillet welded joint.[2]

1.2.7 Finite Element Method [Fracture Mechanics]

As computing hardware and algorithms have advanced making solution times shorter and more accurate, the finite element method incorporating fracture mechanics has been used more extensively to calculate the fatigue life of components and structures. Standard FEA techniques have been developed using the FEA method: British Standards Institution Standard BS 7608 (BSI 1993), ASTM F 722-82, and AWS Structural Welding Code, AWS D1.1.

Fatigue crack analysis is now widely used to predict component failure caused by preexisting small cracks like those found in welded joints, allowing one to take

precautions to prevent further crack growth or to determine the remaining life of the structure. There are many techniques that incorporate FEA to determine component life, and each has its strengths for a particular fatigue process, such as delamination of composite materials. This fatigue process uses the virtual crack closure technique (VCCT) which was initially developed to calculate the energy-release rate of a cracked body. It has since been widely used in the interfacial crack growth simulation of laminate composites, with the assumption that crack growth is always along a predefined path. The most common use of FEA for determining component life is to calculate the stress intensity factors. The stress intensity factors (SIFs) must be evaluated accurately and because it is difficult to determine accurate SIFs using a closed-form analytical solution for cracks in complex structures, finite-element analysis is used instead.

Two approaches are available for evaluating SIFs, the interaction integral method and the displacement extrapolation method. The interaction integral method performs the SIF calculation during the solution phase of the analysis and stores the results for later post processing. The displacement extrapolation method performs the SIF calculation during post processing. This method is limited to problems involving linear elasticity with homogeneous, isotropic materials near the crack region.[3]

The fracture mechanics method analyzes a material's resistance to fracture using solid mechanics principals based on elasticity and plasticity. The analysis uses a fit of the nodal displacements in the vicinity of the crack (Figure 11). The actual displacements at and near a crack for linear elastic materials were determined by Paris and Sih to be[5]:

$$u = \frac{KI}{4G}\sqrt{\frac{r}{2\pi}}\left((2k-1)\cos\frac{\theta}{2} - \cos\frac{3\theta}{2}\right) - \frac{KII}{4G}\sqrt{\frac{r}{2\pi}}\left((2k+3)\sin\frac{\theta}{2} + \sin\frac{3\theta}{2}\right) + 0(r) \quad [4]$$

$$v = \frac{KI}{4G}\sqrt{\frac{r}{2\pi}}\left((2k+3)\sin\frac{\theta}{2} - \sin\frac{3\theta}{2}\right) - \frac{KII}{4G}\sqrt{\frac{r}{2\pi}}\left((2k-1)\cos\frac{\theta}{2} + \cos\frac{3\theta}{2}\right) + 0(r) \quad [5]$$

$$w = \frac{2KIII}{G}\sqrt{\frac{r}{2\pi}}\sin\frac{\theta}{2} + 0(r) \quad [6]$$

where

u, v, w = displacements in a local Cartesian coordinate system as shown in Figure 11.

r, θ = coordinates in a local cylindrical coordinate system also shown in the figure.

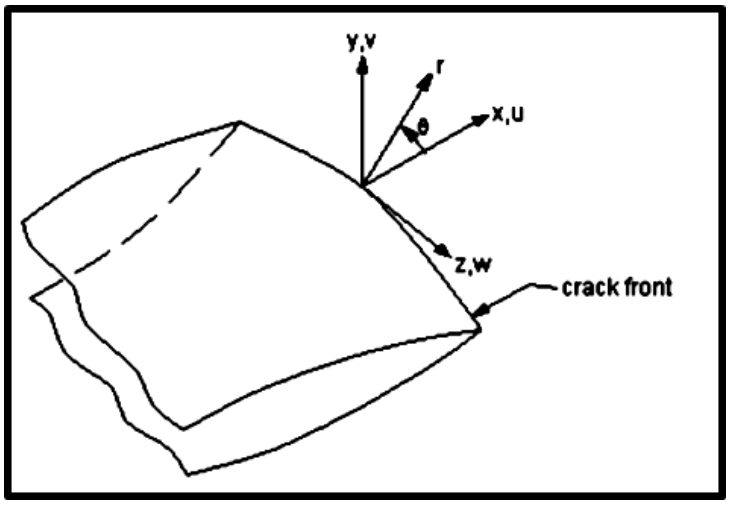

Figure 11. Local Coordinates Measured From a 3-D Crack Front.[3]

G = shear modulus

KI, KII, KIII = stress intensity factors relating to deformation shapes shown in Figure 9.

$$k = \begin{cases} 3 - 4v & if\ plane\ strain\ or\ axisymmetric \\ \dfrac{3 - v}{1 + v} & if\ plane\ stress \end{cases}$$

v = Poisson's ratio

0(r) = terms of order r or higher

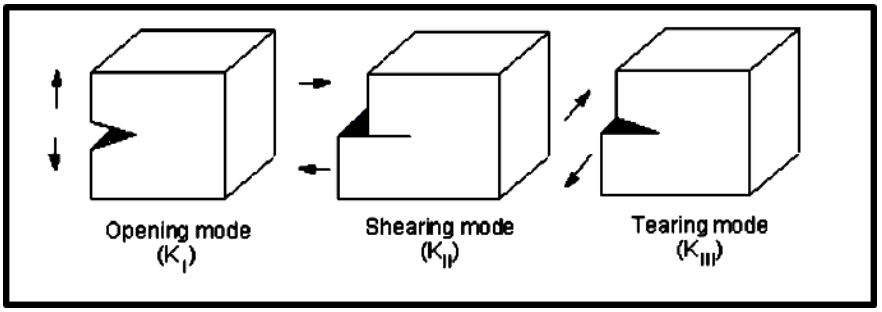

Figure 12. The Three Basic Modes of Fracture.

The stress intensity factors for the three basic modes of fracture shown in Figure 12 are calculated from the nodal displacements using the following equations for no symmetry:

$$K_I = \sqrt{2\pi}\frac{G}{1+k}\frac{|\Delta v|}{\sqrt{r}} \qquad [7]$$

$$K_{II} = \sqrt{2\pi}\frac{G}{1+k}\frac{|\Delta u|}{\sqrt{r}} \qquad [8]$$

$$K_{III} = \sqrt{2\pi}\frac{G}{1+k}\frac{|\Delta w|}{\sqrt{r}} \qquad [9]$$

where Δv, Δu, and Δw are the motions of one crack face with respect to the other.

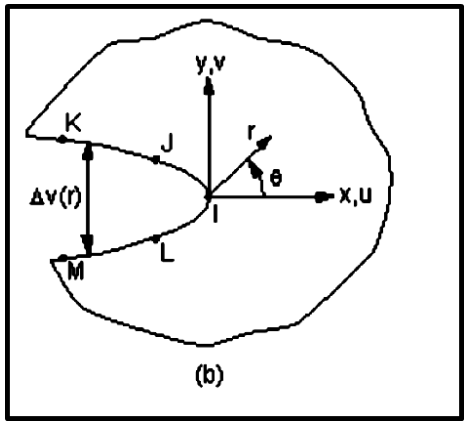

Figure 13. Nodes used for the approximate crack tip displacements.[3]

1.3 Objective of Research

It was the objective of this study to develop a FEM model to predict the fatigue crack growth in a welded joint of a snowplow during normal service loading. Experimental methods were used to validate the FEM fracture results. This technique is intended to aid in predicting the performance of welded joints in snowplows using the finite element method and thus reducing the time and resources required to predict fatigue failure. The study involved investigating the processes involved in the manufacturing, the loading, and the response of a welded joint in a snowplow. This research should lead to a reliable and repeatable procedure for predicting fatigue crack failure for a given joint design, which can be applied to any similarly characterized welded joint.

The study was divided into two major parts, an experimental section in which empirical data about the fatigue life of the particular welded joint of interest were collected and the second section in which the finite element method with fracture mechanics was used to develop a model that aides in predicting crack propagation the joint life accurately.

The experimental section of this study involved fabricating a model of the joint of interest using current production methods at Douglas Dynamics and documenting the critical parameters of the joint. This joint is in a section of a snowplow in which issues with fatigue failures have been reported. The issue was chosen because of the large number of incidences and the failure mode.

The experimental section of the study was based on the procedure presented in the ASTM E 647, and the welded structure method presented by Lassen.[2] The analytical part of the study required the development of a section model that utilized fracture mechanics to compute the stress intensity factor for various crack lengths. The model assumes that there are crack like defects in the welded joints that the crack initiation phase of the process can be neglected. [2]

The test specimens were fabricated using the current processes and materials used in the manufacturing of the product. Each specimen was inspected for compliance with the SOW's (Standard of Work). The fatigue test was developed to replicate the failures seen in the field units. Field load and displacement data was then used to create a load profile for the test. Crack length typical of experimental values were then used to calculate stress intensity factors, K_I using FEM to see how well FEM could predict fatigue crack growth.

A proposed design was then developed to increase the fatigue life of the joint using the afore mentioned process. The design was then implemented and is currently being evaluated by the Manufacturing Group for feasibility and retooling costs.

2 EXPERIMENTAL PROCEDURE

2.1 Fatigue Crack Growth Testing

Since the joint of interest was failing by fatigue, fatigue specimens were developed which duplicated the geometry of the failed snowplow section and provided for fatigue loading in a hydraulic closed loop test system, which simulated actual loading conditions.

2.1.1 Assembly Details

The type of snowplow used for this study is characterized as an expandable-hinged type snowplow assembly. There are two wings (Figure 14) attached to the outer edges of the blade that translate and pivot to provide multiple positions of the wings. Each wing acts independently, providing multiple configurations of the plow. Each wing is powered by a double-acting hydraulic cylinder, and an extension spring assembly. The snowplow blade width varies from 8-1/2' to 10'. The blade can pivot about the center in either direction 30 degrees. The full snowplow assembly in the "scoop" configuration is shown in Figure 14 and the "retracted" configuration is shown in Figure 15.

The joint of interest for this study is located at the outer edges of the blade assembly and is an interface between the wing assembly and the blade assembly. There are four main components and three minor components that make up this joint. The detailed dimensional drawing and weld drawing for the blade assembly is shown in Figures 16 and 17 respectively. The fatigue area is shown in both the figures.

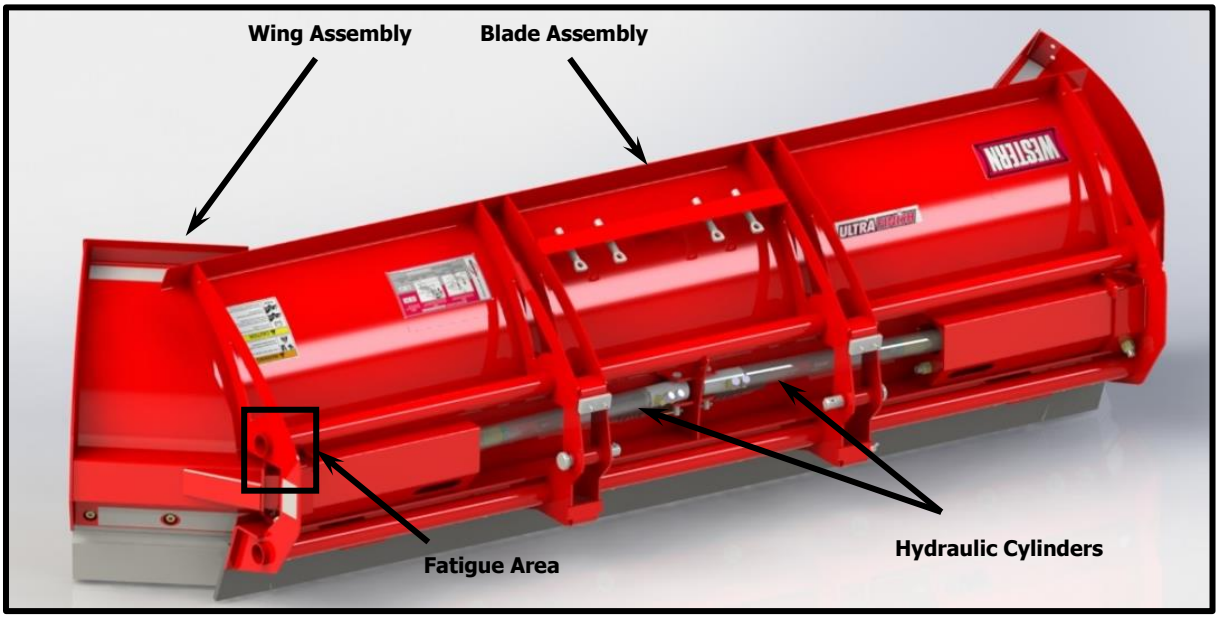

Figure 14. View of the hinged style blade assembly in the scoop mode.

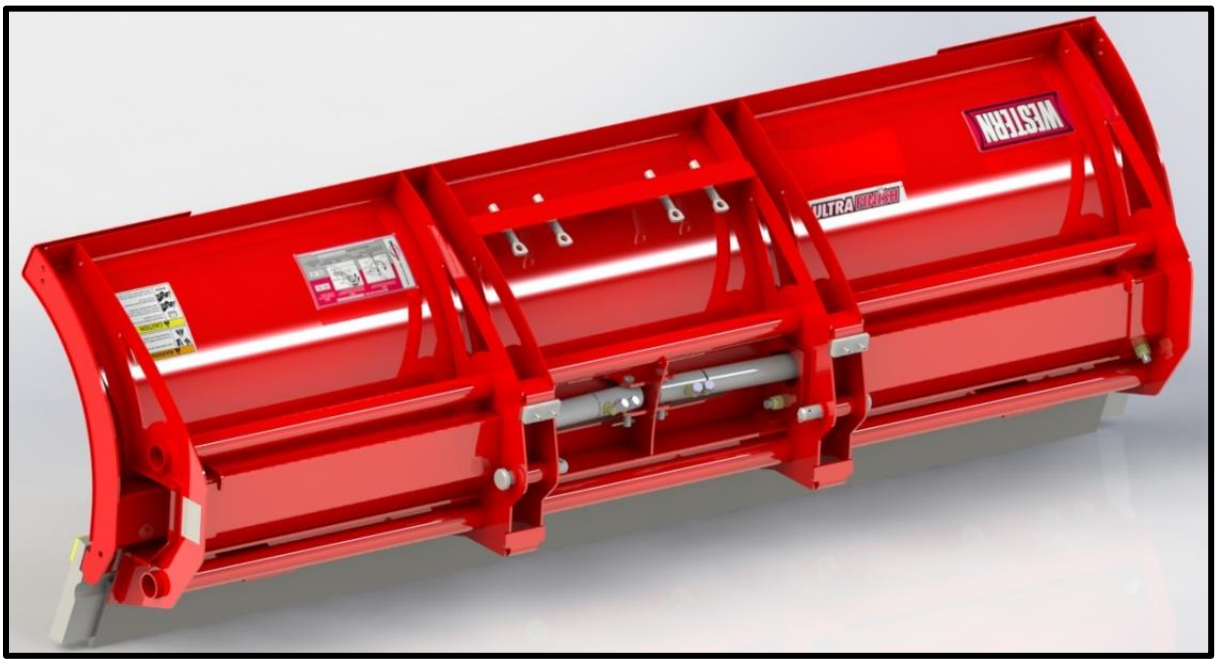

Figure 15. View of the hinge style blade assembly in the retracted mode.

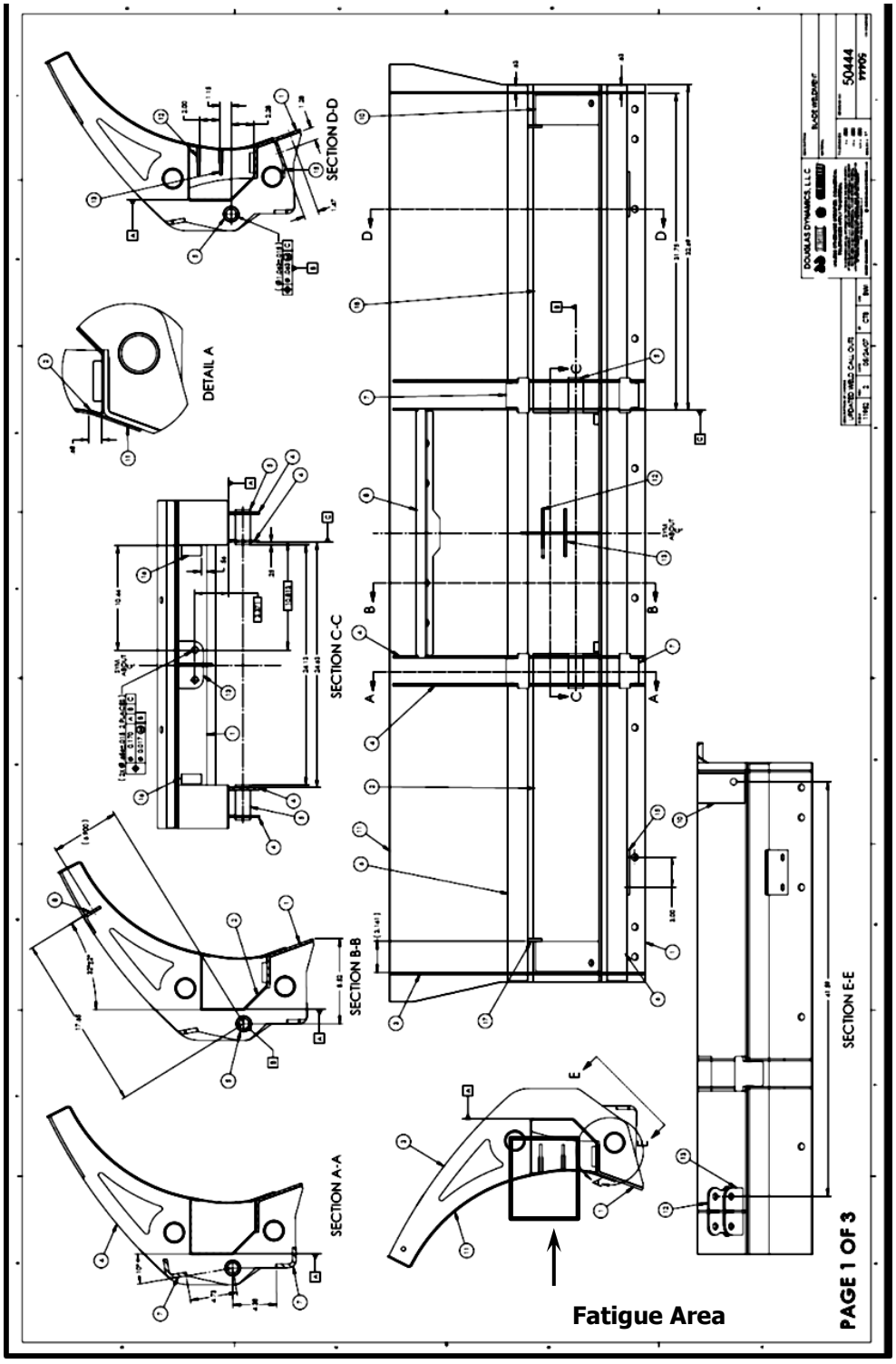

Figure 16. The component position drawing for the hinge snowplow main blade.

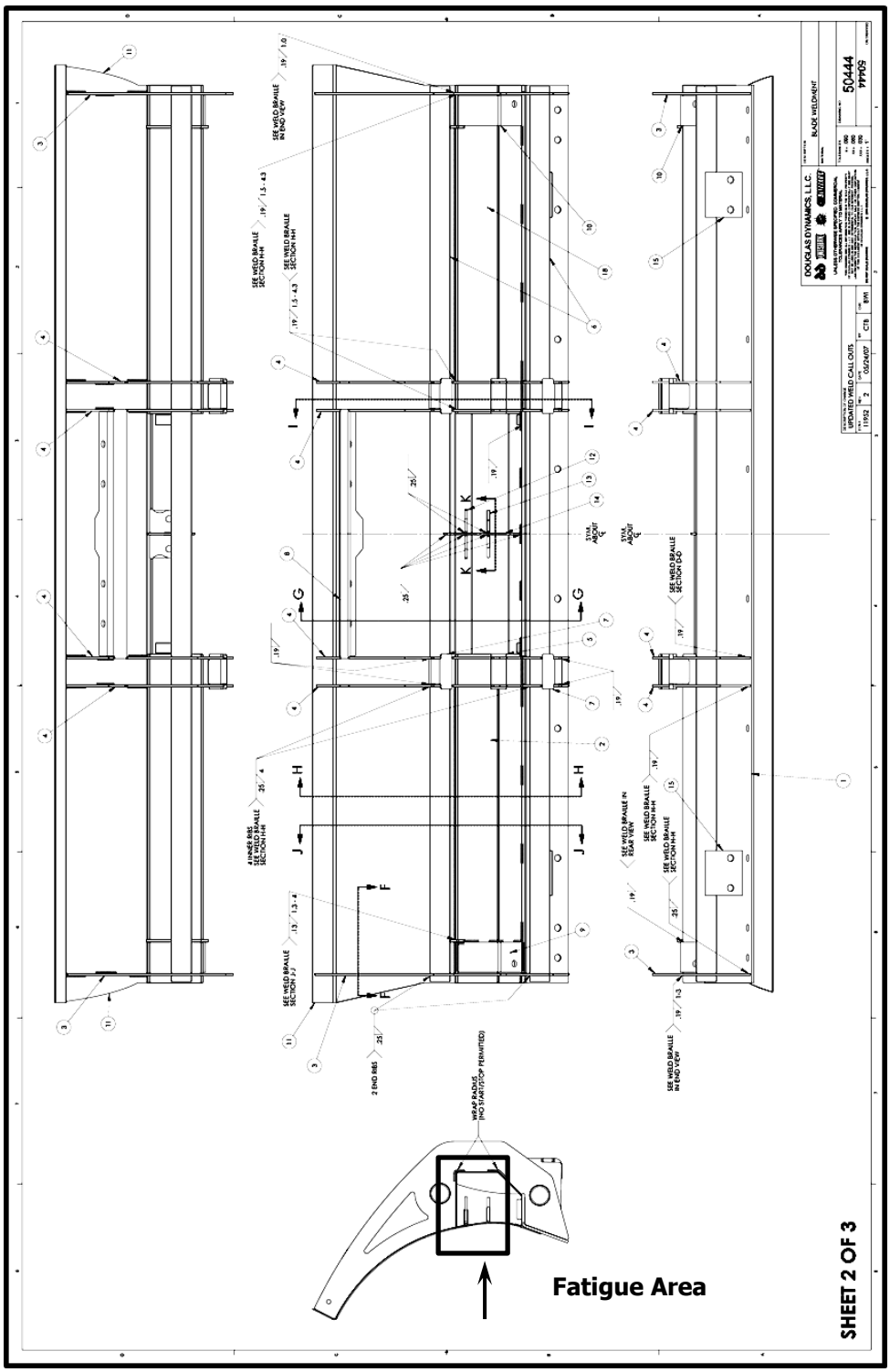

Figure 17. The weld drawing for the hinge snowplow main blade showing the fatigue area.

2.1.2 Specimen Details

The test specimen design incorporates the five components where the joint of interest is located and simplifies other components, so that the specimen fits into the MTS machine's load frame and yet maintains the proper load path. The specimens were manufactured using the current Douglas Dynamics, Inc. Standard Operational Procedures (SOP). The detailed SOPs are located in the Appendices. A model of the assembly showing the 5 components is presented in Figure 18. Material specifications for the components are given in Table 1. A total of seven specimens were manufactured for this study. The specimens were welded with the parameters given in Table 2, and then each specimen was inspected for dimensional and material compliance before testing. The chemical compositions and mechanical properties of component materials are given in Table 3. Specimens 3, 4, and 5 were stress relieved before testing at a temperature of 220°C for 2 hours.

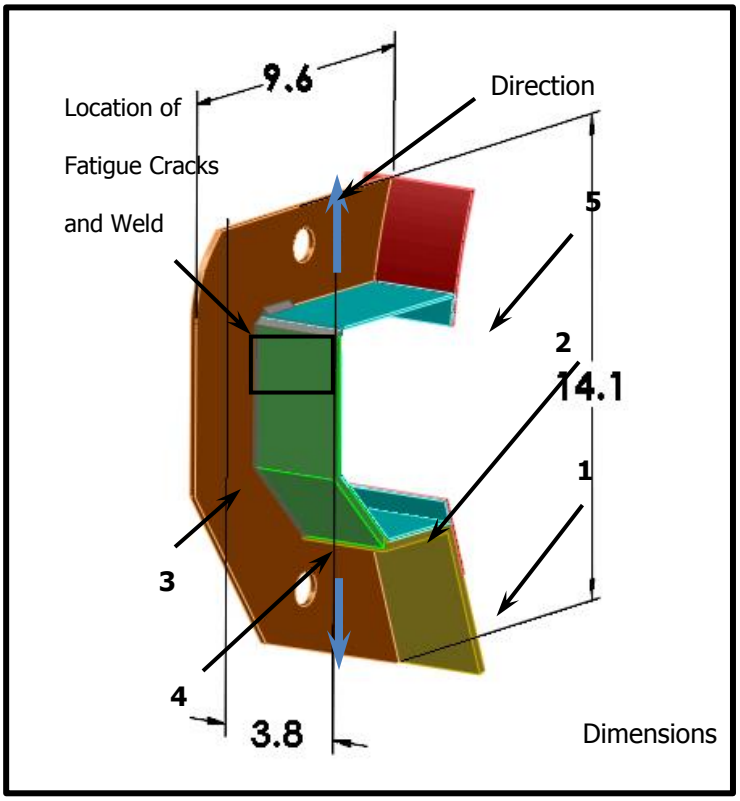

Figure 18. View of the test specimen overall dimensions, and direction of load. (1) formed plate, (2) 5-bend box, (3) outer rib, (4) formed plate, (5) blade sheet.

Table 1. List of specimen component material specifications.

Item ID	Component Description	Material Specification
1	Formed Plate	ASTM A 36
2	5 Bendbox	ASTM A 1011-01A CS TYPE B
3	Outer Rib	ASTM A 36
4	Formed Plate	ASTM A 36
5	Blade Sheet	ASTM A 1011-01A CS TYPE B

Table 2. Welding parameters for the test specimens.

Specimen No.		**1**	**2**	**3**	**4**	**5**	**6**	**7**
Welding Parameters	**Wire Size [in]**	0.035	0.045	0.045	0.035	0.035	0.035	0.045
	Voltage [V]	23.5	19.0	23.5	17.3	23.5	19.0	19.0
	Amps [A]	400	550	310	200	550	310	175
	Wire Speed [in/min]	450	220	220	450	450	450	220
	Gas Mix [$C0_2$/Ar]	95/5						
	Wire Material	ER70S-6						
Weld Size		0.25						
Stress Relieved? Y/N		N	N	N	N	Y	Y	Y

Table 3. Chemical composition and mechanical properties for component materials.

Steel ASTM A1011 Grade 50 Chemistry

% Heat Analysis, Element Maximum unless otherwise shown

C	Mn	P	S	Al	Si	Cu	Ni	Cr	Mo	V	Cb	Ti	N
0.25	1.35	0.035	0.04	...	...	0.2	0.2	0.15	0.06	0.008	0.008	0.025	...

Mechanical Properties

Yield Strength		Tensile Strength		% Elongation in2 in [50mm]
ksi [Mpa] min		ksi [Mpa] min		% for Thickness
50	[340]	66	[450]	17

Weld Material ER70S-6 Chemistry

% Heat Analysis, Element Maximum unless otherwise shown

C	Mn	P	S	Al	Si	Cu	Ni	Cr	Mo	V	Cb	Ti	N
0.06-0.15	1.40-1.85	0.025	0.035	...	0.80-1.15	0.5	0.15	0.15	0.15	0.03	...	...	...

Mechanical Properties

Yield Strength		Tensile Strength		% Elongation in2 in [50mm]
ksi [Mpa] min		ksi [Mpa] min		
80-85	[550-586]	85-90	[586-620]	28

ASTM A36 Chemistry

% Heat Analysis, Element Maximum unless otherwise shown

C	Mn	P	S	Al	Si	Cu	Ni	Cr	Mo	V	Cb	Ti	N
0.06-0.15	1.40-1.85	0.025	0.035	...	0.80-1.15	0.5	0.15	0.15	0.15	0.03	...	...	...

Mechanical Properties

Yield Strength		Tensile Strength		% Elongation in2 in [50mm]
ksi [Mpa] min		ksi [Mpa] min		
36				

2.1.3 Test Specimen Inspection

Each specimen was inspected for compliance with the production material and dimensional values. The following values were recorded:

- The steel type, chemical composition, and mechanical properties.
- Welding procedure, method, electrodes, number and sequences of passes, heat input.
- Global specimen geometry and local weld geometry, axial or angular distortion.
- Estimate of residual stresses in the specimens.
- Microscopy of the heat-affected zone [HAZ].

Several welding process variables were varied to determine their impact on the fatigue life of the joint. These variables were the wire size, weld voltage, weld amperage, feed rate, and stress relief. All other variables were held constant in the manufacturing of the specimens. Seven test specimens were fabricated and tested in this investigation. The welding parameters are presented in Table 2.

The weld geometry of each specimen was characterized on cross sections through welds after fatigue testing near the location at which fatigue cracks developed. The location of the cross section is shown in Figure 18. The cross sections of welds were cut from this location with a vertical band saw and then sectioned with a LECO CM15 cut off wheel. The cross sections were mounted in plastic (LECOSET 100) and then polished and etched for metallographic examination. The specimens were polished through 1.0 μm Al_2O_3 and etched with 3% Nital for about 5 seconds. Macro photos were then obtained with a Canon XT Rebel camera equipped with a Canon macro lens. Figure 19

presents a macro photo of the cross section from Specimen 6 showing the four weld measurements (weld toe radius, horizontal leg length, and vertical leg length) obtained. A total of 28 measurements of the toe radii and a total of 14 measurements of each leg length were made using an Olympus PME3 metallograph and a Spot Insight camera with software for making measurements of the radii and leg lengths. Figure 20 presents a photomicrograph showing a typical measurement of a toe radius. A summary of the measurements is presented in Table 4.

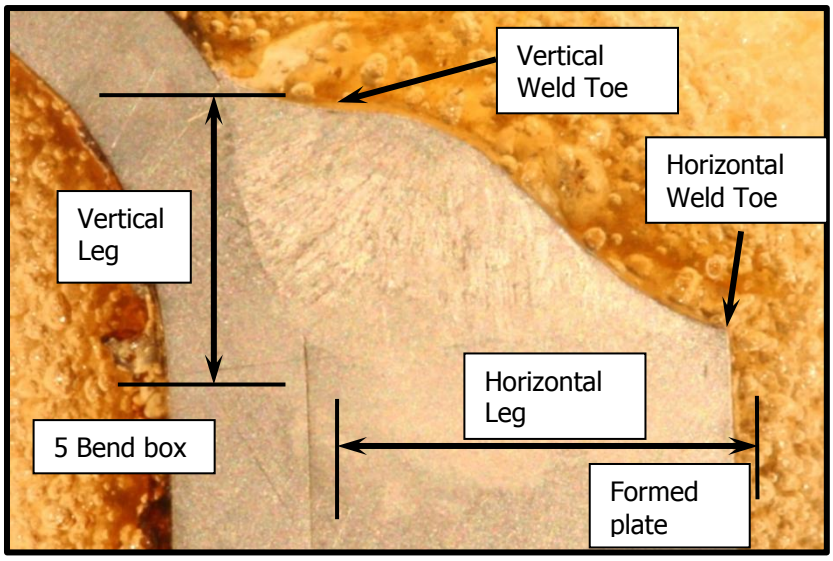

Figure 19. Weld toe measurement locations for specimen 6.

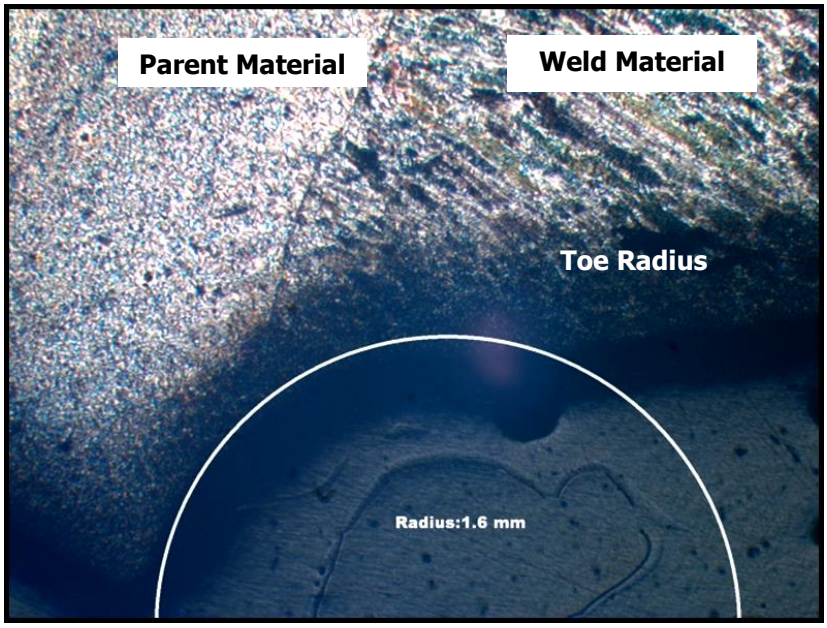

Figure 20. Typical weld toe section showing measurement of the radius.

Table 4. Statistical results from local geometry measurements of a fillet weld.

	Weld Toe Radius, Horiz. Leg [mm]	Weld Toe Radius, Vert. Leg [mm]	Weld Vert. Leg Length [in]	Weld Horz. Leg Length [in]
Number of recordings	**28**	**28**	**14**	**14**
Min value	2.70	0.40	0.118	0.199
Max vaule	5.40	1.60	0.290	0.280
Mean Value	4.15	0.96	0.215	0.245
Std Dev.	1.04	0.52	0.054	0.028
COV	0.25	0.54	0.250	0.116

The mechanical properties of the various parts of the weld cross sections were characterized using Rockwell B measurements. Figure 21 presents a macrophoto of a cross section showing the locations of the measurements. A single measurement was

made for each location using a Wilson Rockwell Series 500 bench top hardness tester. The results are summarized in Table 5. These values are consistent with the yield and tensile strengths reported in Table 3 for the materials involved.

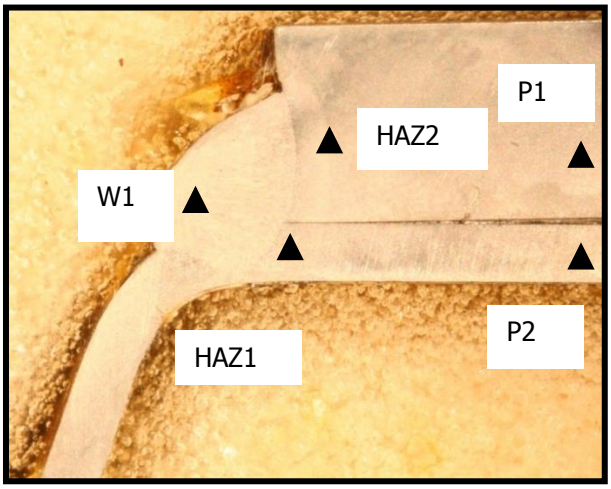

Figure 21. View of the hardness measurement locations for specimen 4.

Table 5. Summary of the hardness measurements for the test specimens.

Spot	HRB [Averaged]
Parent 1	65
Parent 2	67
Weld 1	92
HAZ 1	97
HAZ 2	97

2.2 Fatigue Test Machine

Tests were performed in a 20,000 lbf MTS system using tensile-tensile sinusoidal loading at a frequency of 20 Hz applied to the specimens through pin connection fixtures. Cyclic loads were applied until a crack was initiated. Then crack growth was followed with a traveling microscope. The full set up is shown in Figure 22.

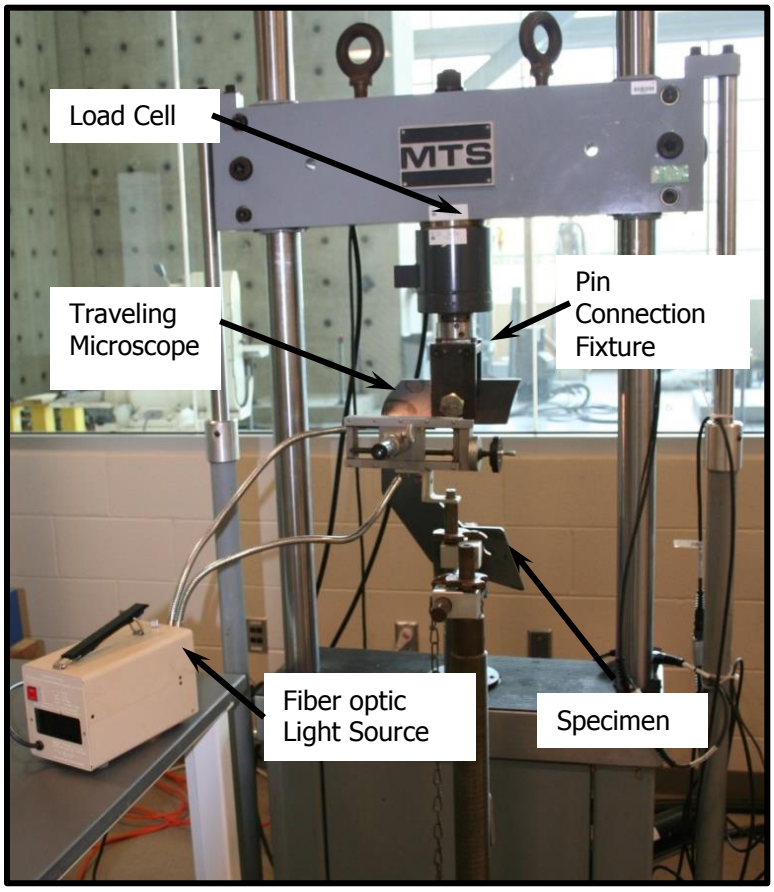

Figure 22. View of the full MTS set up.

2.3 Fixture Design

One of the fixtures for connecting the test specimens to the MTS Hydraulic closed loop test system is shown in Figure 23. These fixtures were designed to produce the load seen by the joint during normal service. The side and top plates in the figure were made from ASTM A 1011 Grade 50 steel; the 0.25” diameter pins were standard dowel pins; and the 3/8 socket head screws were standard screws. The specimens were held in place with 1-5X6 SAE Grade 8 heavy hex bolts and the corresponding hex nuts, and 1" hardened washers. Spiral washers were used to rigidly attach the fixtures to the load cell and actuator of the testing machine.

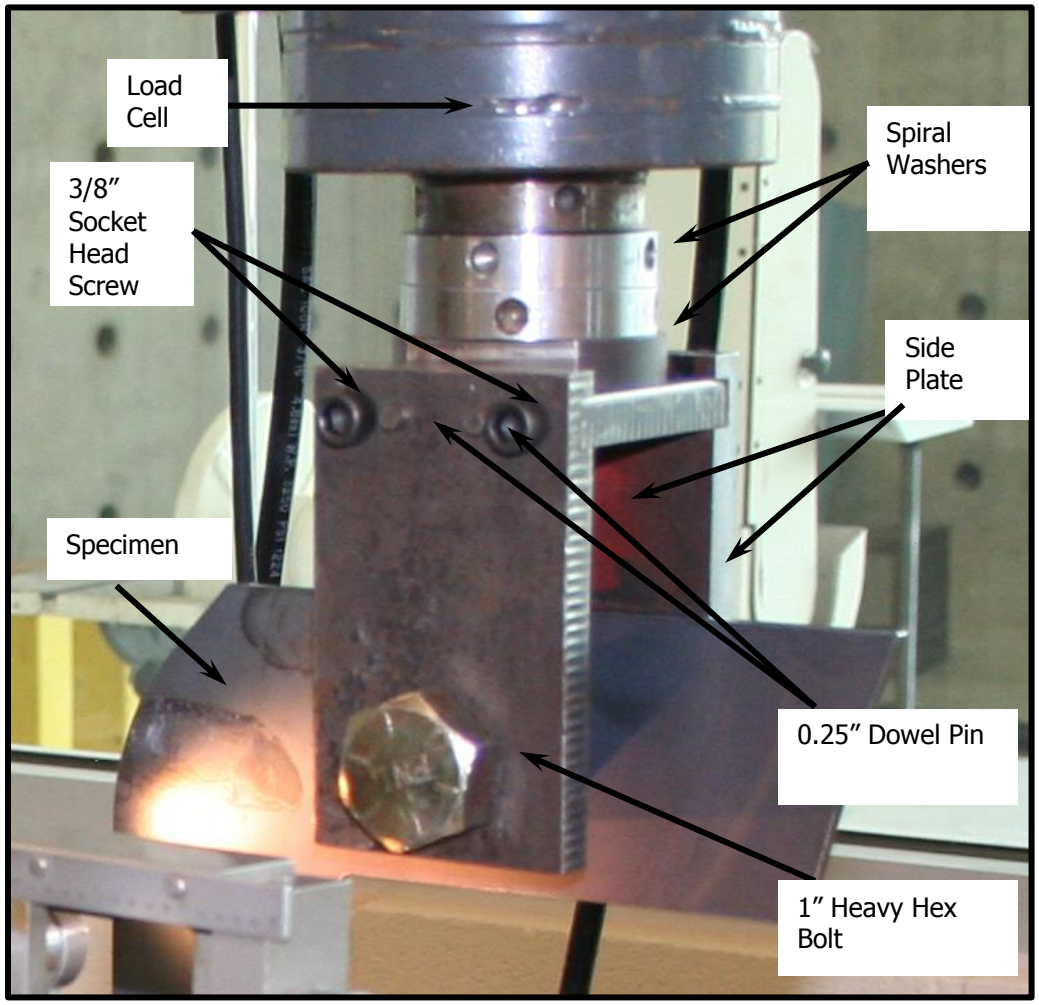

Figure 23. The top test fixture designed for the closed loop hydraulic test system.

2.4 Test Procedure

The test procedure developed for this study was a combination of the ASTM E 647-05 test for measuring crack growth in component specimens and the procedure described in "Fatigue Life Analyses of Welded Structures"[2]. Following this procedure the MTS was fit up with the test fixtures and cycled under displacement control to verify proper positioning of the fixtures. The specimen was then attached using the 1-8 heavy hex SAE Grade 8 bolts, hardened washers, and nuts as shown in Figure 23. The MTS was

then put into load control and the specimen checked for proper alignment. The microscope to follow and measure the crack propagation and the fiber optic light source were then set up and checked as shown in Figure 24. The MTS was then set to cycle at 20 Hz with the loads given in Table 6 and the loads verified using the oscilloscope. The crack length (a) was then taken to be the distance from the first visible crack to the point where the structure could no longer take a load. A growing crack is shown in Figure 25. The point "A" is the lead end of the crack when it just became visible, and point "B" is the lead end of the crack after N cycles.

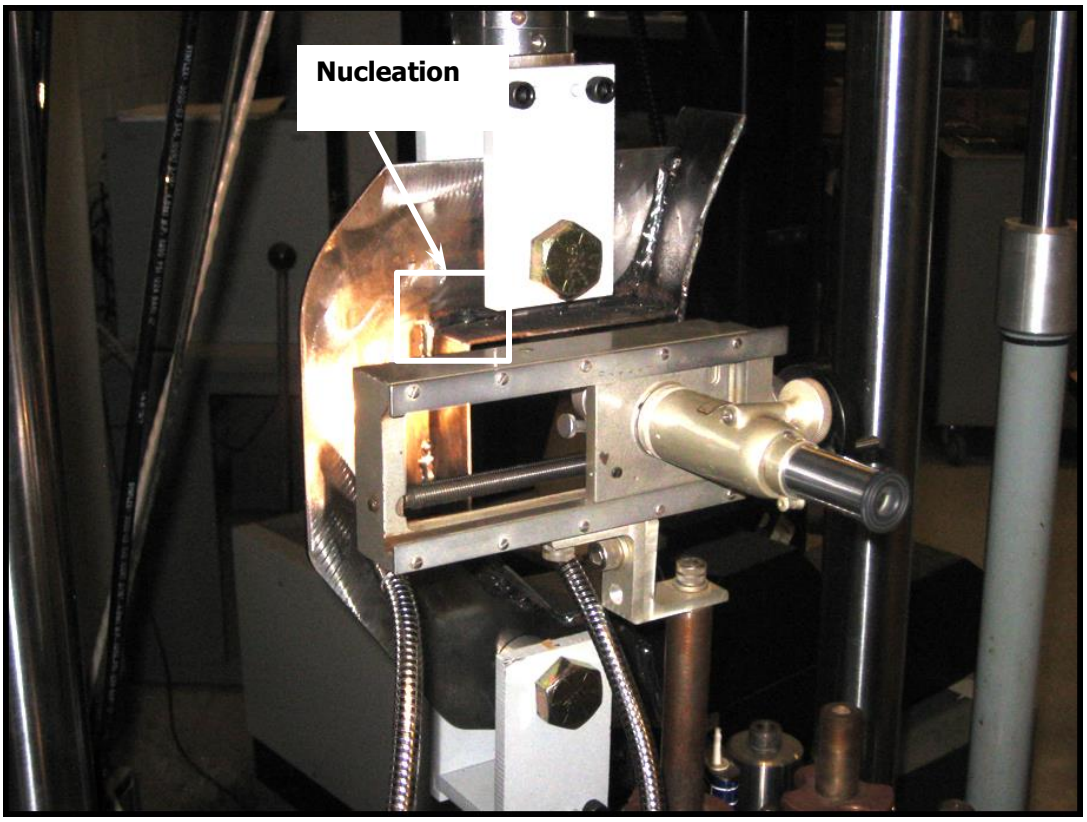

Figure 24. View of the specimen set up in the MTS machine at the start of the test.

Table 6. The MTS Settings for the Fatigue Test.

P_{max} [lbf]	P_{min} [lbf]	P_a [lbf]	Frequency [Hz]
1000	50	950	20

2.5 Running the Test

The test was started after all checks were made to assure that the proper loading was achieved. The specimen was checked every 1000 cycles until a crack was observed, and then the crack length was measured every 5000 cycles until the specimen could no longer carry any load. All cracks were observed to nucleate at the joint between the outer rib and 5-bend box as shown in Figure 26.

Figure 25 shows a close up view of a fatigue crack which initiated at point A and propagated to point B. The end of the test was defined when the components could no longer hold the input load.

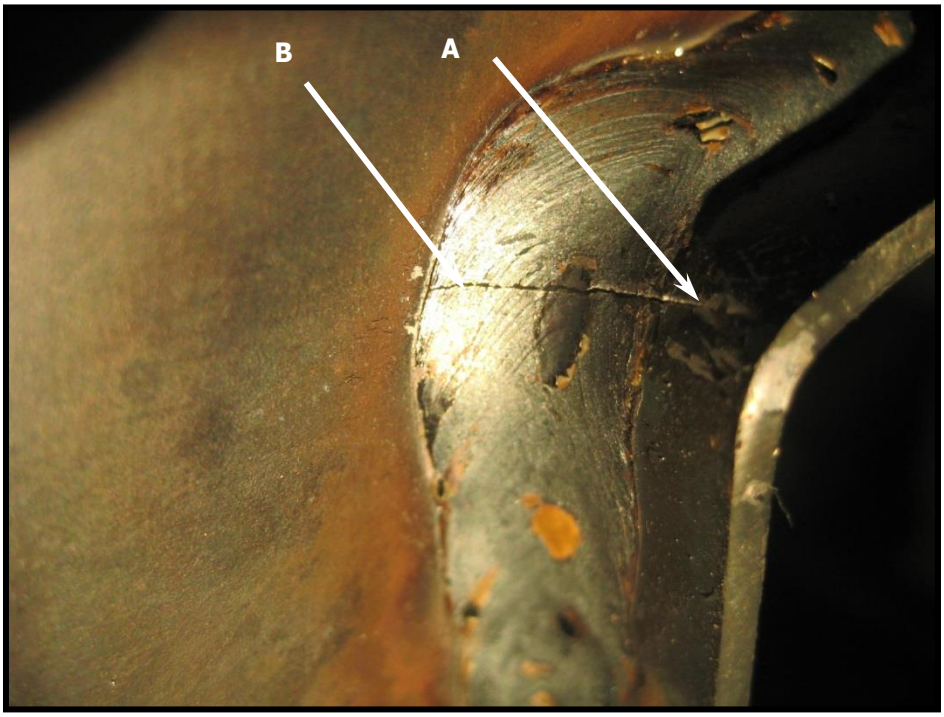

Figure 25. Typical fatigue crack growing from A to B.

2.6 Data Analysis

The crack length (a) and number of cycles (N) were recorded and used to calculate the stress intensity factors [SIF] using the secant method described in ASTM A 647-05 Standard for Measurement of Fatigue Crack Growth Rates.[13] section X1.1. Using the calculated data a curve was developed to determine the stress intensity factors. The data from the specimen inspections and the calculated SIFs were tabulated and correlations examined to obtain a set of crack parameters for use in the FEM study. The crack growth rate, da/dN, and stress intensity range, ΔK, were calculated and plotted on a log-log graph.

3 FINITE ELEMENT PROCEDURE

3.1 Methodology

The fracture mechanics method was used to study the fatigue life of the welded joint specimens described in the experimental section. The method involved the following steps:

- CAD Model creation
- Elastic stress analysis of the pre-cracked geometry
- Creation of the crack
- Crack parametric study
- Crack propagation
- Calculation of stress intensity factors
- Interpretation of results

This type fracture analysis is widely used to predict component failure caused by preexisting small cracks, allowing one to take precautions to prevent further crack growth or to determine the remaining life of the structure.

The 3D solid CAD geometry for the test specimen design (Figure 26) was used in the finite element package ANSYS utilizing the fracture mechanics module. The welds were modeled as solid bodies and meshed with tetrahedron quadratic elements. To obtain the fracture damage, stress intensity factors (SIFs) had to be evaluated accurately. Because it is difficult to determine accurate SIFs using a closed-form analytical solution for cracks in complex structures, finite-element analysis was used instead.

There are two approaches are available for evaluating SIFs:

- The interaction integral method, which performs the SIF calculation during the solution phase of the analysis and stores the results for later postprocessing.

- The displacement extrapolation method which performs the SIF calculation during postprocessing. This method is limited to problems involving linear elasticity with homogeneous, isotropic materials near the crack region.

The interaction integral method is suitable for a wide range of applications. In a finite element analysis, this method is suitably accurate for evaluating mixed mode SIFs and is also a robust tool for heterogeneous models with continuous, discontinuous, or nonlinear material properties. This method yields more accurate results because the contour integral is evaluated at points far away from the crack-tip.[6]

3.1.1 CAD Model

The CAD geometry for the study shown in Figure 26 was developed from the snowplow blade geometry obtained from the manufacturing design. The component descriptions and material specifications are shown Figure 18 and in Table in 1 in Section 2.1.1. Figure 26 shows the CAD geometry.

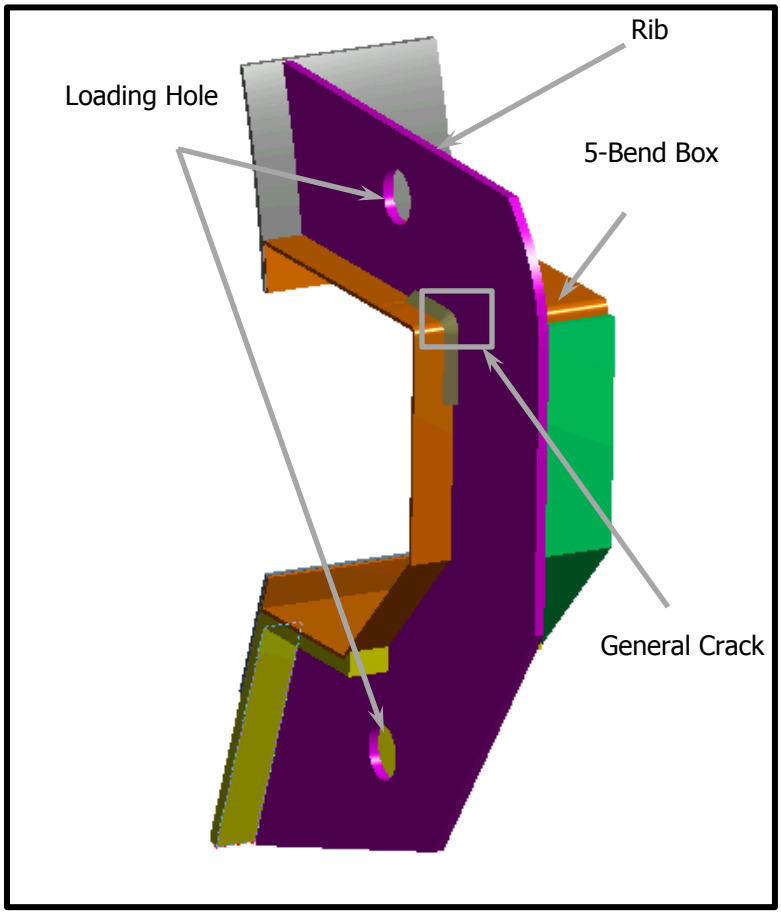

Figure 26. The CAD geometry used to generate the finite element model for the fracture mechanics analysis.

3.1.2 Development of the crack model

The crack geometry was developed using the fatigue testing data collected in the experimental part of the study. This part of the study showed that the cracks started either at location A on the top outside radius of the 5-bend box (Figure 27) or at location B on the top outside weld of the 5-bend box to rib (Figure28). Figure 29 shows actual fatigue cracks that formed at these two locations. Crack parameters required for the FEA are the major and minor radii, the crack opening and the crack location. The crack

parameters are given in Table 7, and the detailed diagram of the crack geometry is shown in Figure 30.

The Mode 1 Stress Intensity Factor (K1) is computed along the crack front using the interaction integral method. The interaction integral method for the stress intensity factor calculation applies volume integration for 3D problems and area integration for 2D problems. The traditional displacement extrapolation method is less accurate and requires greater mesh requirements than the interaction integration method.

The interaction integral is defined as:

$$I = -\oint \frac{q_{i,j}\left(\sigma_{k,j}\varepsilon_{k,j}^{aux}\delta_{i,j} - \sigma_{k,j}^{aux}u_{k,i} - \sigma_{k,j}u_{k,i}^{aux}\right)dV}{\int \delta q_n \, ds} \quad [9]$$

Where,

$\sigma_{ij}, \varepsilon_{ij}, u_i$ are the stress, strain and displacement,

$\sigma_{ij}^{aux}, \varepsilon_{ij}^{aux}, u_{ij}^{aux}$ are the stress, strain, and displacement of the auxiliary field, and qi is the crack extension vector.

The interaction integral is associated with the stress intensity factor as

$$I = \frac{2}{E^*}(K_1 K_1^{aux} + K_{21} K_2^{aux}) + \frac{1}{\mu} K_3 K_3^{aux} \quad [10]$$

where K_i (i = 1, 2, 3) are mode I, II, III, stress intensity factors, and K_i^{aux} (i = 1, 2, 3) are auxiliary mode I, II, III, stress intensity factors. E* = E for plane stress and

$E^* = E / (1 - \upsilon^2)$ for plane strain, E is the Young's modulus, υ is the Poisson ratio, and μ is the shear modulus.

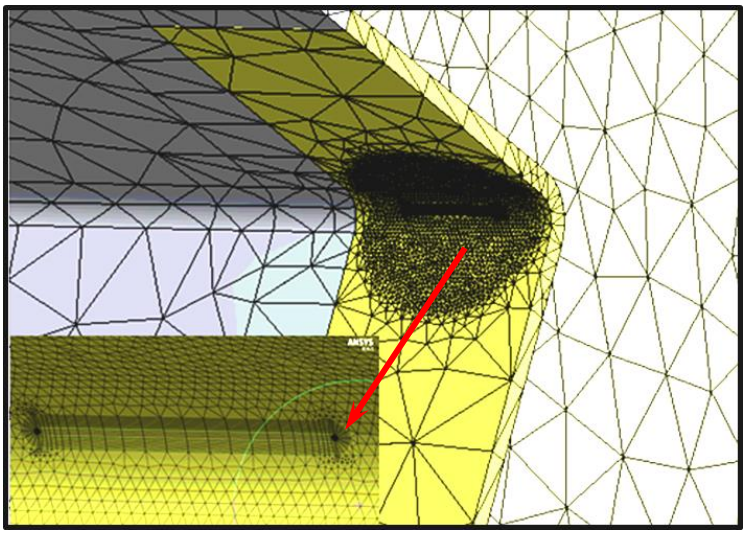

Figure 27. Meshed geometry including crack mesh for location [A].

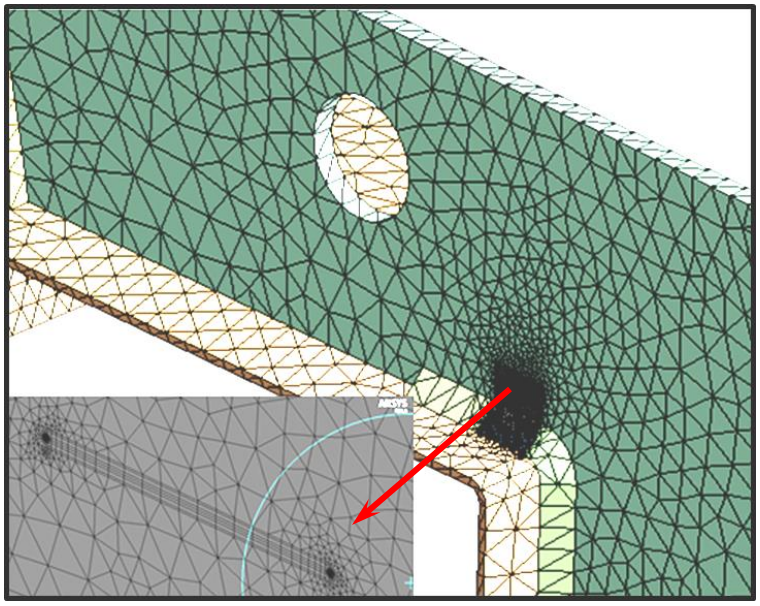

Figure 28. Meshed geometry including crack mesh for location [B].

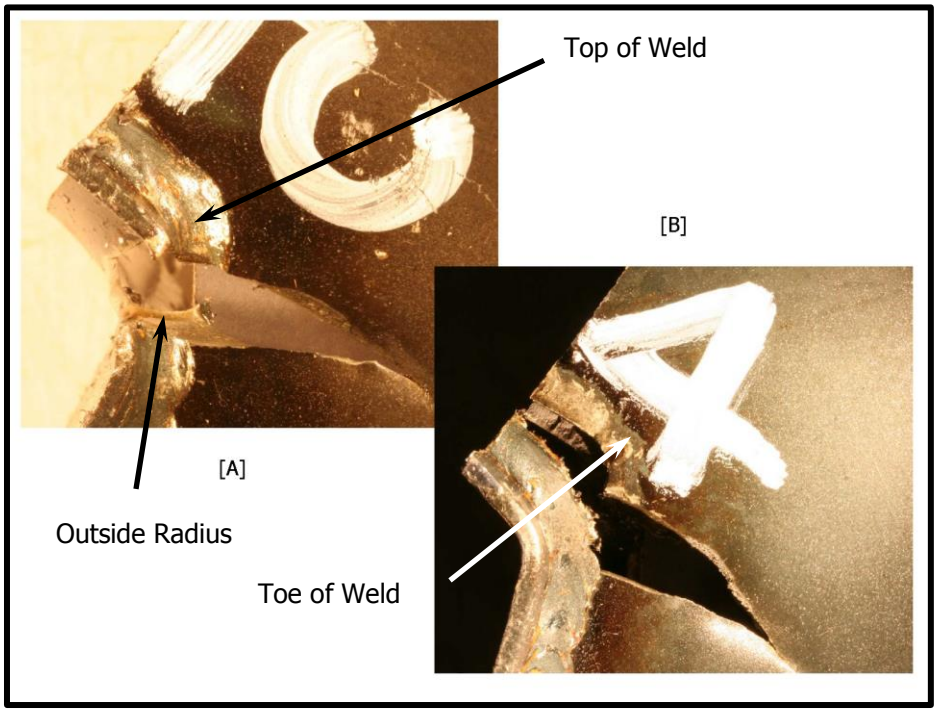

Figure 29. Fatigue cracks at the two locations of crack initiation, [A] 5 bend box, [B] top weld toe.

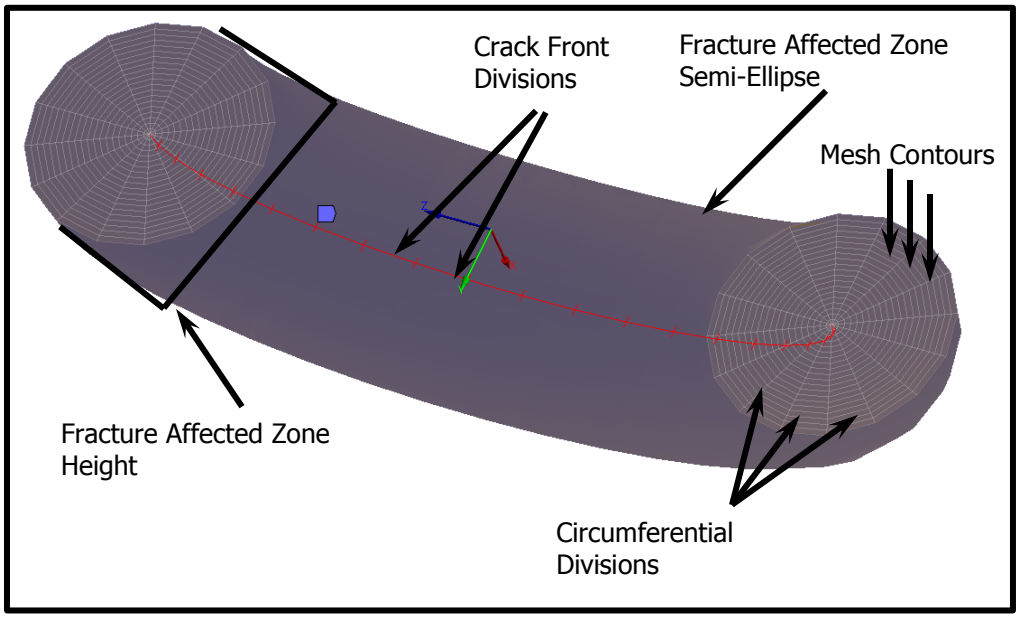

Figure 30. Details of the crack model.

Table 7. Crack parameters.

Crack Location	A	B
Major Radius [in]	0.0150	0.03
Minor Radius [in]	0.0115	0.01
Fractrure Affected Zone Height [in]	0.0150	0.05
Largest Contour Radius [in]	0.0025	0.001
Circumferential Divisions	16	16
Mesh Contours	20	20
Crack Front Divisions	20	20

3.1.3 ANSYS Database

The software used for this study was ANSYS Mechanical Release 14.5.1. The process to develop the database to solve the stress intensity range involves importing the CAD geometry via Design Modeler, a software CAD module that works inside the Workbench environment. Once inside ANSYS the CAD geometry was developed to generate an acceptable mesh (Figure 31) that was checked using the quality factor algorithm. The quality factor is computed for each element of a model (excluding line and point elements). The element quality option provides a composite quality metric that ranges between 0 and 1. This metric is based on the ratio of the volume to the edge length for a given element. A value of 1 indicates a perfect cube or square while a value of 0 indicates that the element has a zero or negative volume. Figure 32 shows the element quality plot for the mesh. A quality factor is computed for each element of a model (excluding line and point elements). The minimum element quality ratio for acceptable results is a value of 0.6 in the region of interest.

The parametric study was used to determine the stress intensity factors for the particular crack length. From the experimental data, the initial crack length was determined to be approximately 0.03" [1.0 mm]. The crack length was increase by 0.05" until a maximum length that would allow a converged solution. The parameter values are shown in Table 8.

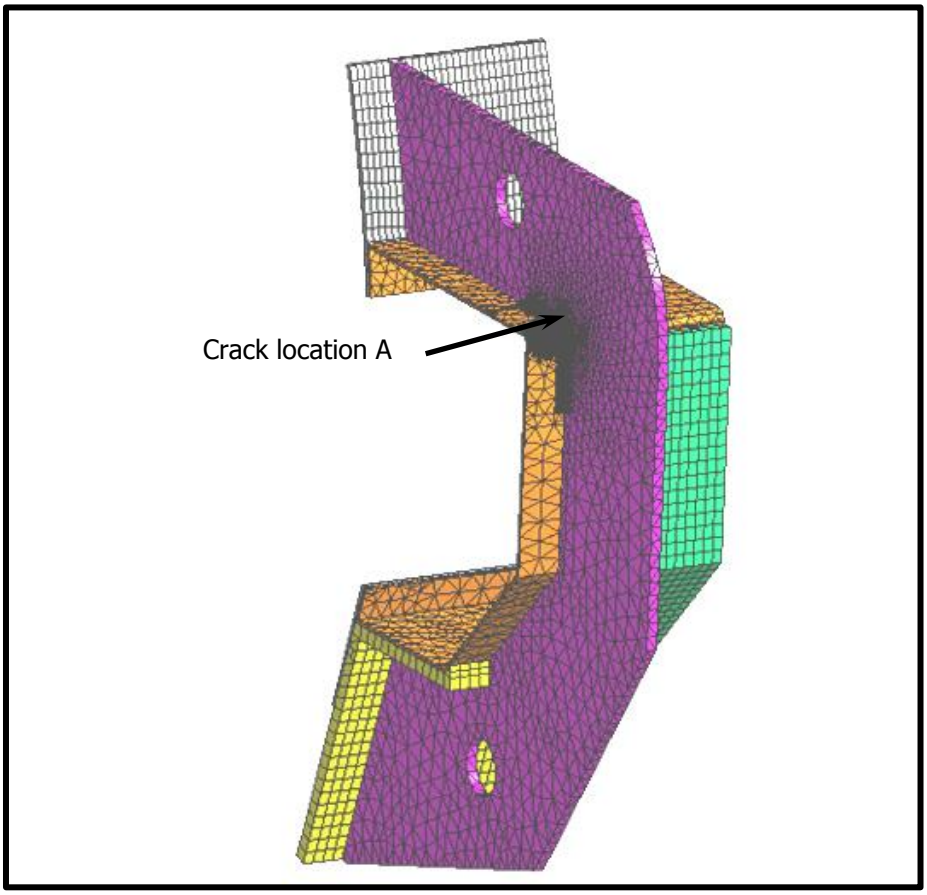

Figure 31. Meshed CAD model with the crack generated.

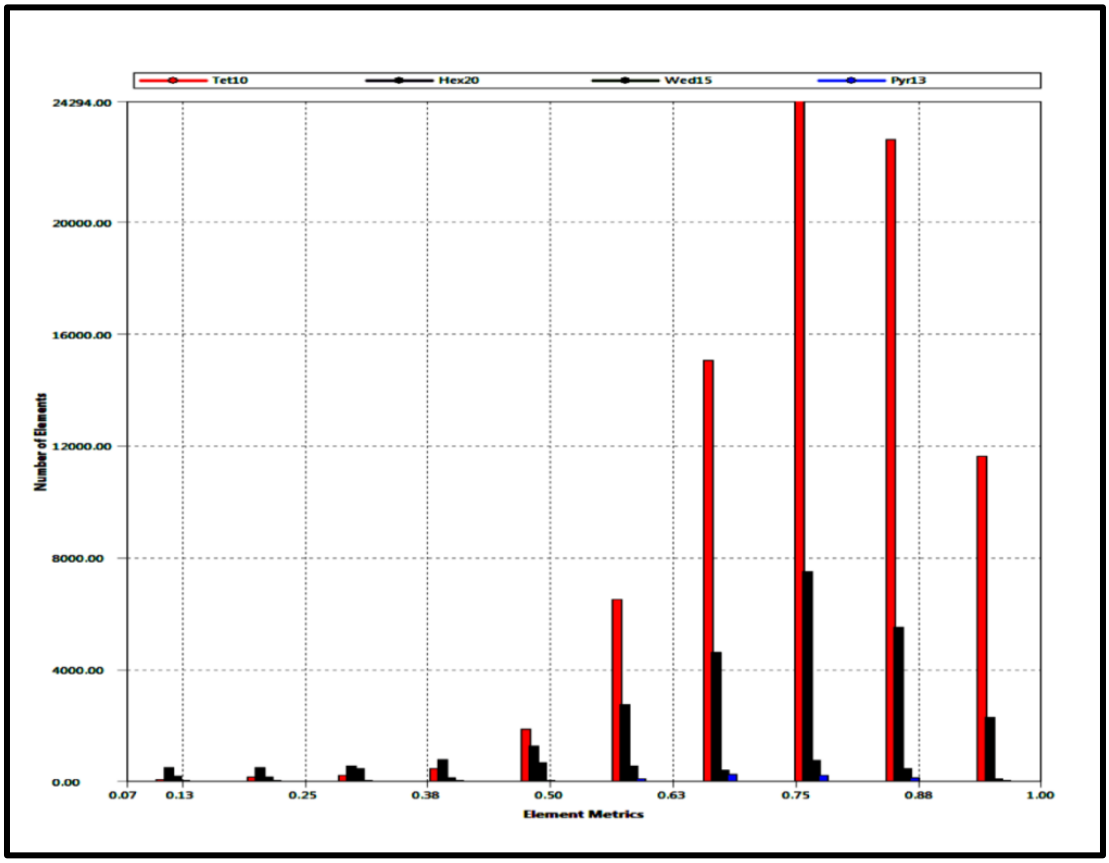

Figure 32. Element quality graph.

Table 8. Parametric Study Variables.

Parameter	Crack Location A	Crack Location B
Major Radius	0.05	0.05
	0.10	0.08
	0.15	0.10
	0.18	0.12

The recommended element type for 3-D models for cracks is SOLID186 (Figures 27, 28, and 31), the 20-node brick element, as shown in Figure 33. The first row of elements around the crack front should be singular elements. Notice that the element is

wedge-shaped, with the KLPO face collapsed into the line KO. Stress and deformation fields around the crack tip generally have high gradients. The precise nature of these fields depends on the material, geometry, and other factors. To capture the rapidly varying stress and deformation fields, a refined mesh in the region around the crack tip.

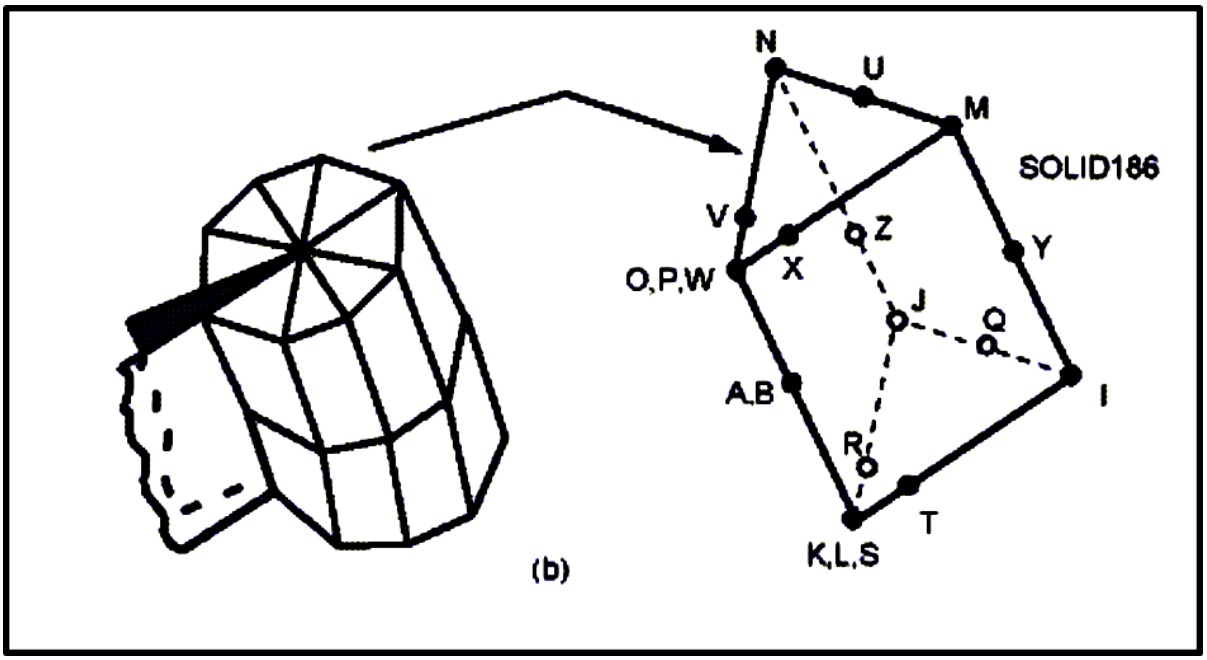

Figure 33. Singularity at the crack tip.

Element size recommendations are the same as for 2-D models. In addition, aspect ratios should not exceed approximately 4 to 1 in all directions. For curved crack fronts, the element size along the crack front depends on the amount of local curvature. A general guideline is to have at least one element every 15° to 30° along a circular crack front. All element edges should be straight, including the edge on the crack front.

The model was loaded between the holes connecting the test specimens to the MTS closed loop system. The cyclic load parameters were defined as: P_{max} = 1000 lbf, P_{min}

= 50 lbf, ΔP = 950lbf, P_a = 475 lbf, P_m = 525 lbf. The lower hole was held with one displacement normal to the outside surface of the rib and a cylindrical restraint on the hole surface (Figure 35). The force was applied to the top hole surface (Figure 34), and a displacement normal to the outside surface of the rib (Figure 35). The lower restraint was modeled using a displacement normal to the outside surface of the rib (Figure 36) and a cylindrical restraint applied to the top hole surface, with the radial DOF set to "fixed", the axial and tangential DOF were set to "free" (Figure 37).

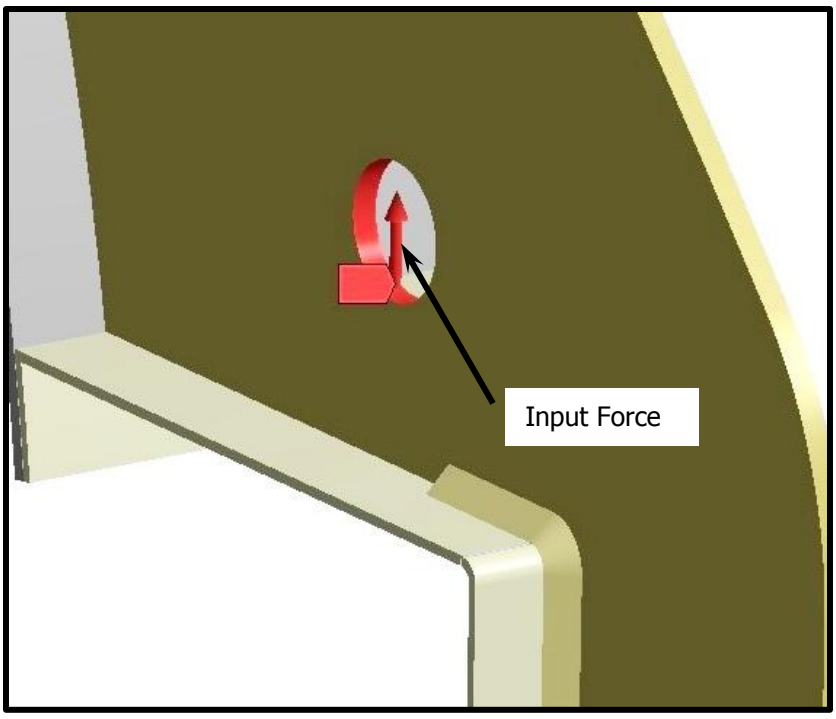

Figure 34. Force applied to the inside surface of the top hole of the specimen.

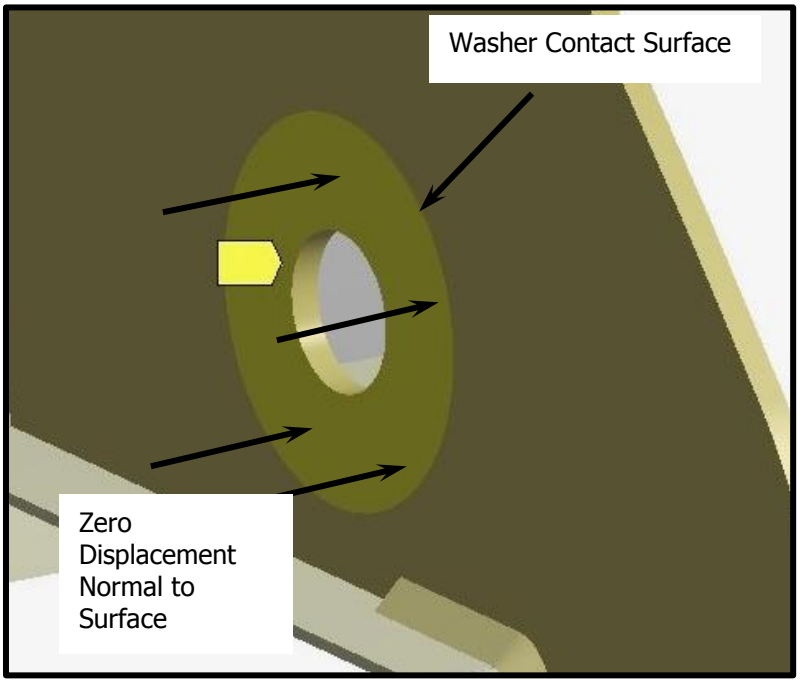

Figure 35. Zero Displacement applied to the surface of the rib at the top hole.

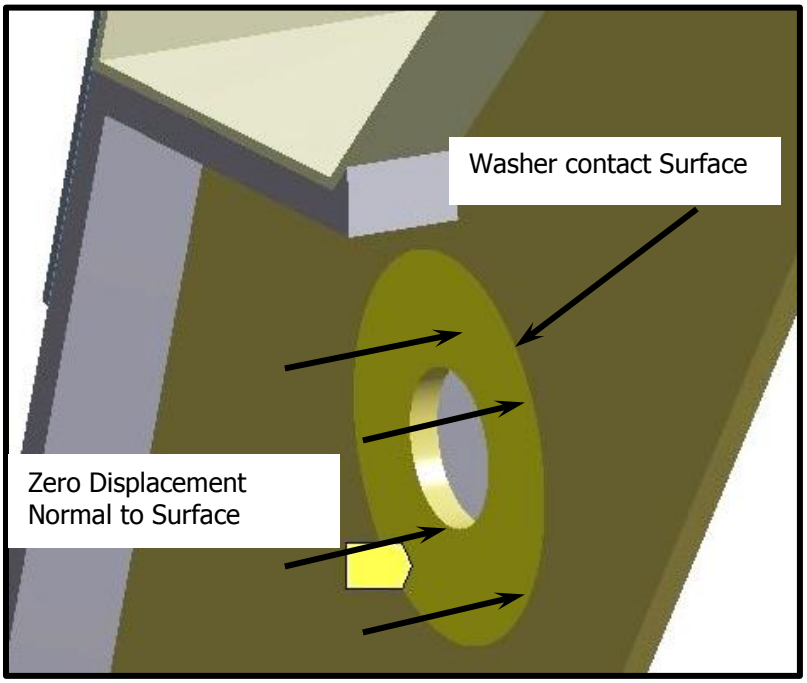

Figure 36. Zero Displacement applied to the surface of the rib at the bottom hole.

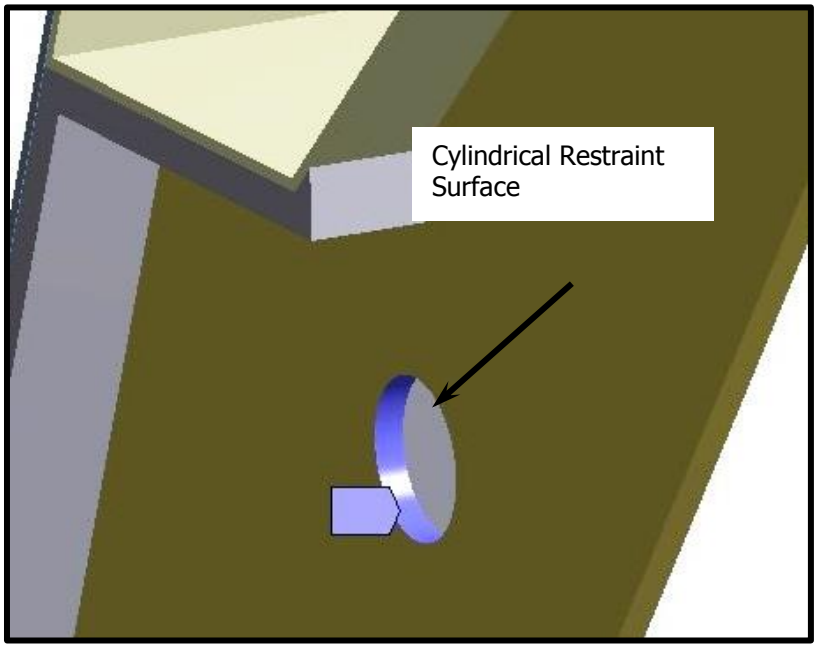

Figure 37. Cylindrical restraint at the lower hole, radial DOF is fixed, axial and tangential DOFs are free.

3.1.4 Solution Procedure

The first step to determine the stress intensity factors was to create a crack in the areas of initiation, of which there were two (Figures 17, 28 and 29) observed during testing, both in the field and in the lab. The next step was to apply the restraints and force to the correct surfaces. The washers were represented as zero displacements normal to the outer rib, the lower fastener was represented by a cylindrical restraint with the radial DOF set to fixed, and the axial and tangential DOF's set to free. The solution settings are given in Table C2.

4 RESULTS

4.1 Fatigue Testing Results

As pointed out in Section 3 fatigue cracks initiated at one of the two locations shown in Figure 29, either at the top inside formed edge of the 5 bend box (Location A) or at the top corner weld toe (Location B). For the seven specimens cracks initiated at Location A in five and at Location B in two. The initiation of the crack was fairly fast compared to the total life cycle of the joint. The number of cycles required for crack initiation was a very small percentage of the total fatigue life. The average fatigue life of a test specimen was approximately 177,000 cycles, and the average number of cycles until a crack was observed was 11,000 cycles or approximately 6%. This is consistent with the assumption that, as pointed out in Section 1.2.6, crack initiation can be neglected in the determination of fatigue life and that the number of cycles to propagate a crack to failure determines the fatigue life.

The basic fatigue crack growth data of crack length (a) and numbers of cycles (N) for each test specimen are tabulated in Table 9 and are graphically presented in Figures 38 – 46. Figure 45 shows all of the data plotted on a single graph. As can be seen the crack growth rates (slopes of the plots) increase as the cracks get longer. Figure 45 also shows that the crack growth behavior is about the same for all specimens. From this crack growth data the ASTM A 647-05 secant method was used to calculate the crack growth rate, da/dN. The secant method uses a point to point technique,

$$\left(\frac{da}{dN}\right) = \frac{\left(a_{i_{+_1}} - a_i\right)}{(N_{i+1} - N_i)} \qquad [11]$$

where a is the crack length and N is the number of cycles. The variable a_i is the crack length measured at cycle N_i, and a_{i+1} is the crack length measured at cycle N_{i+1}.

The stress intensity factor range, ΔK was calculated using the average crack size, $\bar{a}$, over the interval of cycles, ΔN using

$$\Delta K_i = \frac{\Delta P}{B}\sqrt{\frac{\pi a_i}{2W}\left[\sec\left(\frac{\pi a_i}{2}\right)\right]} \qquad [12]$$

$$a_i = \frac{2\bar{a}_i}{W} \qquad [13]$$

$$\bar{a} = \frac{a_{i_{+1}} + a_i}{2} \qquad [14]$$

ΔP is the load range, (P_{max} – P_{min}), B is the thickness , W is the width of the plate , and a_i is the crack length at N cycles.

$$\Delta K = (1 - R)K_{maz} \qquad for\ R \geq 0 \qquad [15]$$

$$\Delta K = K_{max} \qquad for\ R \leq 0 \qquad [16]$$

The force ratio is the algebraic ratio of the minimum to maximum force in a cycle,

$$R = \frac{P_{min}}{P_{max}} \qquad [17]$$

The force ratio was equal to 0.048, Thus, from Equation 14 $\Delta K_I = (1 - R)K_{max}$ or $(0.952)K_{max}$.

Table 10 shows the calculated da/dN and ΔK_I values for all seven tests and Figures 46 through 52 present the individual da/dN versus ΔK curves for the seven test specimens, and Figure 53 shows all of the data on one graph. As can be seen in this figure, the data falls in a

broad band which shows similar crack growth in all of the test specimens. This suggests that the variation in the welding parameters and stress relief had no significant effect on the overall fatigue life of the joint. This is most likely due to the fact that the existence of a crack in the weld area is much more significant than the weld parameters.

Table 9. Experimental Crack Length and Number of Cycles Data.

Reading No.	Specimen 1		Specimen 2		Specimen 3		Specimen 4	
	Crack Length, a [mm]	Number of Cycles, N	Crack Length, a [mm]	Number of Cycles, N	Crack Length, a [mm]	Number of Cycles, N	Crack Length, a [mm]	Number of Cycles, N
1	1.03	10100	1.09	10020	1.00	10120	1.20	12120
2	1.25	20050	1.26	20120	1.16	19800	1.36	22800
3	1.50	30200	1.41	30300	1.35	30120	1.45	31120
4	1.75	40050	1.65	40050	1.55	41050	1.65	45050
5	2.00	50060	2.10	51000	2.00	50090	2.40	54090
6	2.36	60300	2.46	62300	2.36	61300	2.66	64300
7	2.98	70200	3.18	70130	2.80	70090	2.80	72090
8	4.00	80040	4.10	82050	3.71	81050	3.79	81050
9	6.00	90100	6.20	90230	6.20	91030	6.20	87030
10	9.00	100050	8.76	103020	9.00	101080	9.70	104080
11	12.50	110030	11.97	110080	12.25	110060	12.50	118060
12	17.10	120100	16.99	120500	17.21	121500	17.21	123500
13	22.00	130050	22.25	131000	20.00	131020	20.36	139020
14	25.90	140300	24.60	140200	24.90	140200	24.90	148200
15	29.50	150040	30.25	152000	27.50	145500	29.50	155500
16	33.60	160020	35.10	163000	35.60	154700	38.60	165700
17	37.35	170115			38.33	161948		
18	42.19	179980			42.78	175136		
19	47.03	189995			48.30	192324		

	Specimen 5		Specimen 6		Specimen 7	
Reading No.	Crack Length, a	Number of Cycles,	Crack Length, a	Number of Cycles,	Crack Length, a	Number of Cycles,
1	1.30	10700	1.20	10120	1.16	10120
2	1.45	20200	1.36	19800	1.21	21120
3	1.64	31000	1.41	30120	1.31	32300
4	1.75	42900	1.65	41050	1.45	40850
5	1.92	51800	2.20	50290	1.90	53000
6	2.26	60200	2.46	61300	2.46	62305
7	2.58	71000	2.80	71090	3.18	70135
8	3.17	80300	3.51	81250	4.15	82050
9	5.02	90056	5.20	91030	6.29	90230

Table 10. Summary ΔK and da/dN values for Fatigue Tests.

Specimen 1	
ΔK [ksi√in]	da/dN [mm/cycle]
16.5	2.21E-05
18.2	2.46E-05
19.7	2.54E-05
21.2	2.50E-05
22.9	3.52E-05
25.3	6.26E-05
29.0	1.04E-04
34.8	1.99E-04
43.0	3.02E-04
52.2	3.51E-04
62.9	4.57E-04
75.5	4.92E-04
88.2	3.80E-04
100.7	3.70E-04
116.1	4.11E-04
136.5	3.71E-04
168.8	4.91E-04
237.0	4.83E-04
452.9	4.28E-04

Specimen 2	
ΔK [ksi√in]	da/dN [mm/cycle]
16.8	1.68E-05
17.9	1.47E-05
19.2	2.46E-05
21.2	4.11E-05
23.4	3.19E-05
26.0	9.20E-05
29.6	7.72E-05
35.4	2.57E-04
42.9	2.00E-04
51.2	4.55E-04
62.0	4.82E-04
75.6	5.01E-04
86.6	2.55E-04
99.7	4.79E-04
121.4	4.41E-04

Specimen 3	
ΔK [ksi√in]	da/dN [mm/cycle]
16.1	1.65E-05
17.3	1.84E-05
18.6	1.83E-05
20.6	4.98E-05
22.9	3.21E-05
24.9	5.01E-05
28.0	8.30E-05
34.7	2.49E-04
43.3	2.79E-04
51.9	3.62E-04
62.7	4.34E-04
72.9	2.93E-04
83.7	5.34E-04
95.4	4.91E-04
116.1	8.80E-04
146.1	3.77E-04
176.6	3.37E-04
259.6	3.21E-04

Specimen 4	
ΔK [ksi√in]	da/dN [mm/cycle]
17.5	1.50E-05
18.4	1.08E-05
19.3	1.44E-05
22.0	8.30E-05
24.7	2.55E-05
25.6	1.80E-05
28.2	1.10E-04
34.8	4.03E-04
44.3	2.05E-04
53.1	2.00E-04
63.0	8.66E-04
73.4	2.03E-04
84.2	4.95E-04
98.9	6.30E-04
128.4	8.92E-04

Specimen 5	
ΔK [ksi√in]	da/dN [mm/cycle]
18.2	1.58E-05
19.3	1.76E-05
20.2	9.24E-06
21.0	1.91E-05
22.4	4.05E-05
24.1	2.96E-05
26.3	6.34E-05
31.5	1.90E-04
37.0	1.03E-04
41.3	1.75E-04
48.4	2.88E-04
61.6	8.00E-04
81.5	9.33E-04
98.9	2.60E-03
116.1	5.60E-04
142.9	8.77E-04
194.1	1.06E-03
328.7	8.48E-04

Specimen 6	
ΔK [ksi√in]	da/dN [mm/cycle]
17.5	1.65E-05
18.2	4.84E-06
19.2	2.20E-05
21.5	5.95E-05
23.7	2.36E-05
25.1	3.47E-05
27.6	6.99E-05
32.5	1.73E-04
40.0	2.61E-04
49.3	4.15E-04
60.4	4.12E-04
71.6	3.98E-04
83.7	4.02E-04
93.8	1.20E-04
116.1	1.91E-03
189.1	1.91E-03

Specimen 7	
ΔK [ksi√in]	da/dN [mm/cycle]
16.9	4.55E-06
17.4	8.94E-06
18.2	1.64E-05
20.0	3.70E-05
22.9	6.02E-05
26.0	9.20E-05
29.7	8.14E-05
35.6	2.62E-04
43.3	1.68E-04
50.8	4.21E-04
59.7	6.49E-04
71.5	8.72E-04
82.9	4.79E-04
92.1	2.41E-04
105.7	7.29E-04
131.7	1.22E-03
178.7	1.22E-03
354.8	1.15E-03

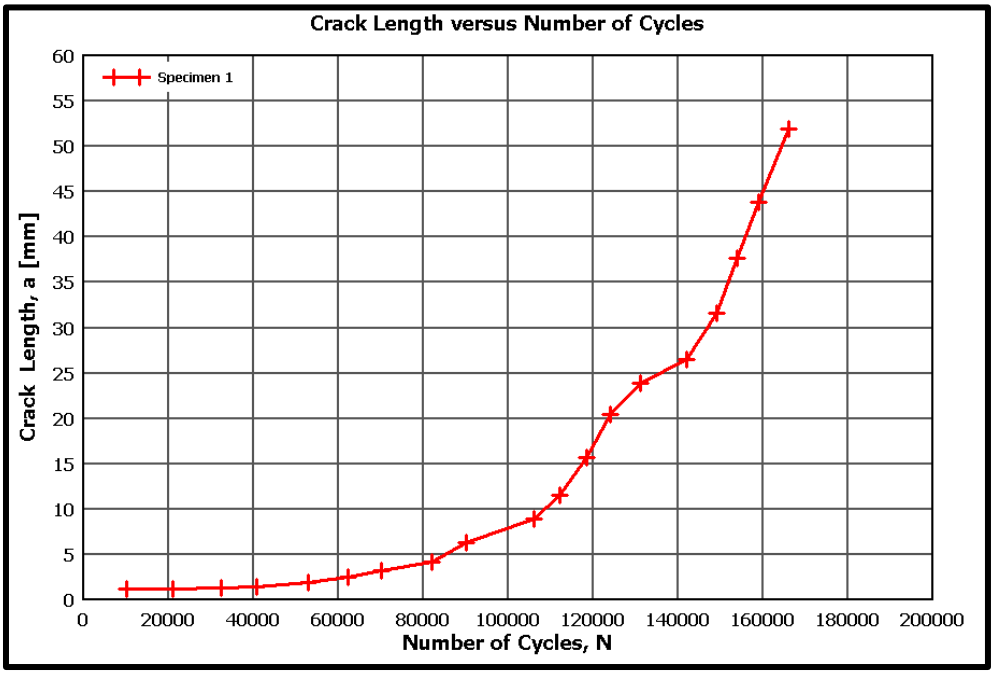

Figure 38. Plot of a versus N for Specimen 1.

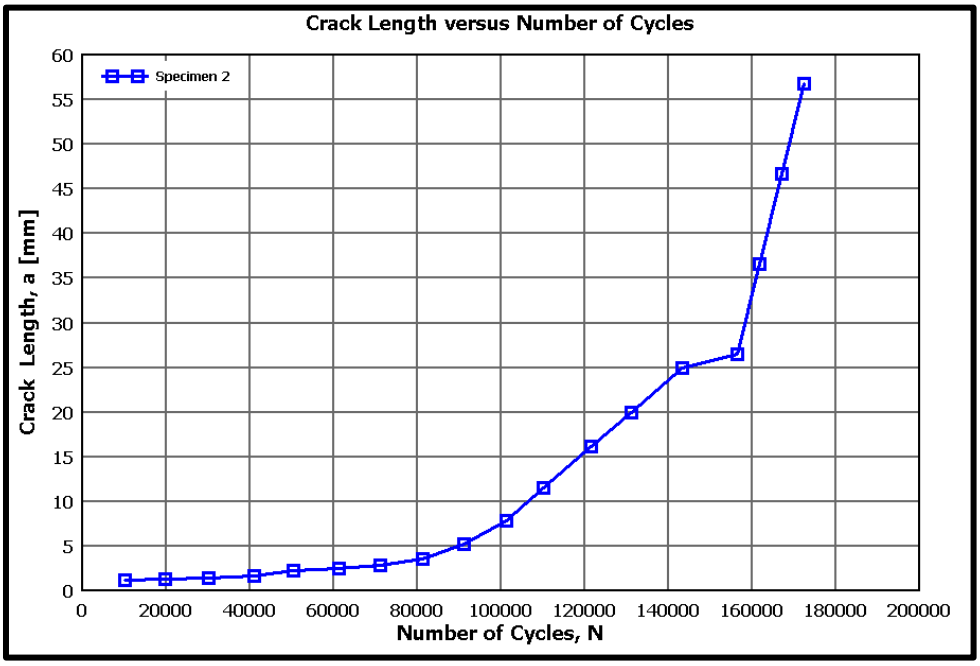

Figure 39. Plot of a versus N for Specimen 2.

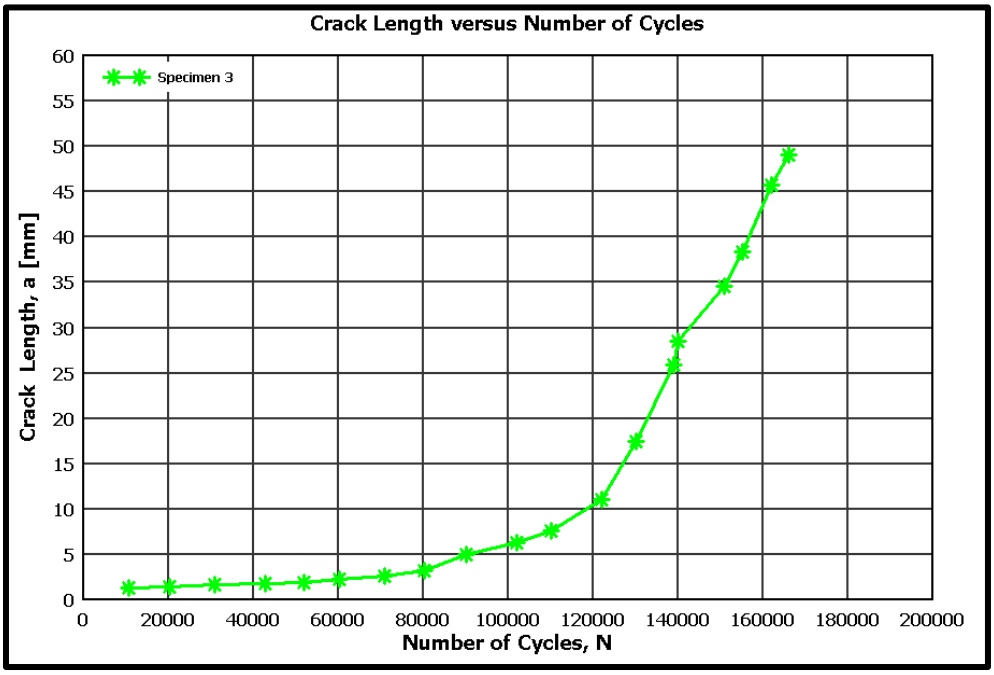

Figure 40. Plot of a versus N for Specimen 3.

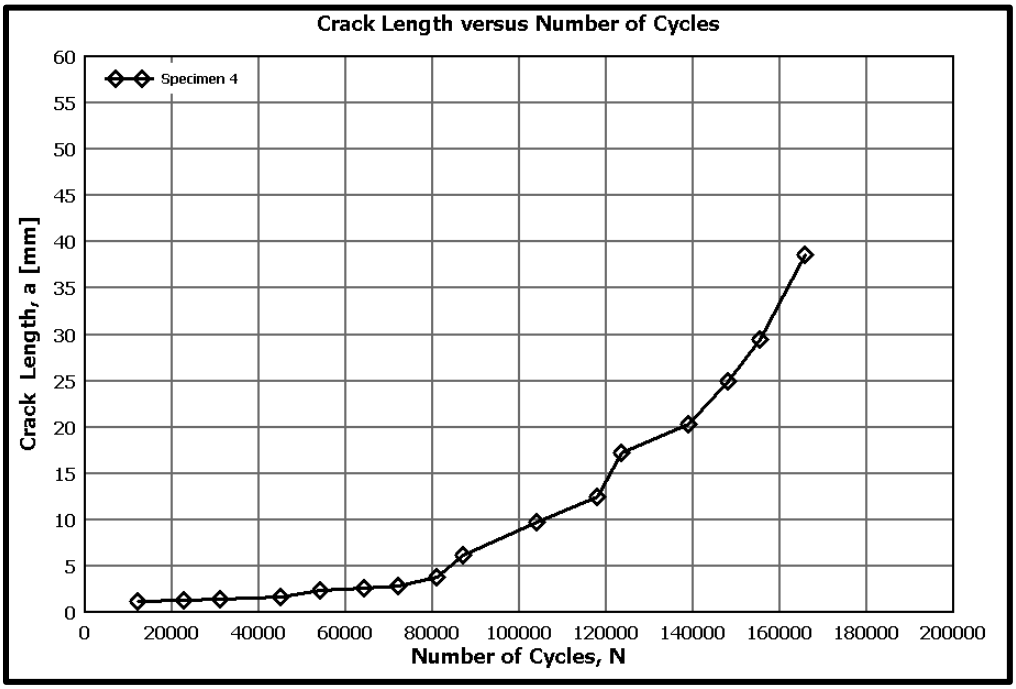

Figure 41. Plot of a versus N for Specimen 4.

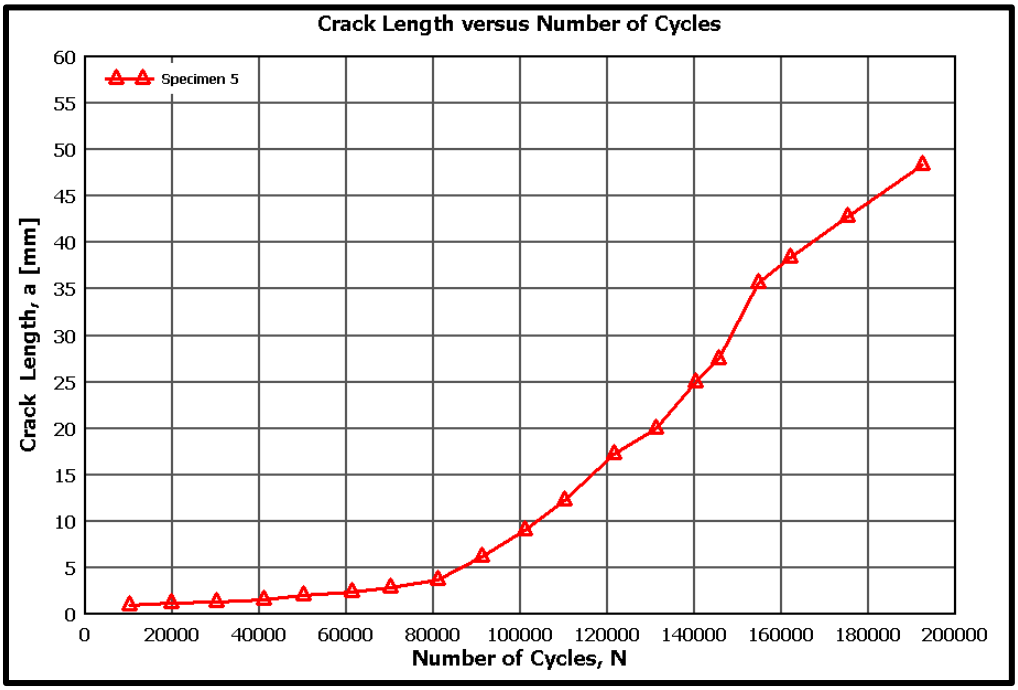

Figure 42. Plot of a versus N for Specimen 5.

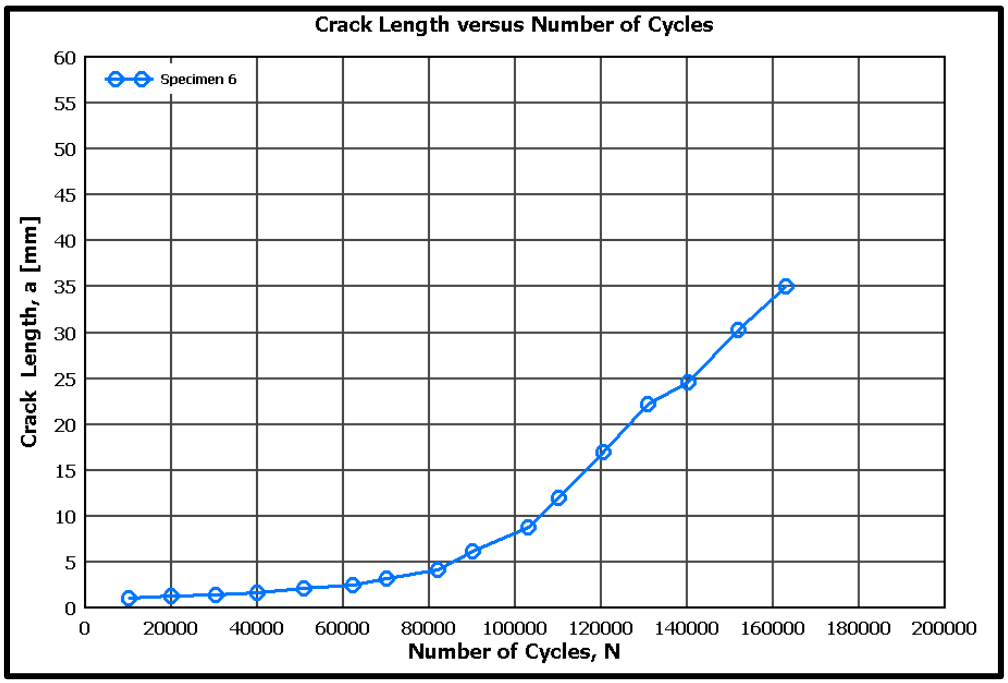

Figure 43. Plot of a versus N for Specimen 6.

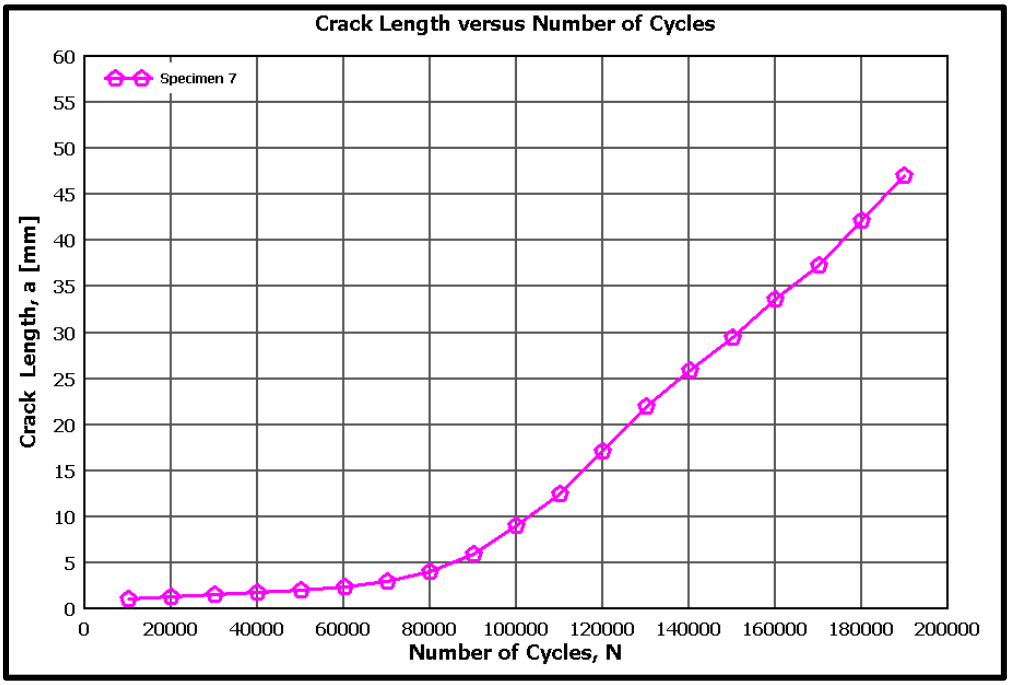

Figure 44. Plot of a versus N for Specimen 7.

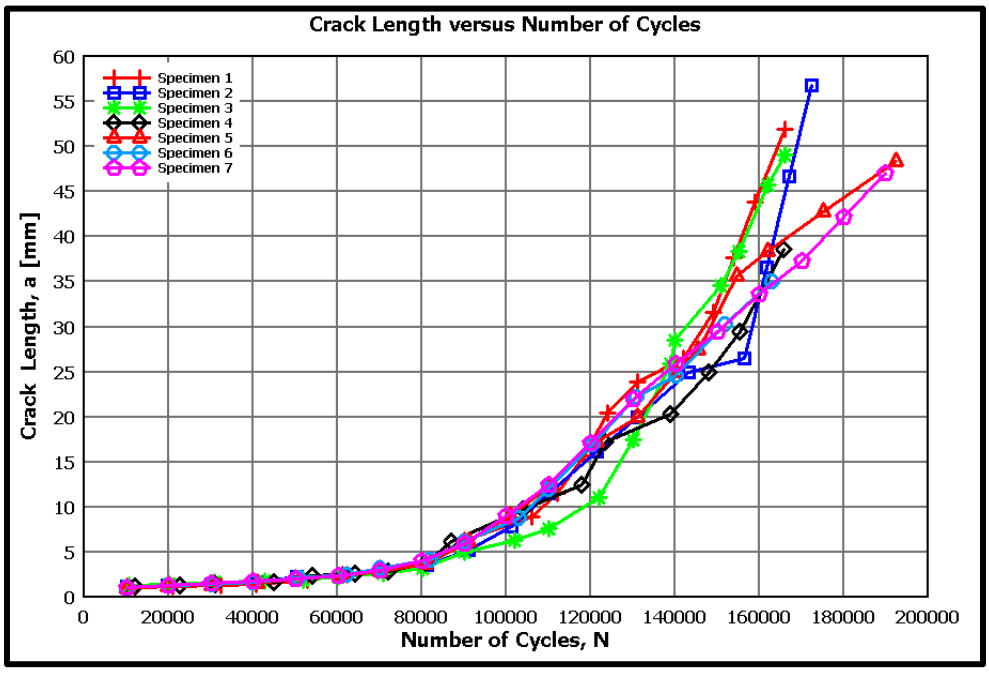

Figure 45. Plot of a versus N for all Specimens.

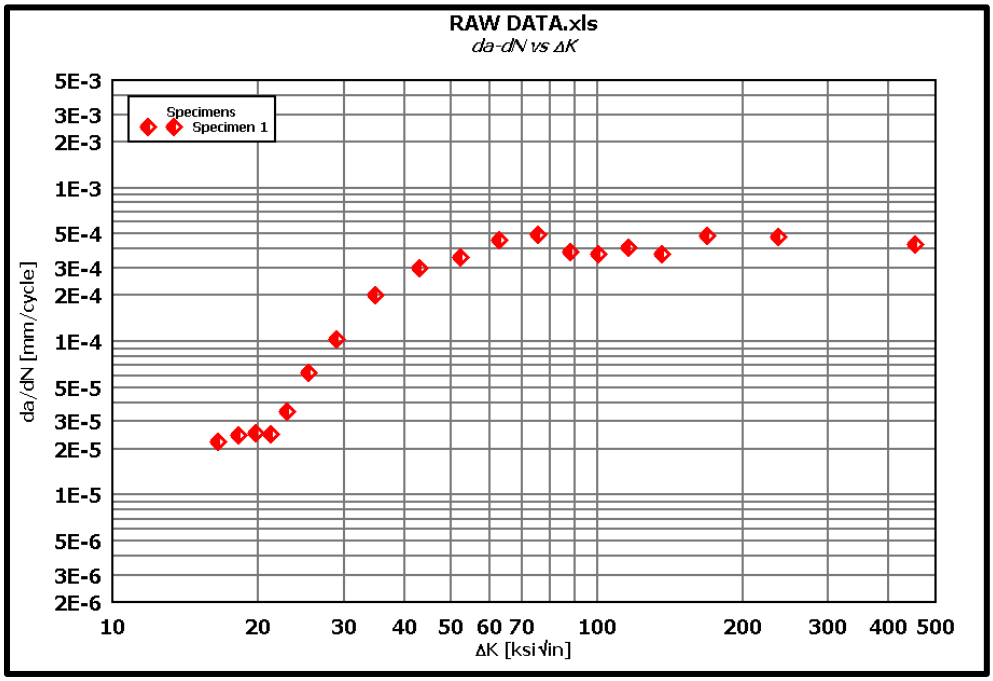

Figure 46. Plot of the calculated da/dN vesus ΔK data Specimen 1.

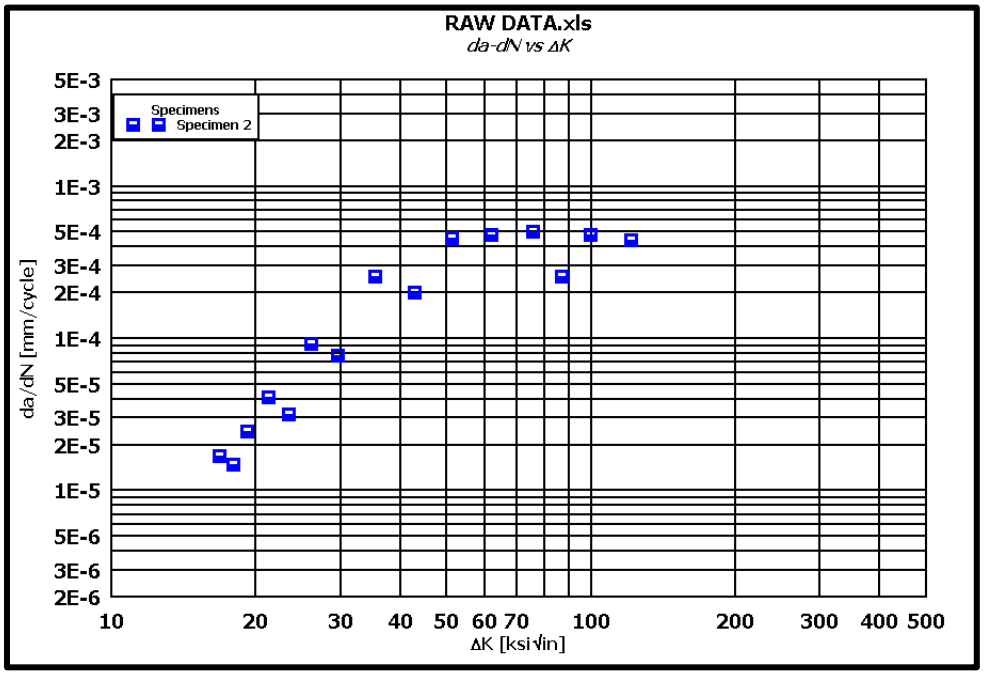

Figure 47. Plot of the calculated da/dN vesus ΔK data Specimen 2.

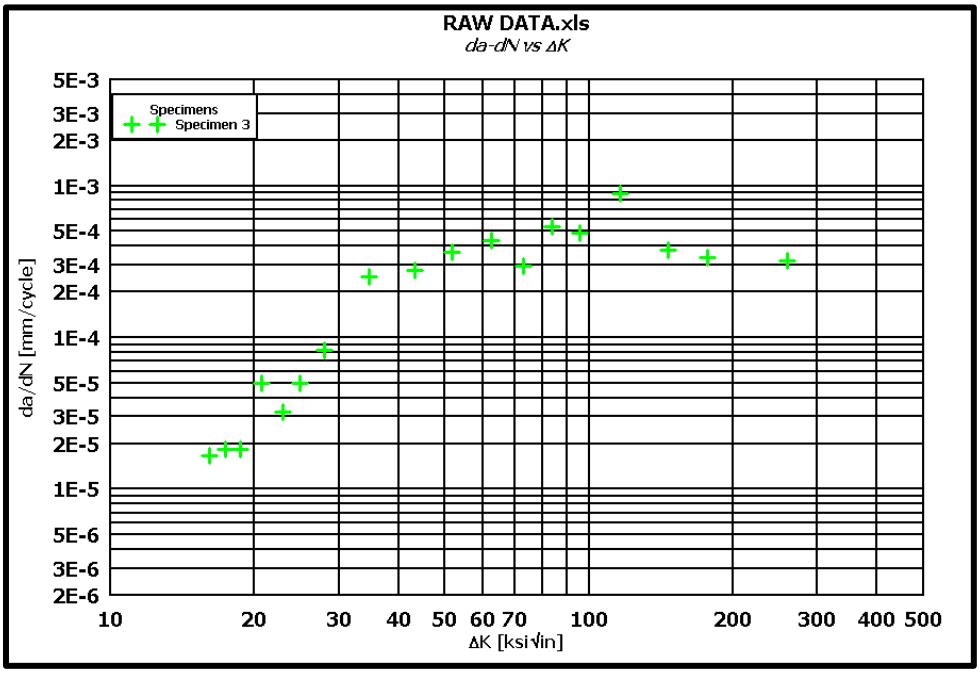

Figure 48. Plot of the calculated da/dN vesus ΔK data Specimen 3.

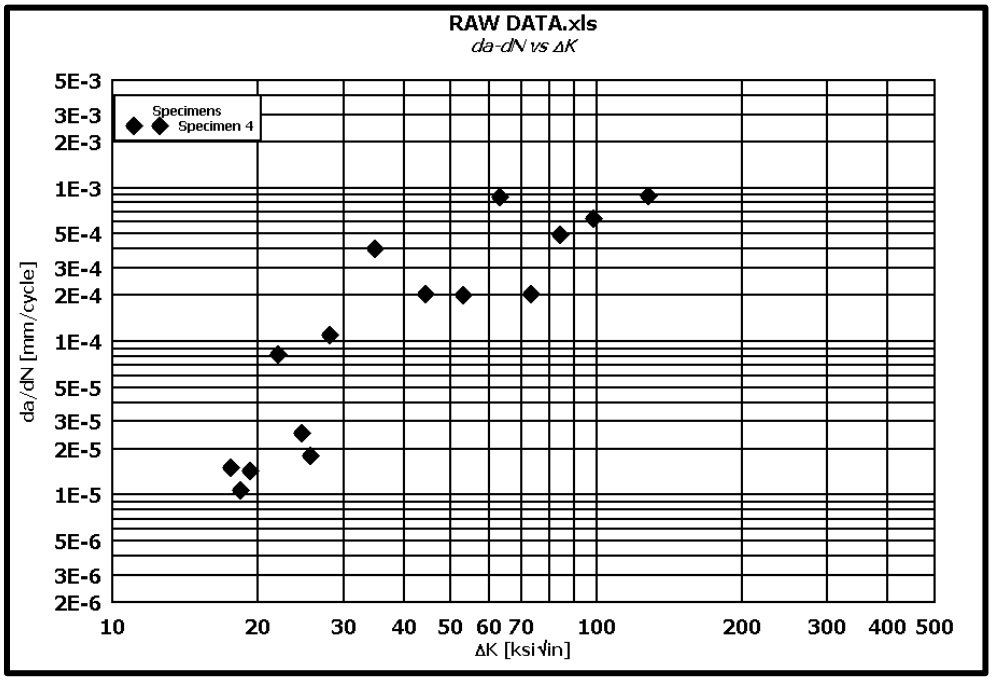

Figure 49. Plot of the calculated da/dN vesus ΔK data Specimen 4.

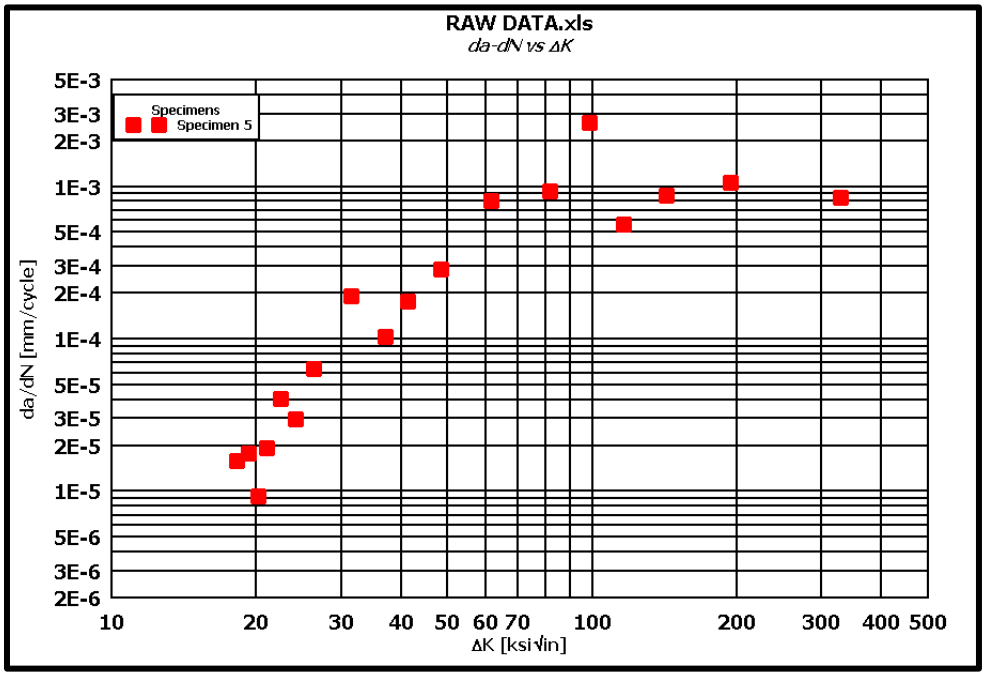

Figure 50. Plot of the calculated da/dN vesus ΔK data Specimen 5.

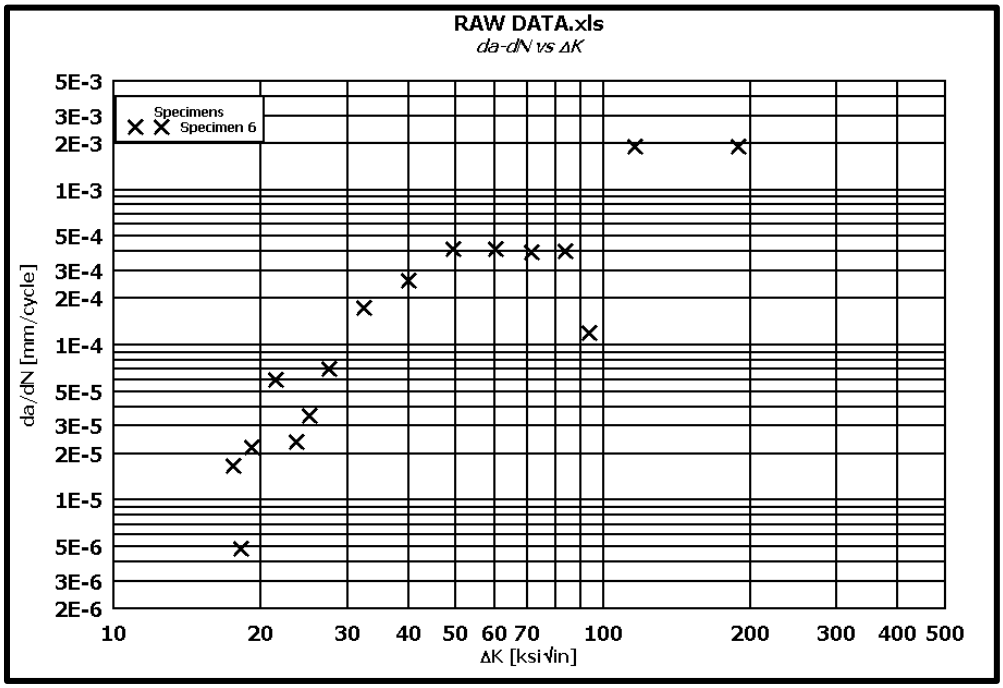

Figure 51. Plot of the calculated da/dN vesus ΔK data Specimen 6.

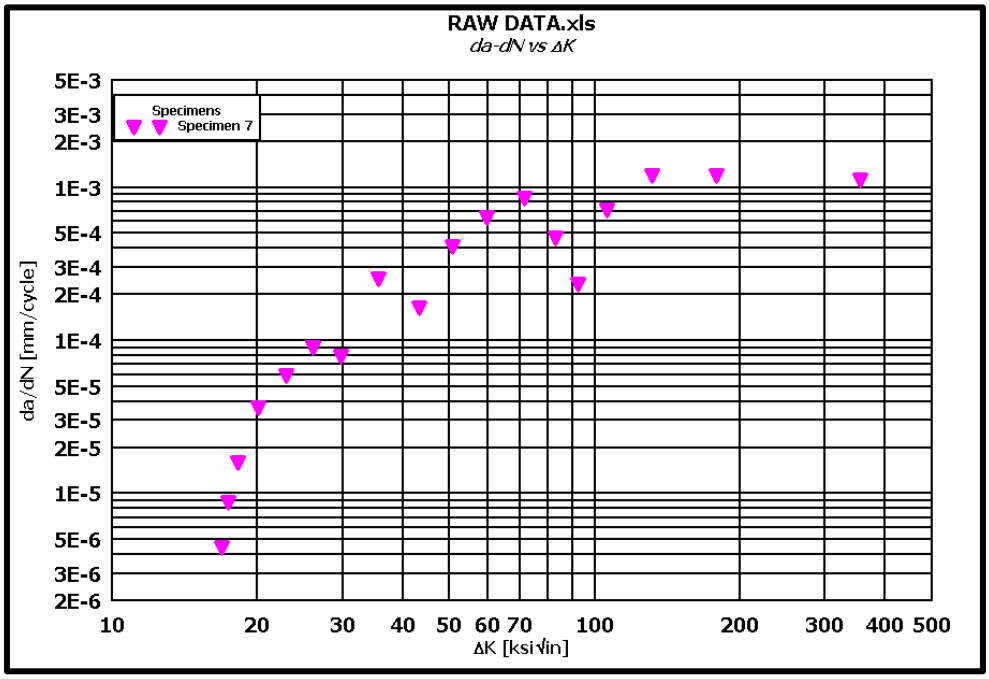

Figure 52. Plot of the calculated da/dN vesus ΔK data Specimen 7.

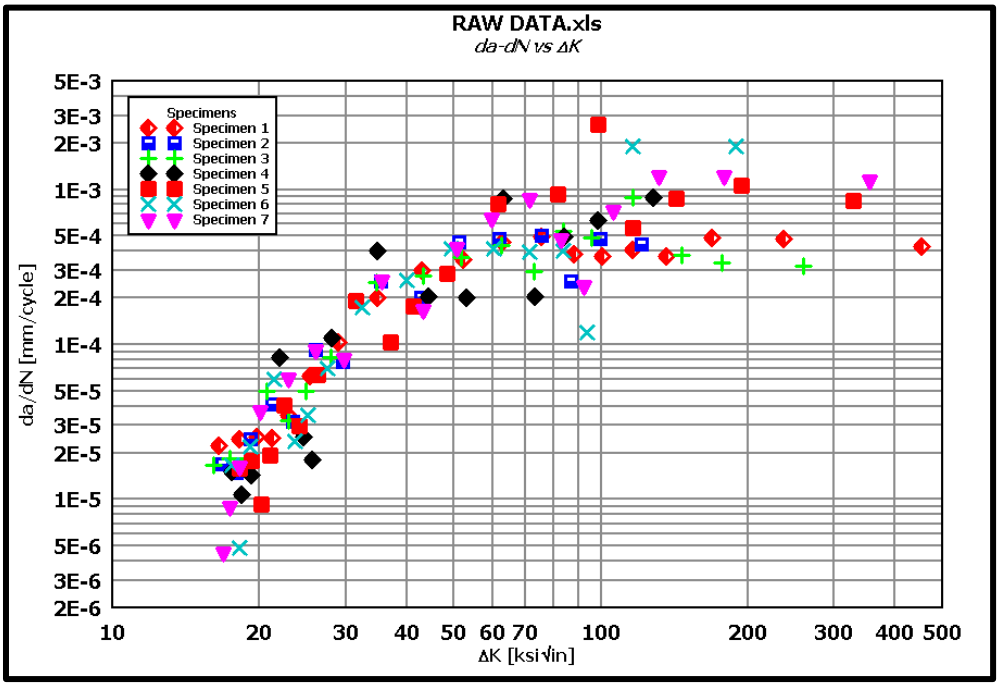

Figure 53. Plot of the calculated da/dN vesus ΔK data All Specimens.

4.2 Finite Element Method

Presented in Figures 54 – 63 are the results for the crack analysis for Location A. Figure 54 presents the von Mises stress plot for the general area of the crack. This figure shows that the von Mises stress in the general area of the crack is approximately 5.0 ksi, well below the yield of the parent material, which is 50 ksi. But at the crack tip and crack front the von Mises stresses are in excess of 90 ksi. Figure 55 presents the detailed crack mesh and major diameter (Crack Length) at Location A. Figure 56 presents the detailed crack profile on the face of the inside radius of the 5-bend box. The contours for the fracture affected zone are also shown in this figure. Figure 57 presents the cross section of the crack mesh at Location A. The minor radius (depth of crack) is shown in the figure. Figure 58 presents a top cross section of the crack mesh at Location A showing the minor radius and fracture affected zone. Figure 59 presents the von Mises stress plot for the cross sectional profile of the crack front. Notice the zero stress at the crack opening. Figure 60 presents the von Mises stress plot for the cross sectional profile of the crack showing the butterfly pattern associated with a crack front. Figure 61 shows the von Mises stress plot for the inside crack tip area, it also has the butterfly pattern of stress. Figure 62 presents the K_I (SIF) plot of the crack front. The highest K_I is located at the inside inner most contour of the crack mesh. Figure 63 shows Specimen 3 at approximately 100,000 cycles with the crack formed at the radius of the 5-bend box. The large heat affected zone in the area of the crack is associated with the weld of the rib to the 5-bend box.

Presented in Figures 64 – 72 are the results for the crack analysis for Location B. Figure 64 presents the von Mises stress plot for the general area of the crack. This figure shows that the von Mises stress in the area of the crack is approximately 5.0 ksi, well below the yield of the parent material which is 50 ksi. Figure 65 presents the detailed crack mesh and major diameter (Crack Length) at Location B. Figure 66 presents the detailed crack profile on the face of the rib.

The contours for the fracture affected zone are also shown in this figure. Figure 67 presents the cross section of the crack mesh at Location B. The minor radius (depth of crack) is shown in the figure. Figure 68 presents a top cross section of the crack mesh at Location B showing the minor radius and fracture affected zone. Figure 69 presents the von Mises stress plot for the cross sectional profile of the crack front. Notice the zero stress at the crack opening. Figure 70 presents the von Mises stress plot for the cross sectional profile of the crack showing the butterfly pattern associated with a crack front. Figure 70 shows the von Mises stress plot for the inside crack tip area, it also has the butterfly pattern of stress. Figure 71 presents the K_I (SIF) plot of the crack front. The highest K_I is located at the inner most contour of the crack mesh. Figure 72 shows Specimen 6 at approximately 125,000 cycles with the crack formed at the weld toe between the 5-bend box and outer face of the rib.

Figures 73 – 75 show the experimental ΔK and finite element K_I results versus the crack length. The crack length calculation for the FEA were selected from the experimental range of values. The major radius for the crack mesh is the crack length and the minor radius is the depth of the crack. The experimental ΔK values were determined by using the data points from the crack length versus the number of cycles (a vs N) data presented in Figures 38 – 45 and the da/dN versus ΔK data points presented in Figures 46 – 53. The load ratio, R, was assumed to be 1, which allows for the assumption that ΔK is equal to K_{max}.

As can be seen in Figure 73 the K_I values calculated by the FEA of the minor radius correlated well with the experimental values although they are about 50% higher as can be seen in Figure 74. Better agreement might be obtained by plotting the distance from the major axis at the crack in Figure 62 to the location of the maximum K_I. Figure 74 for location B shows the K_I values for the minor radius extrapolates well to the experimental ΔK values. Figure 75 shows all the curves for the experimental ΔK's and the FEA K_I values plotted versus the crack length, a.

The plots show that the minor radius direction of crack growth correlates well with both locations.

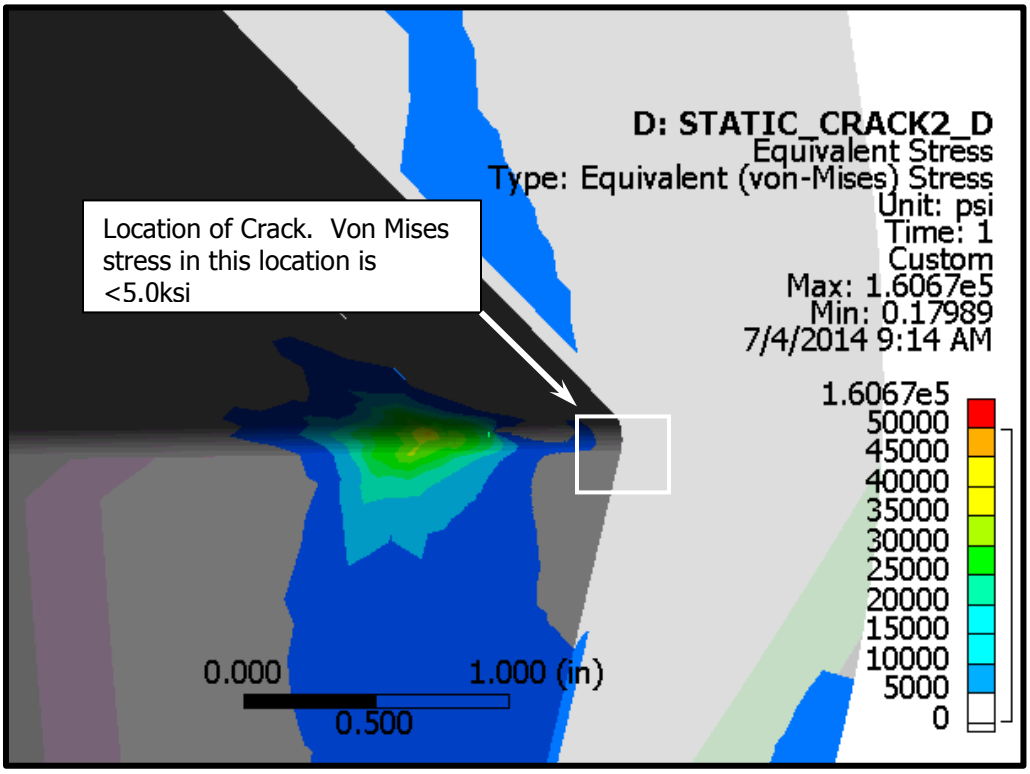

Figure 54. The von Mises stress plot for the general area of the crack at Location A.

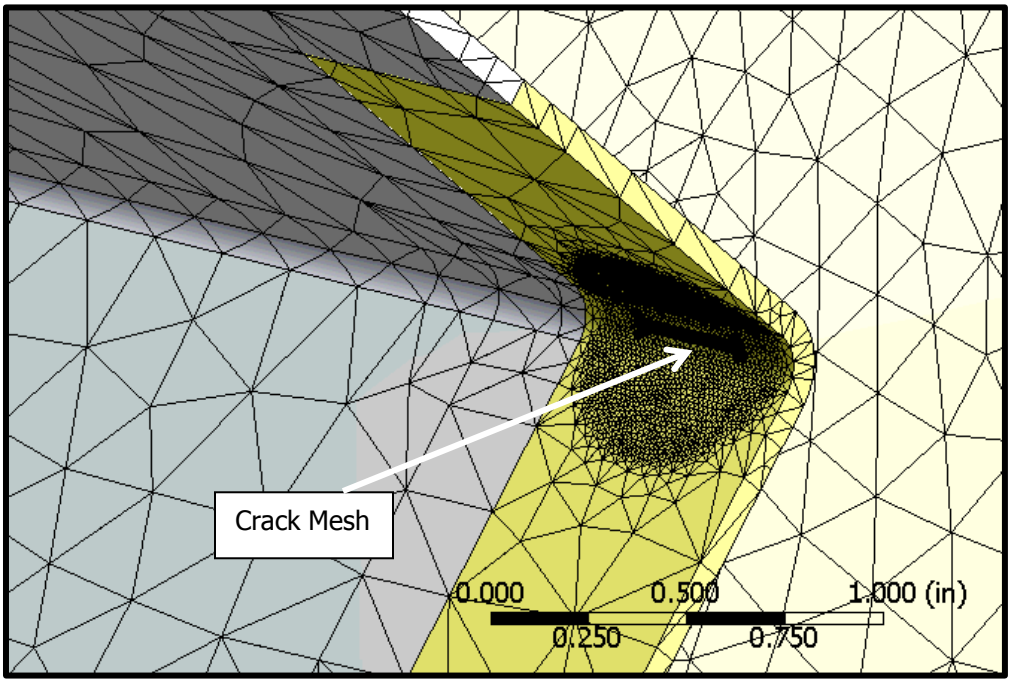

Figure 55. The detailed crack mesh and major diameter (Crack Length) at Location A.

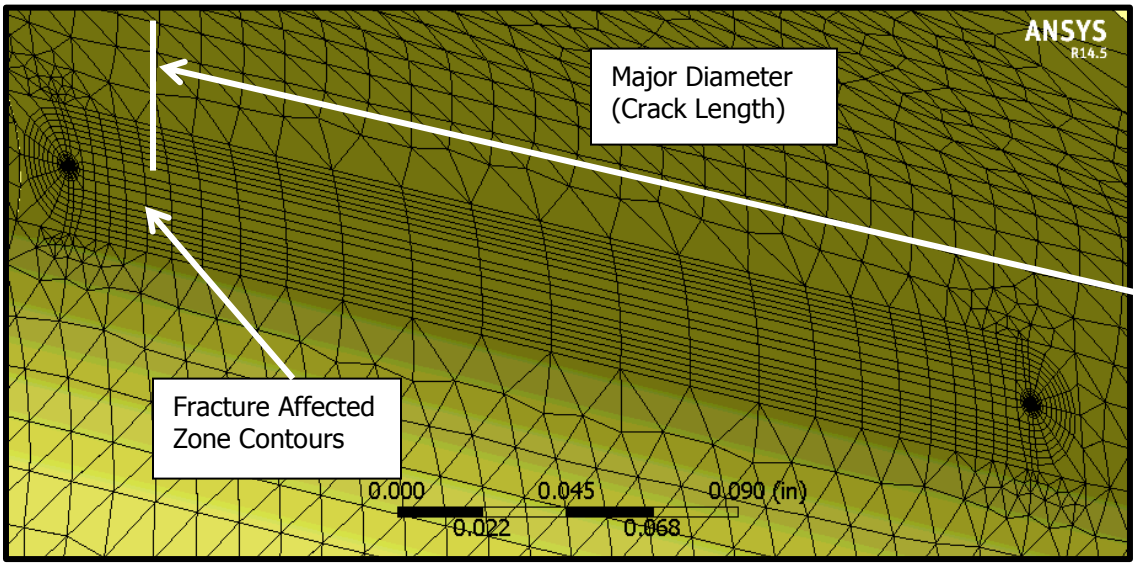

Figure 56. The detailed crack profile on the face of the inside radius of the 5-bend box.

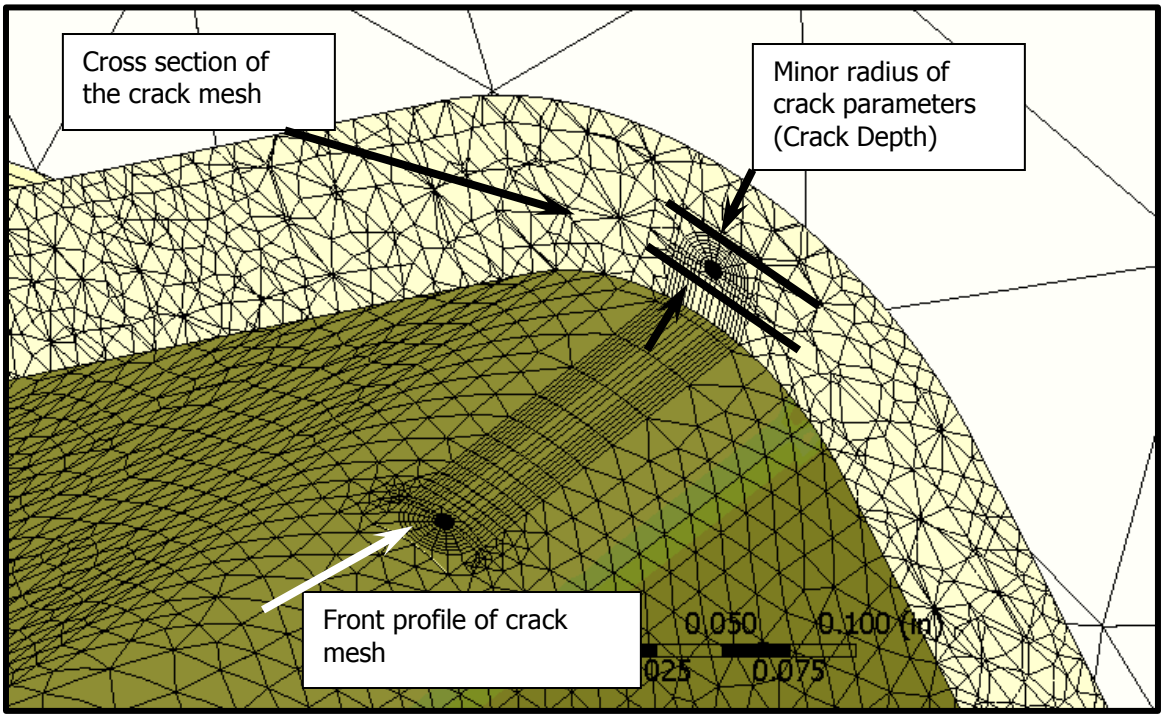

Figure 57. The cross section of the crack mesh at Location A. The minor radius (depth of crack) is shown in the figure.

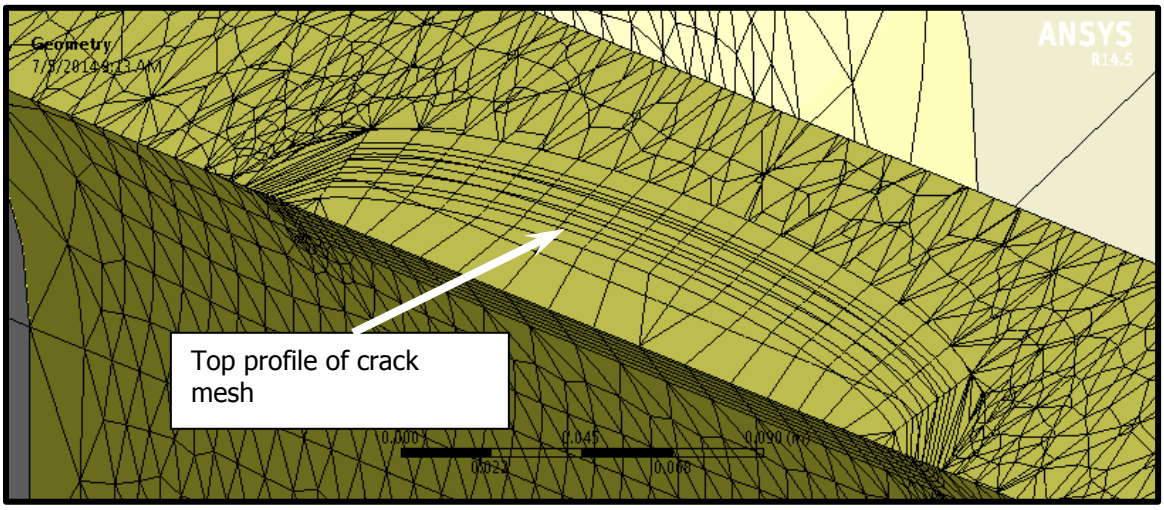

Figure 58. A top cross section of the crack mesh at Location A showing the minor radius and fracture affected zone.

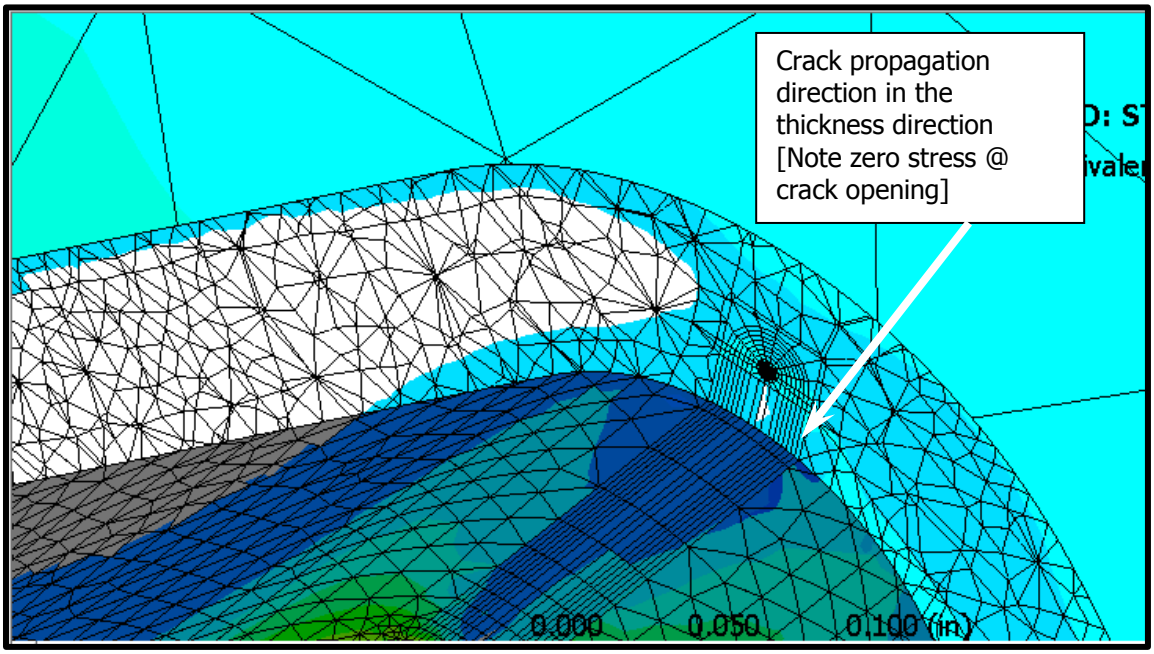

Figure 59. The von Mises stress plot for the cross sectional profile of the crack front.

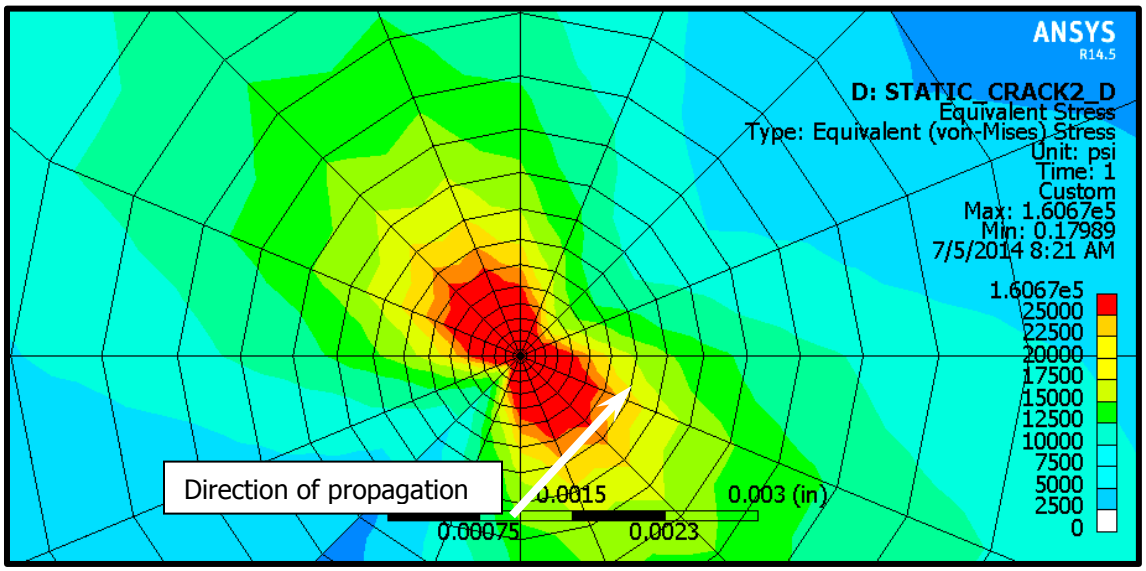

Figure 60. The von Mises stress plot for the cross sectional profile of the crack showing the butterfly pattern associated with a crack front.

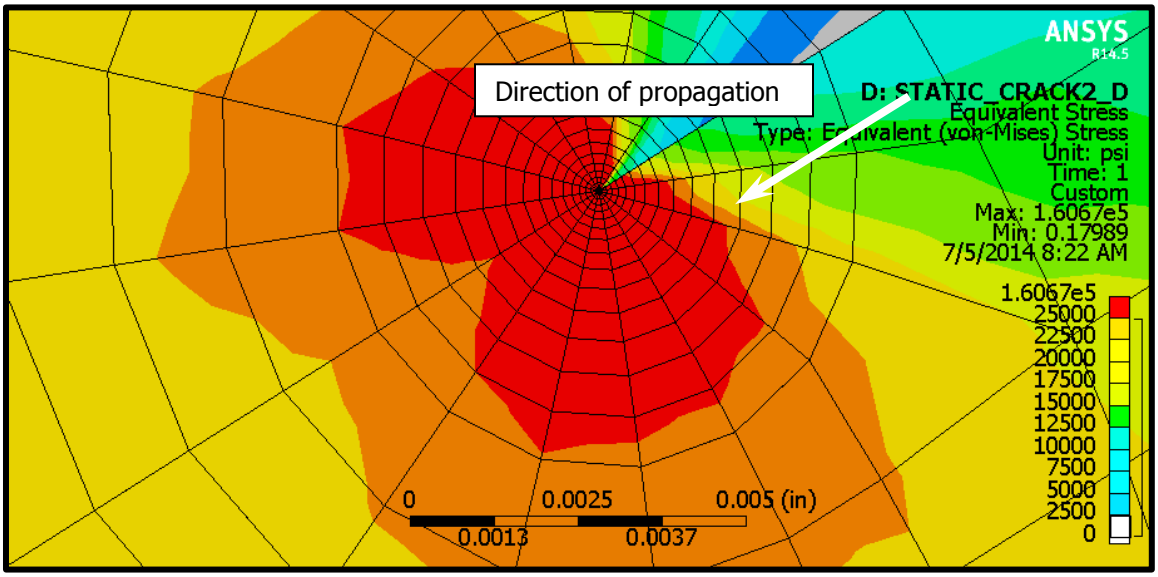

Figure 61. The von Mises stress plot for the inside crack tip area showing the butterfly pattern of stress.

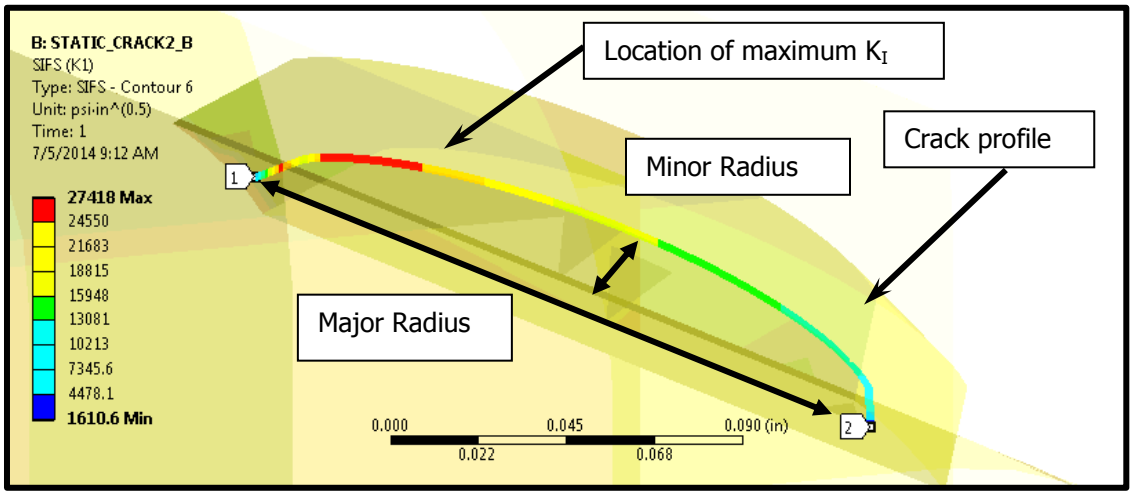

Figure 62. Plot of the K_I for the crack front showing the maximum K_I at the inside edge of the crack front.

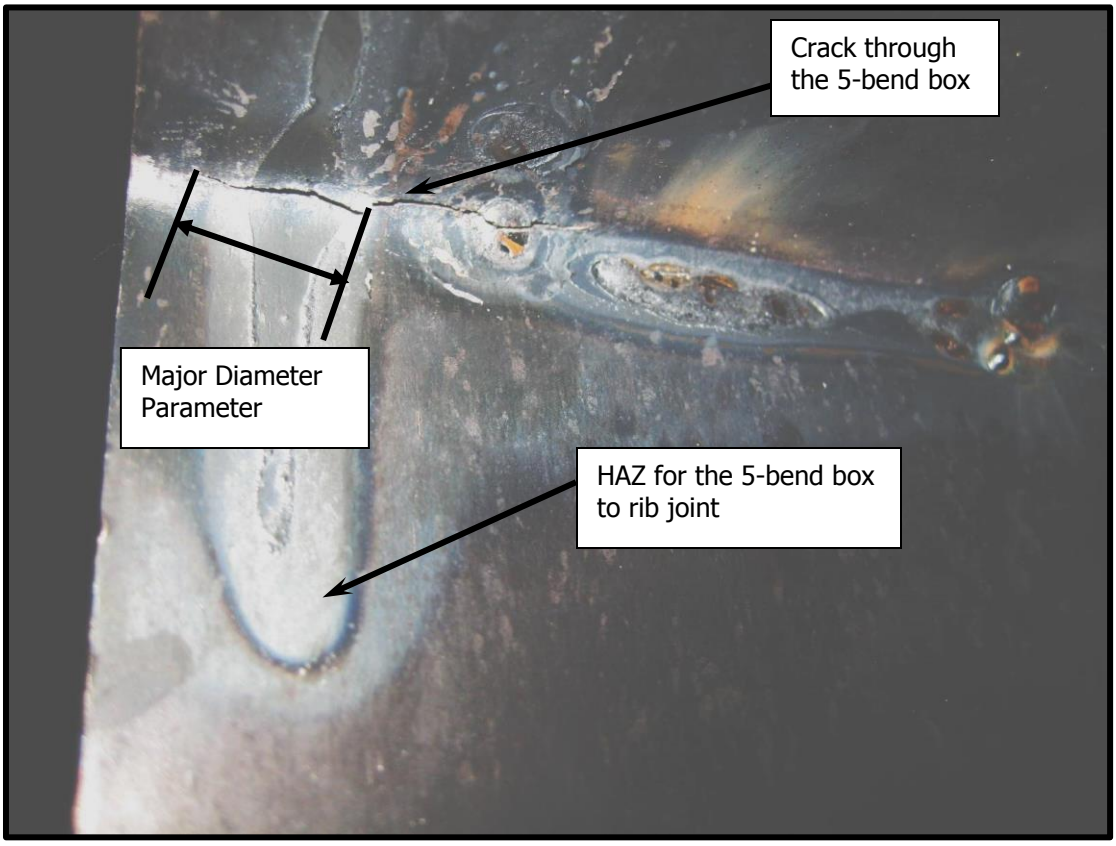

Figure 63. Specimen 3 at approximately 100,000 cycles with the crack formed at the radius of the 5-bend box. Notice the large heat affected zone in the area of the crack.

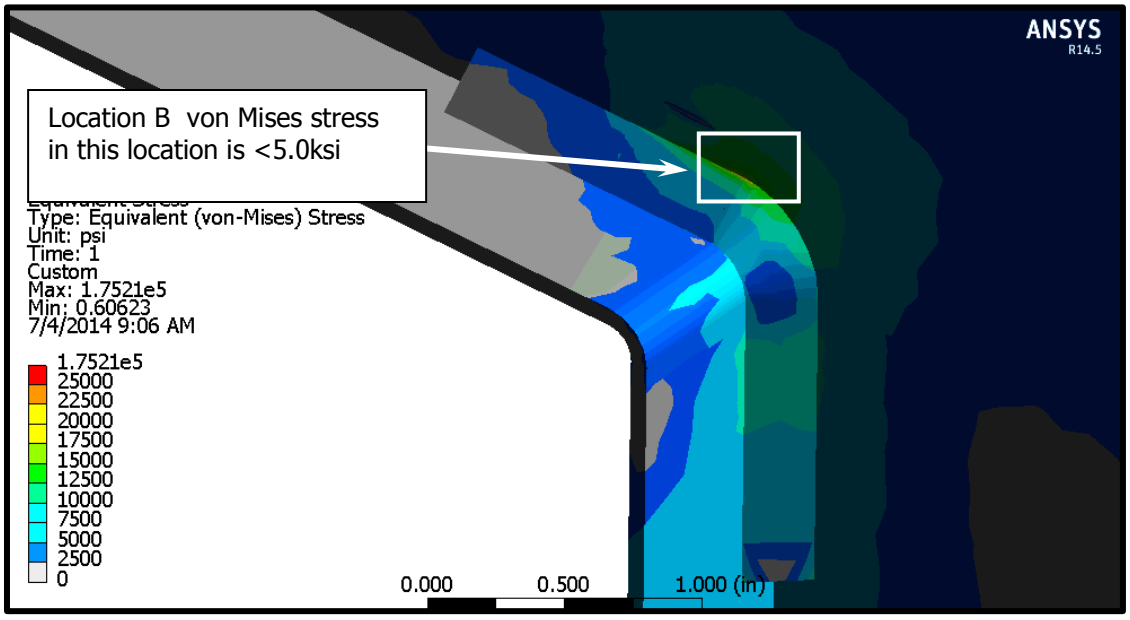

Figure 64. von Mises stress plot of the 0.12" crack length at Location B.

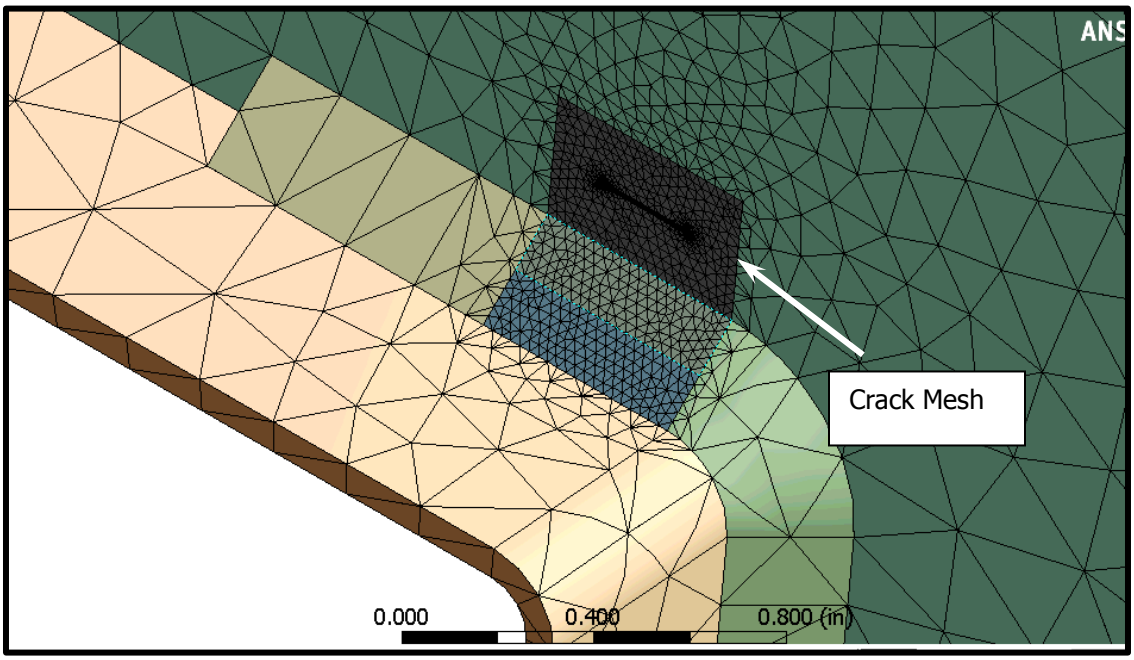

Figure 65. View of the mesh of the crack at the weld toe at Location B.

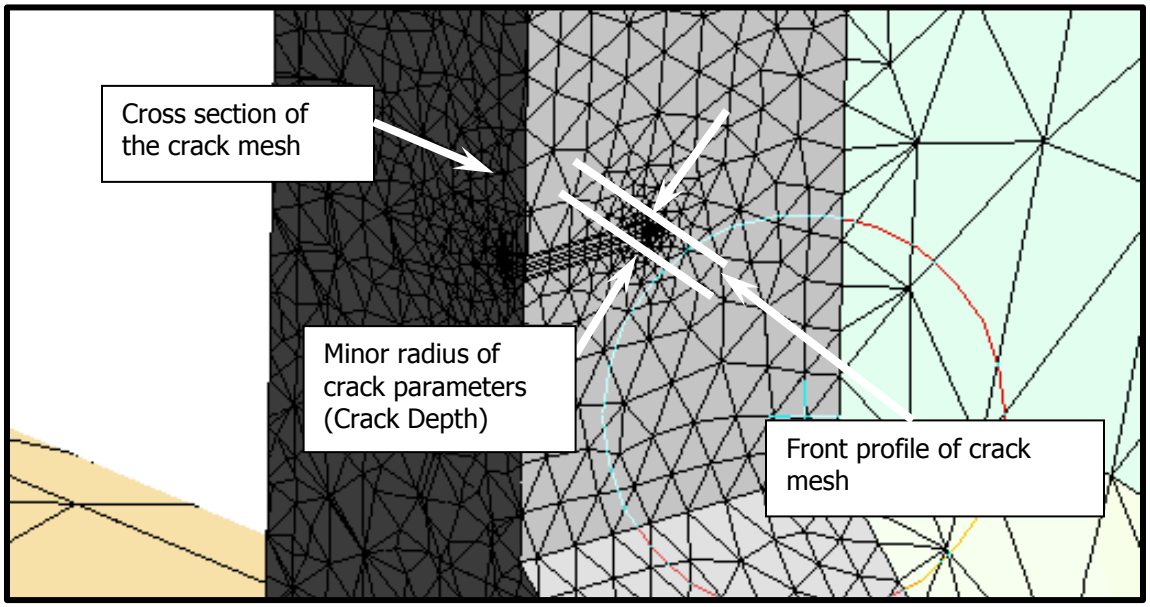

Figure 66. Side section view of the crack mesh at Location B.

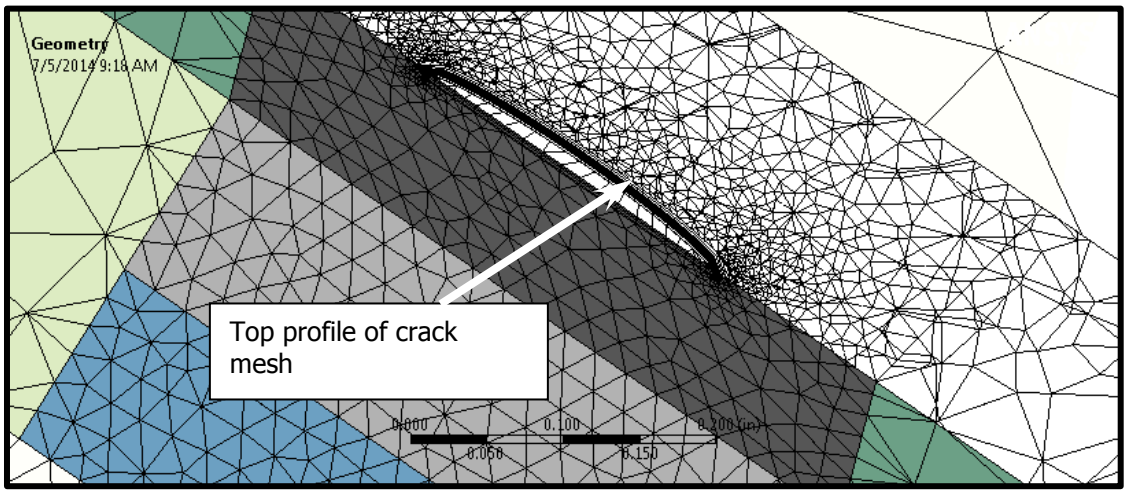

Figure 67. Top section view of the crack mesh at location B.

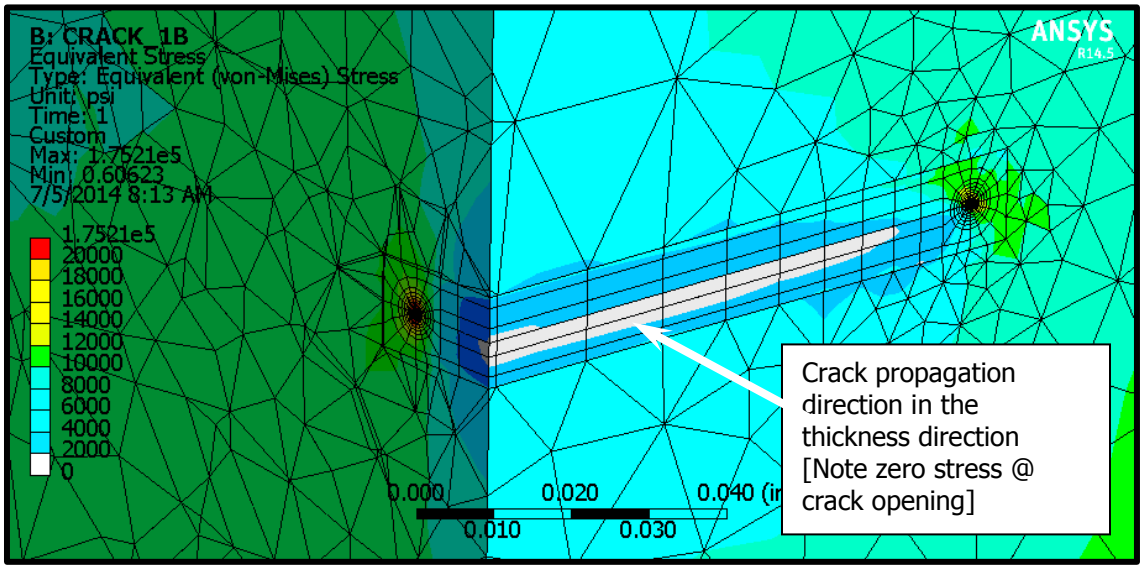

Figure 68. von Mises stress plot of the crack front and crack corner at Location B.

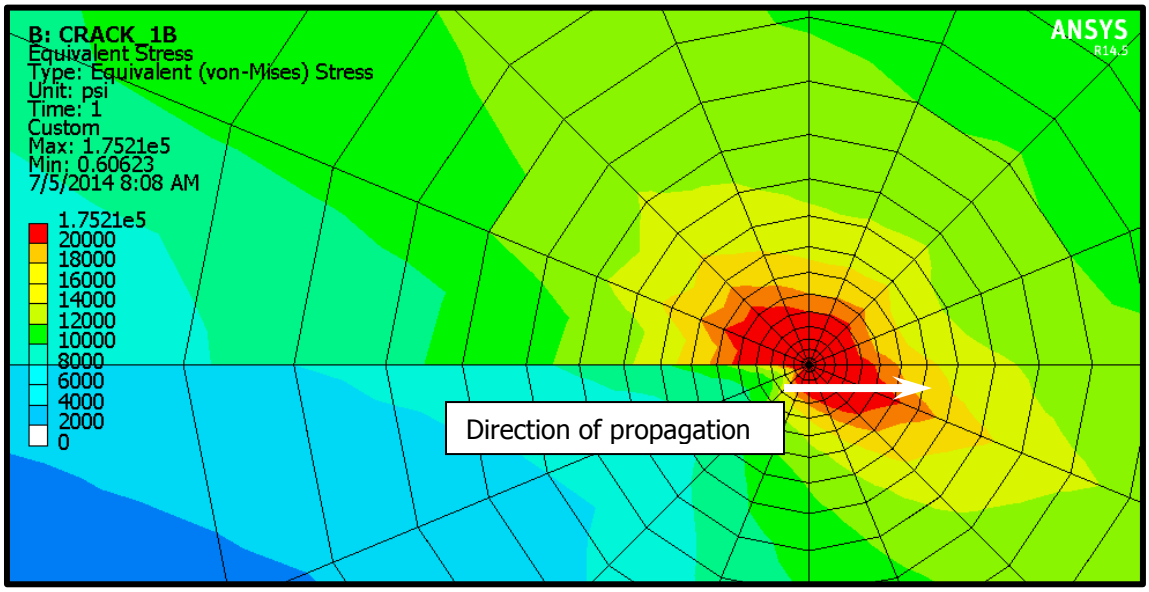

Figure 69. von Mises stress plot of the crack corner at Location B.

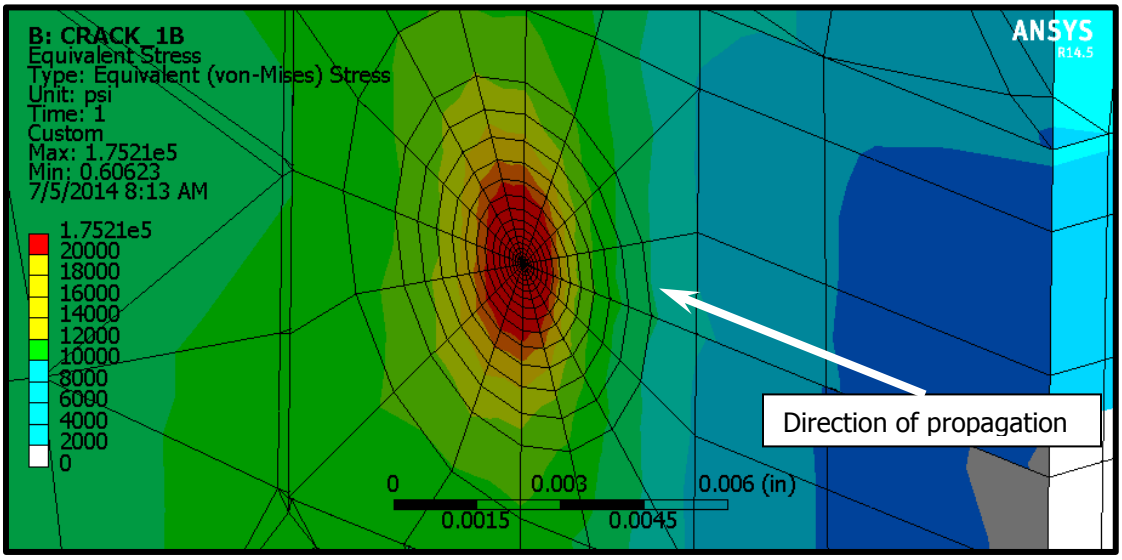

Figure 70. von Mises stress plot of the crack front at Location B.

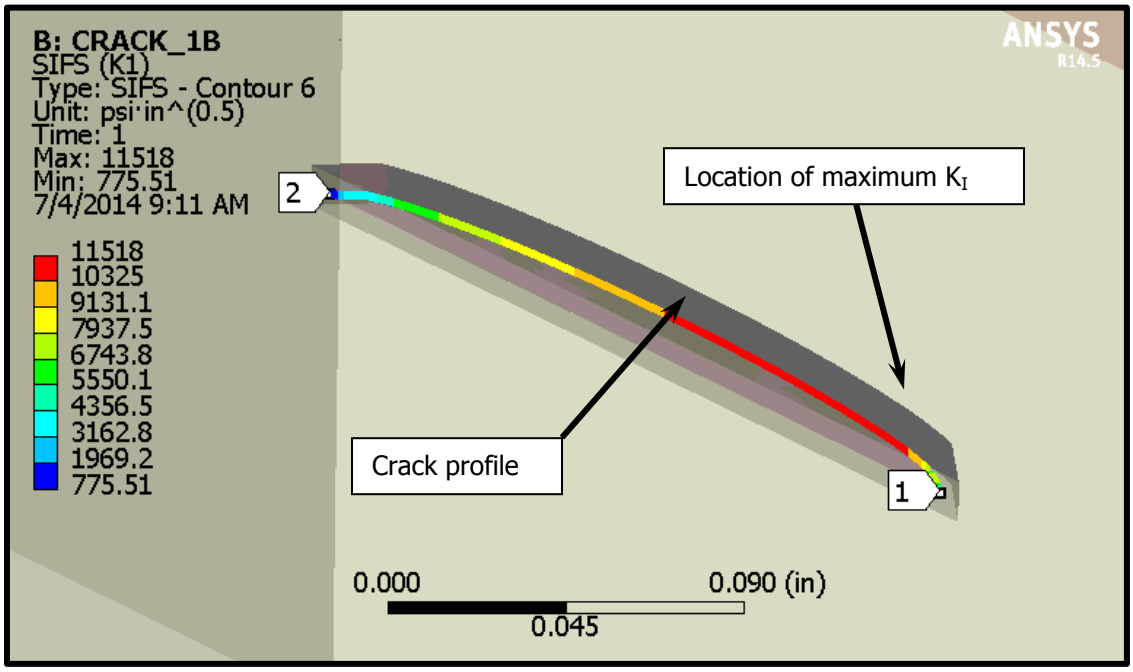

Figure 71. Plot of K_I for the crack length of 0.12" at Location B.

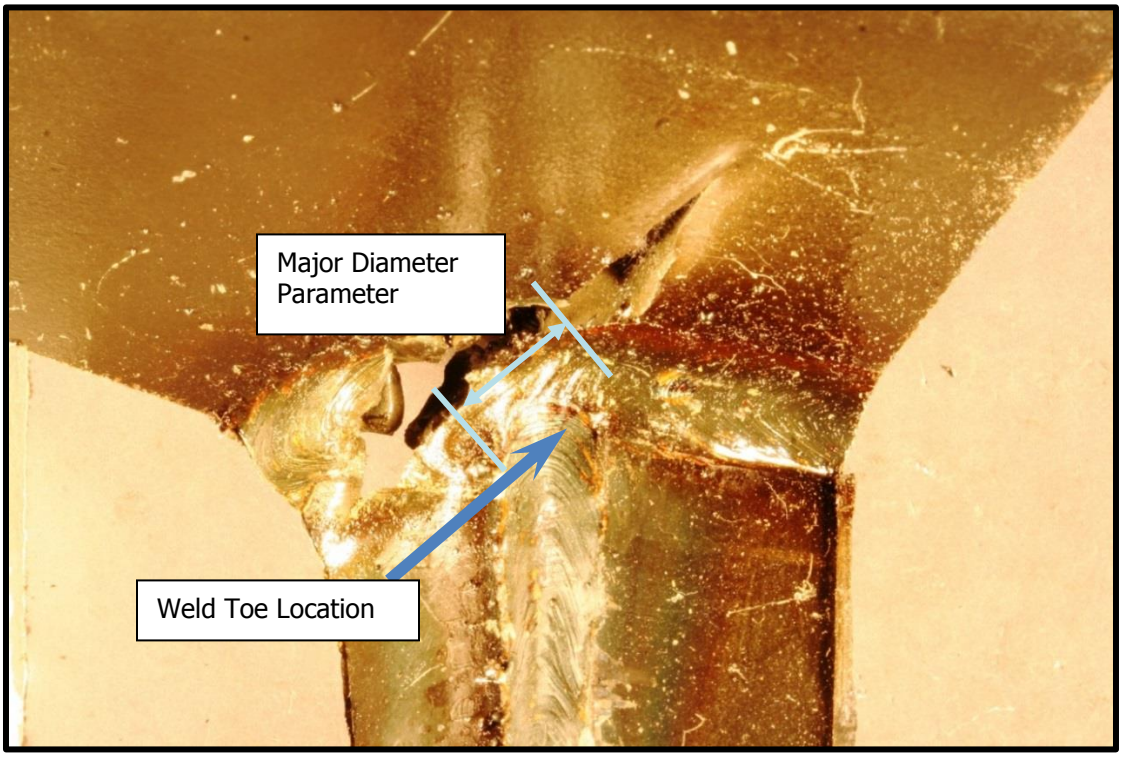

Figure 72. Specimen 6 with the top weld toe crack initiation point at Location B.

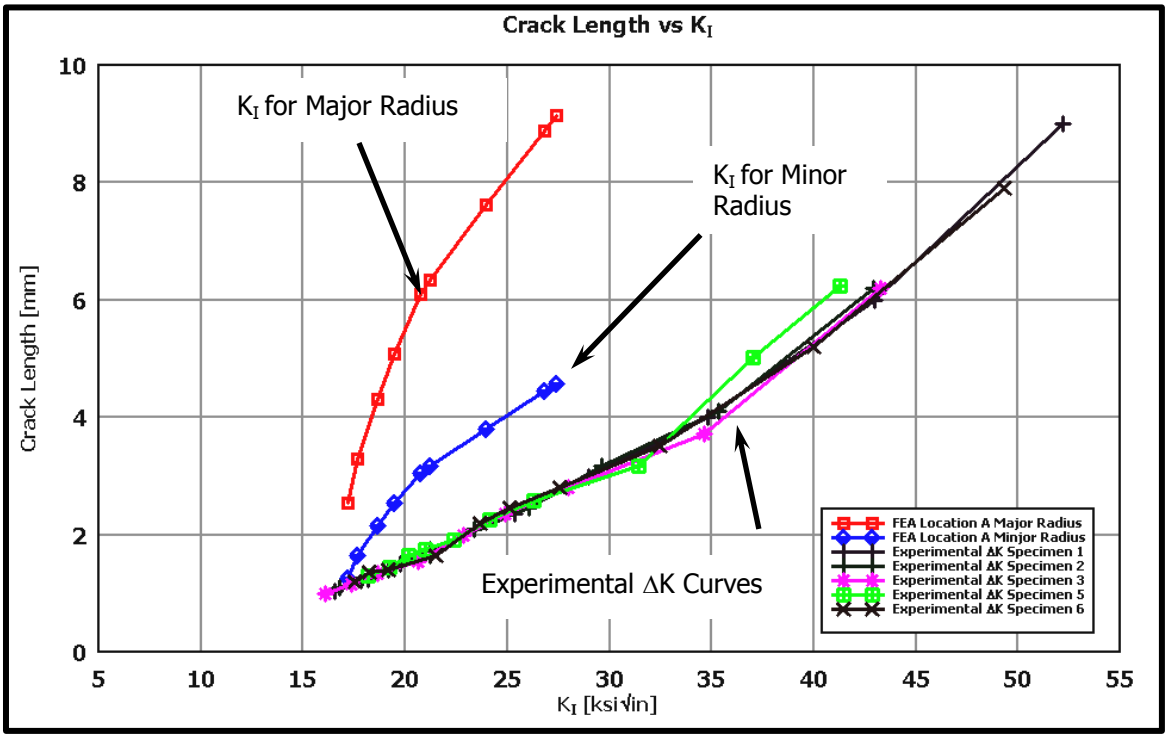

Figure 73. Plots of the crack length (a) versus the experimentally determined ΔK values for the specimens with cracks in Location A and plots of FEA calculated K_I values for both the major and minor crack radii.

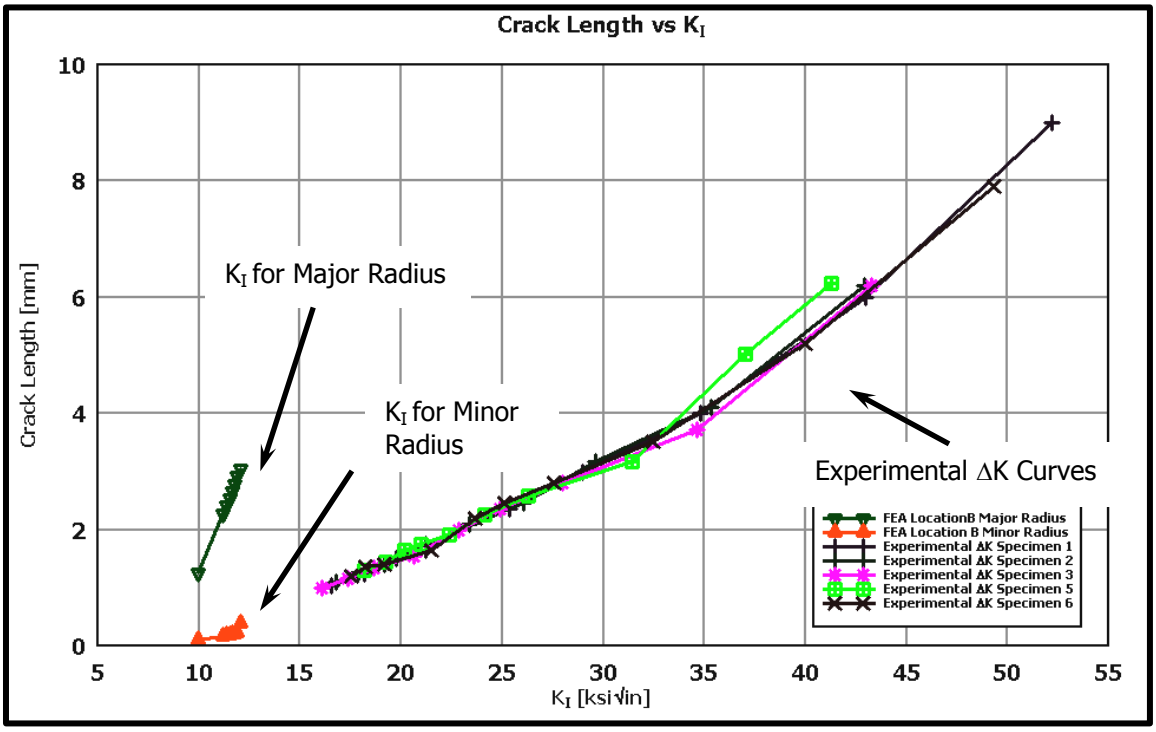

Figure 74. Plots of the crack length (a) versus the experimentally determined ΔK values for the specimens with cracks in Location B and plots of FEA calculated K_I values for both the major and minor crack radii.

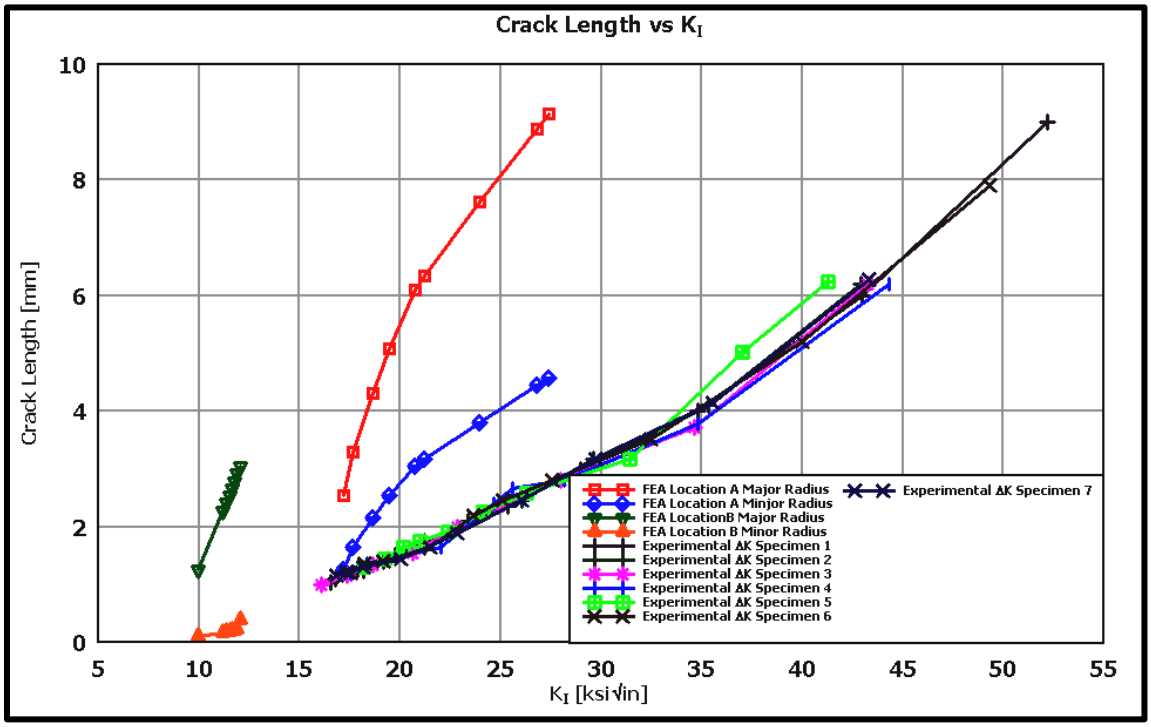

Figure 75. Plots of all curves presented in Figures 73 – 74. Showing that the experimental growth of the cracks is the same regardless of the origin of the crack.

5 DISCUSSION

The crack nucleation locations and resultant propagation were consistent with the field failure incidents as shown in Figures F1 – F4. The crack propagation for both initiation locations were also consistent with the field failure reports.

The crack propagation in the test specimens was very similar as seen in the plots of crack length (a) versus number of cycles (N) in Figures 38 – 45. This indicates that the welding parameters in Table 2 had little effect on fatigue in these specimens. The ΔK values calculated from the experimental data was also consistent between specimens and gives a high confidence level in the results.

The FEA predictions for the K_I values are conservative but that should be expected because the solutions were based on linear elastic behavior. A more accurate solution would involve including nonlinearities in the material properties for the crack region. The experimental plots show that the maximum K_I for the crack range was between 10 ksi$\sqrt{in}$ and 50 ksi$\sqrt{in}$ for the crack growth phase of the process.

The simulation model could be refined by studying the properties of the heat affected zone. The amount of variation can be attributed to the welding process used to manufacture the joint. The material selection and process becomes critical when there is no preheat or post process stress relief performed on the structure. Although this study found no direct correlation to post process stress relief, it is strongly believed that if tighter controls on manufacturing where held, post process stress relief would be of a benefit.

The K_I values for the minor axis correlate well with the experimental values as shown in Figures 73 – 74. The K_I values for the major axis do not correlate as well as the minor axis values. This may be attributed to crack growing in the direction of the minor axis.

6 CONCLUSIONS

The experimental fatigue test resulted in fractures which simulated actual field failures. The experimental results were very consistent for all seven specimens from which it can be conclude that the location of crack initiation had little effect on the final crack growth path. The wire speed, voltage, gas mixture, and stress relief did not show any significant changes in the overall crack growth process. This leads to the conclusion that the presence of a crack created during the welding process was far more detrimental to fatigue life than the variations in the welding process.

The FEA results confirm that the crack growth path does progress to the rib, and that there is significant energy to propagate a crack. The results could be refined and more accurate if nonlinear material parameters and meshing techniques, such as life-death of elements were used.

REFERENCES

[1] Dowling, Norman E., *Mechanical Behavior of Materials*, Prentice Hall, New Jersey, 1999, pp. 357-379.

[2] Lassen, Tom, Fatigue Life analysis of Welded Structures, ISTE Ltd, United States and Great Britain, 2006, pp. 15-30.

[3] ANSYS, 2012, ANSYS Mechanical User Guide, Canonsburg.

[4] Rolyance, David, (2001) Fatigue, Department of Materials Science and Engineering, Massachusetts Institute of Technology, Cambridge, Maine, USA.

[5] Brockenbrough, R. L. and Johnston, B. G., Steel Design Manual, United States Steel Corporation, ADUSS 27-3400-04, January 1981.

[6] T.Nakazawa, S.Suzuki, T.Sunami and Y.Sogo, Application of High-Purity Ferritic Stainless Steel Plates to Welded Structures, ASTM STP, 706 (1980), 99.Hold

[7] Ekberg, Anders, Low Cycle Fatigue, Solid Mechanics, Chalmers, Göteborg, Sweden, 2013.

[8] Wardenier, (2009), Introduction to Fatigue, University of Oslo, Norway.

APPENDICES

Appendix A. Experimental Crack Growth Photos

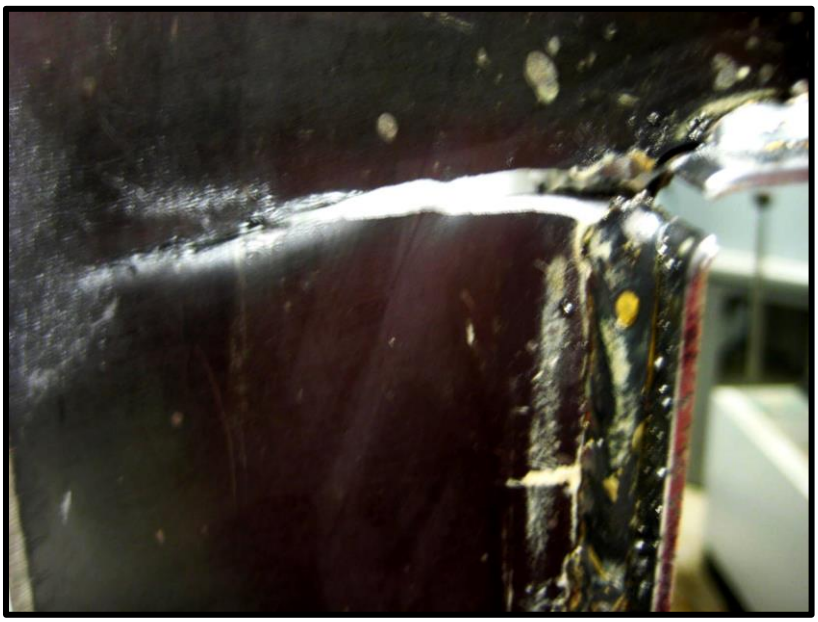

Figure A1. Photo of the final crack length of a test specimen.

Figure A2. Photo of the end of test for Specimen 1.

Figure A3. Photo of the end of test for Specimen 2.

Figure A4. Photo of the crack sectioned at the end of test of Specimen 1.

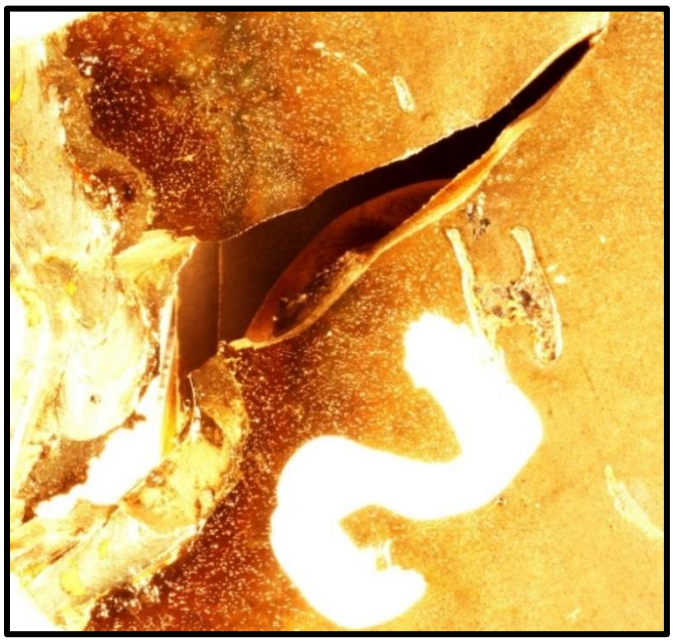

Figure A5. Photo of the crack sectioned at the end of test of Specimen 2.

Figure A6. Photo of the crack sectioned at the end of test of Specimen 3.

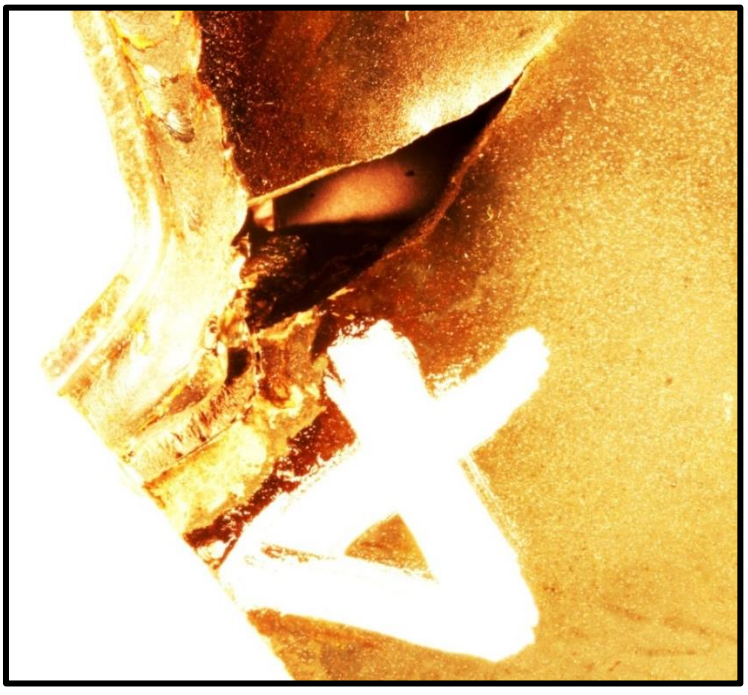

Figure A7. Photo of the crack sectioned at the end of test of Specimen 4.

Figure A8. Photo of the crack sectioned at the end of test of Specimen 5.

Figure A9. Photo of the crack sectioned at the end of test of Specimen 6.

Appendix B. Weld Joint Geometry and Data

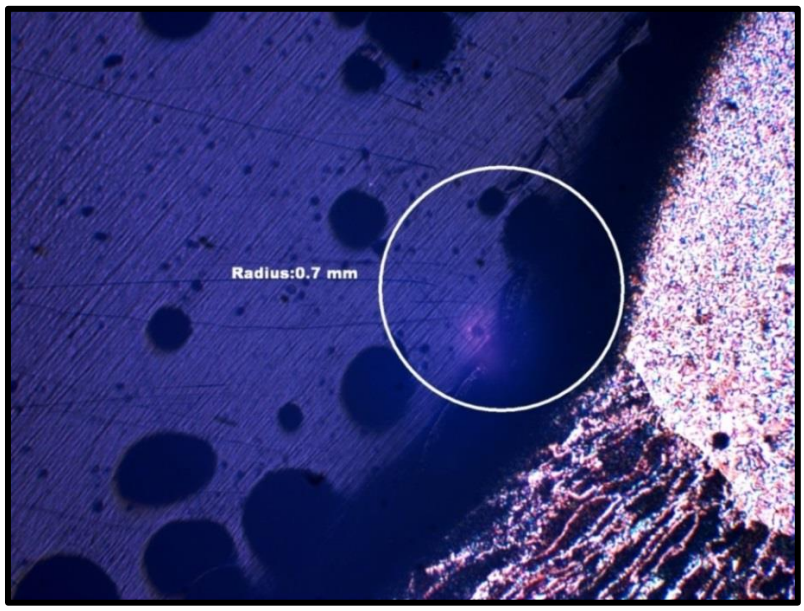

Figure B1. Weld toe measurement of a test specimen.

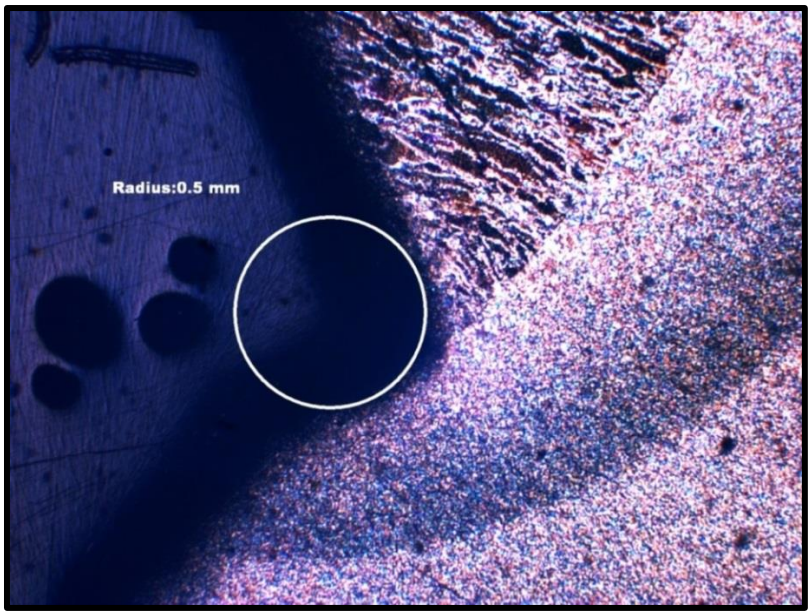

Figure B2. Weld toe measurement of a test specimen.

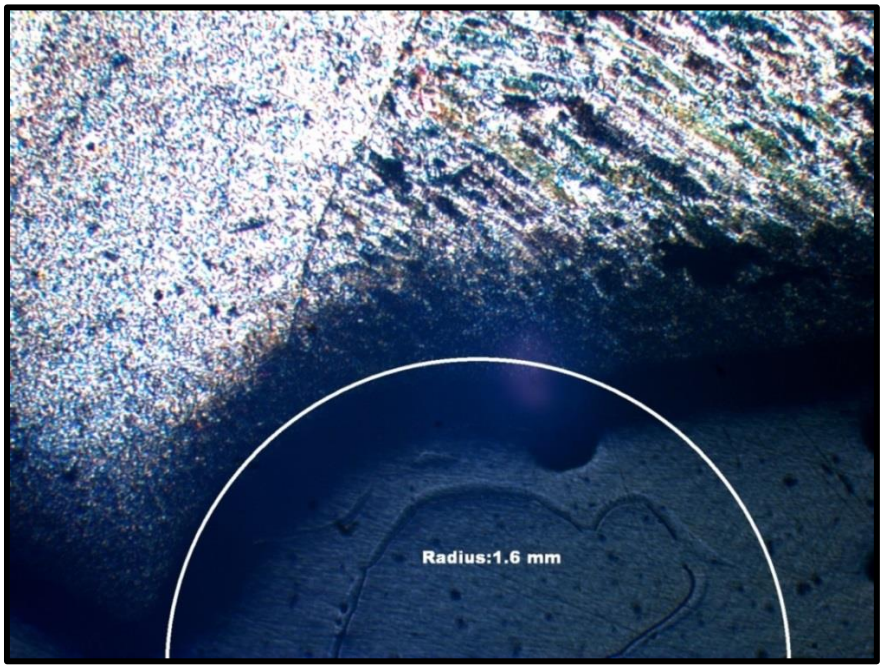

Figure B3. Weld toe measurement of a test specimen.

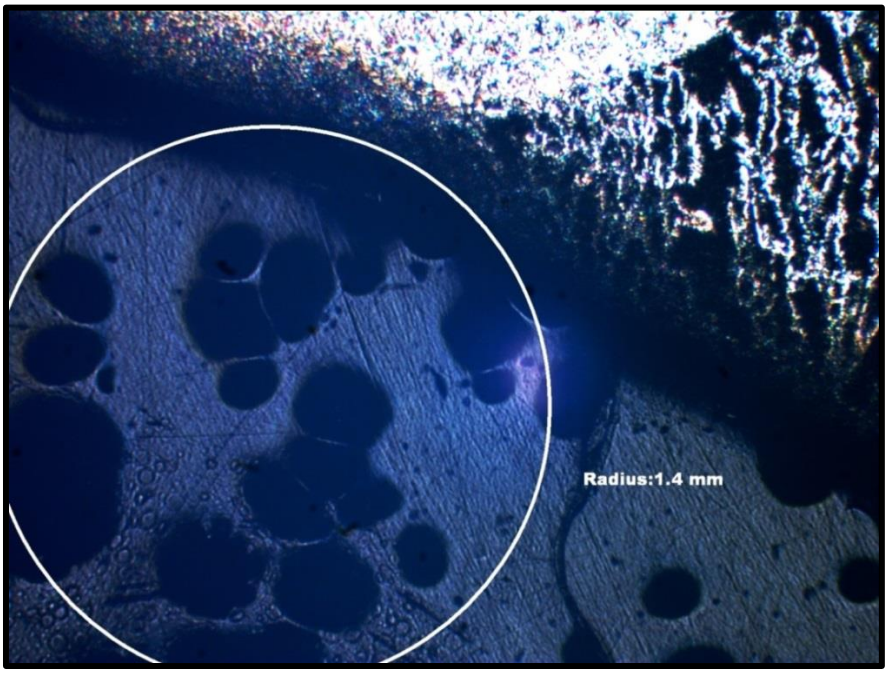

Figure B4. Weld toe measurement of a test specimen.

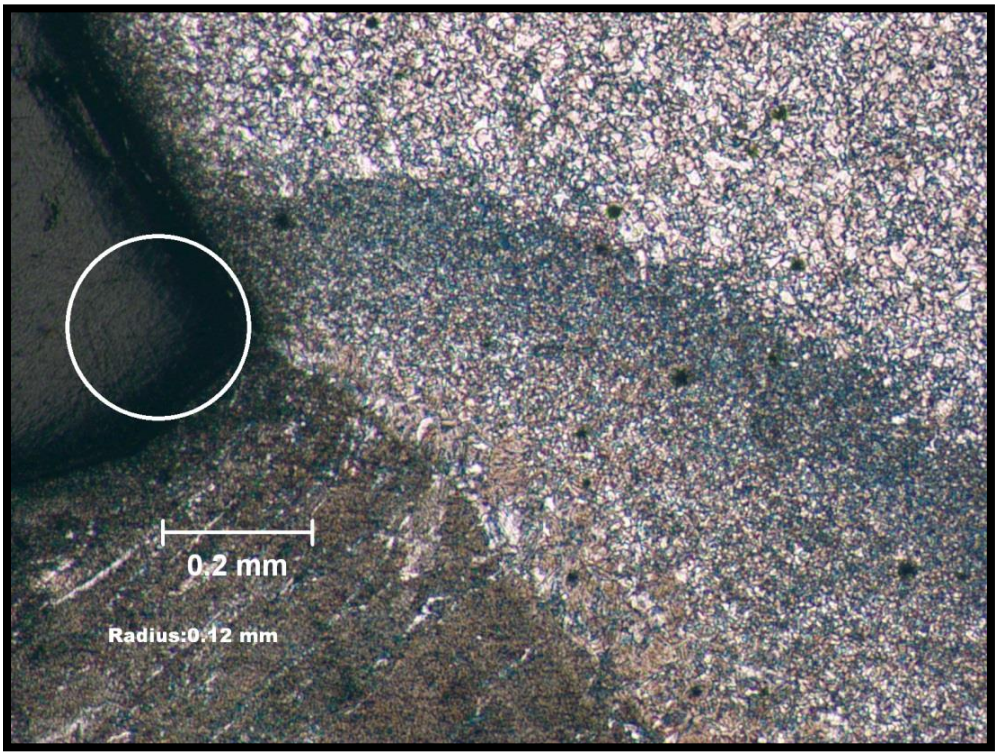

Figure B5. Weld toe measurement of a test specimen.

Appendix C. Finite Element Study

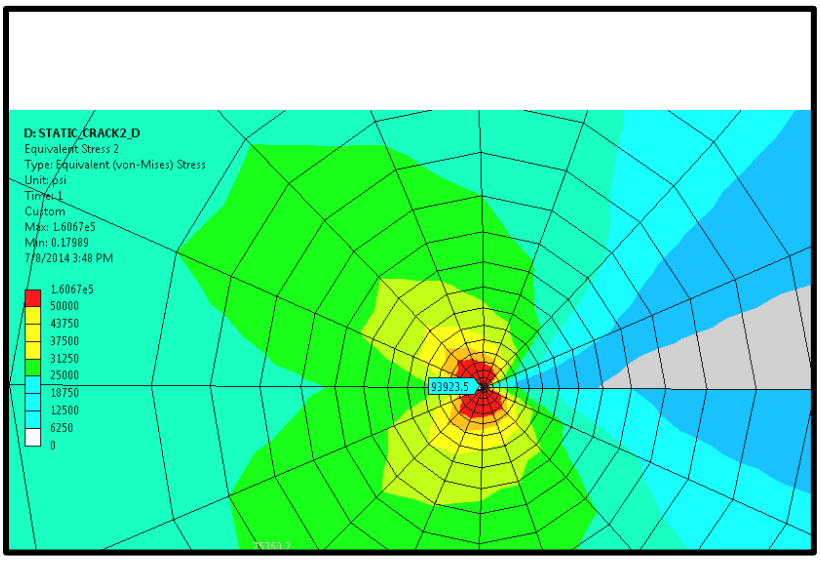

Figure C1. Plot of the von Mises stress at the crack tip.

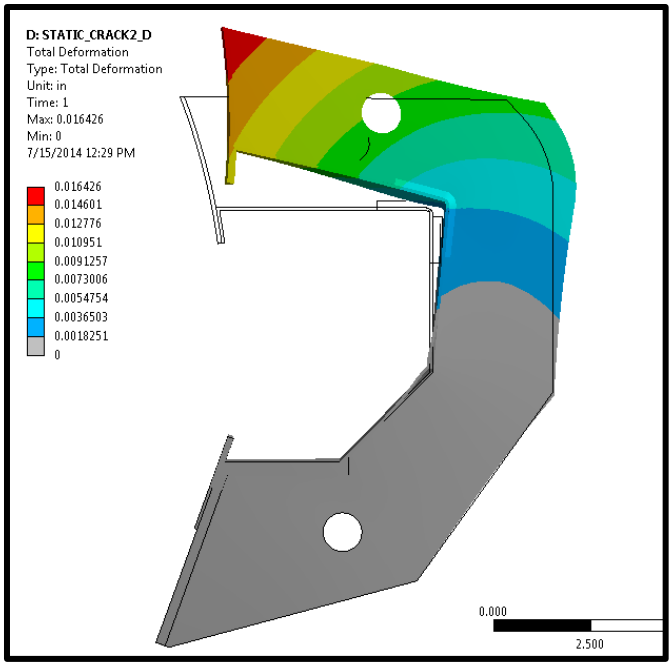

Figure C2. Displacement plot for Location A

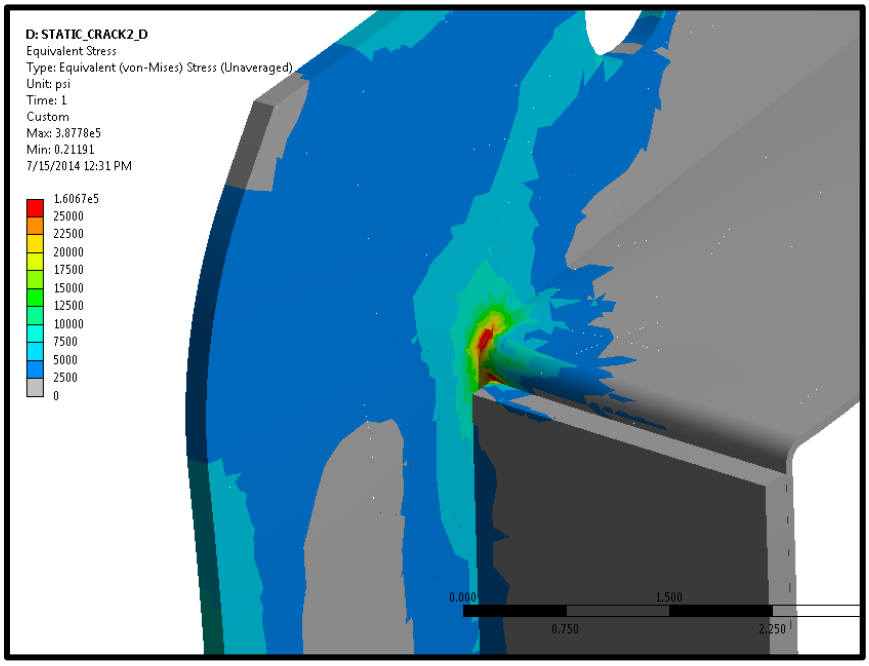

Figure C3. von Mises stress plot for Location A viewing from the opposite side.

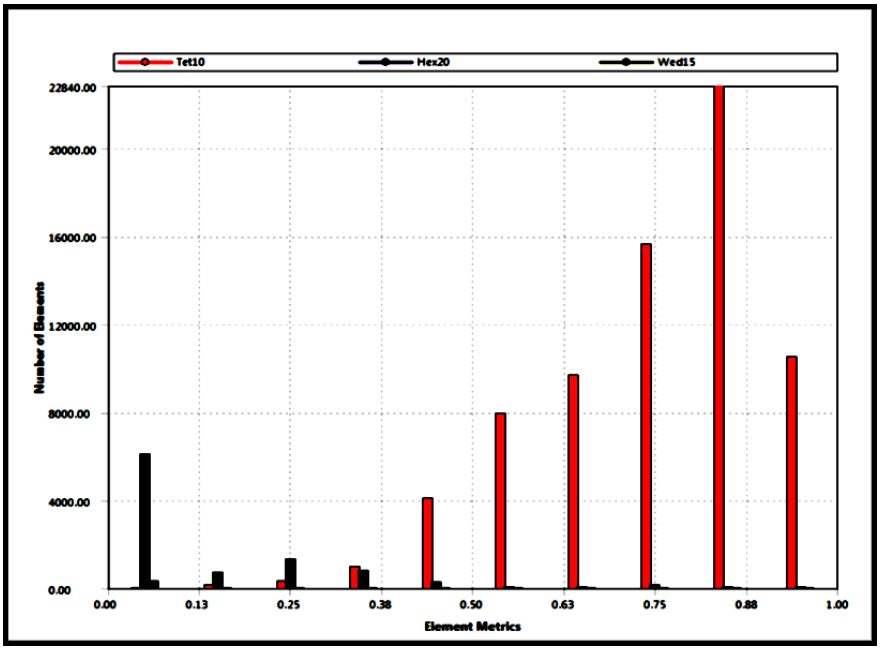

Figure C4. Plot of the mesh quality.

Table C1. Maximum K_I values for the Crack Profile.

Location A			Location B		
Maximum KI [ksi√in	Major Radius Crack Length [mm]	Minor Radius Crack Length [mm]	Maximum KI [ksi√in	Major Radius Crack Length [mm]	Minor Radius Crack Length [mm]
27.41787	4.572	0.50800	12.03982	3.048	0.0150
26.80596	4.445	0.40005	11.89683	2.921	0.0086
23.96091	3.810	0.34290	11.77071	2.794	0.0083
21.19337	3.175	0.28575	11.65198	2.667	0.0079
20.76423	3.048	0.27432	11.51845	2.540	0.0075
19.46342	2.540	0.22860	11.33703	2.413	0.0071
18.68117	2.159	0.19431	11.18257	2.286	0.0068
17.63170	1.651	0.14859	9.935465	1.270	0.0038
17.21420	1.270	0.11430			

Table C2. Solution Settings.

Step Controls	
Number Of Steps	1
Current Step Number	1
Step End Time	1. s
Auto Time Stepping	On
Define By	Substeps
Initial Substeps	1
Minimum Substeps	1
Maximum Substeps	10
Solver Controls	
Solver Type	Direct
Weak Springs	Program Controlled
Large Deflection	Off
Inertia Relief	Off
Fracture	On
Restart Controls	
Generate Restart Points	Manual
Load Step	Last
Substep	Last
Retain Files After Full Solve	Yes
Nonlinear Controls	
Force Convergence	Program Controlled
Moment Convergence	Program Controlled
Displacement Convergence	Program Controlled
Rotation Convergence	Program Controlled

Appendix D. ANSYS Solver Output for the Fracture Mechanics Solution

```
*****  ANSYS COMMAND LINE ARGUMENTS  *****
BATCH MODE REQUESTED (-b)    = NOLIST
INPUT FILE COPY MODE (-c)    = COPY
4 PARALLEL CPUS REQUESTED
START-UP FILE MODE           = NOREAD
STOP FILE MODE               = NOREAD
00352168          VERSION=WINDOWS x64     RELEASE= 14.5     UP20120918
CURRENT JOBNAME=file  14:33:49  JUN 18, 2014 CP=      1.544
PARAMETER _DS_PROGRESS =     999.0000000
/INPUT FILE= ds.dat  LINE=       0
MAXIMUM NUMBER OF DATA SETS ON RESULT FILE(NRES)=      10
DO NOT WRITE ELEMENT RESULTS INTO DATABASE
*GET  _WALLSTRT  FROM  ACTI  ITEM=TIME WALL  VALUE=  14.5636111
TITLE=
FRACTURE_MECHANICS_1--Static Structural (A5)
SET PARAMETER DIMENSIONS ON  _WB_PROJECTSCRATCH_DIR
TYPE=STRI  DIMENSIONS=      248        1        1
PARAMETER _WB_PROJECTSCRATCH_DIR(1) = D:\!1Share\THESIS
MODELS\_ProjectScratch\ScrCF58\
SET PARAMETER DIMENSIONS ON  _WB_SOLVERFILES_DIR
TYPE=STRI  DIMENSIONS=      248        1        1
PARAMETER _WB_SOLVERFILES_DIR(1) = D:\!1Share\THESIS
MODELS\FRACTURE_MECHANICS_1_files\dp0\SYS\MECH\
SET PARAMETER DIMENSIONS ON  _WB_USERFILES_DIR
TYPE=STRI  DIMENSIONS=      248        1        1
PARAMETER _WB_USERFILES_DIR(1) = D:\!1Share\THESIS
MODELS\FRACTURE_MECHANICS_1_files\user_files\
--- Data in consistent BIN units.
U.S. CUSTOMARY INCH UNITS SPECIFIED FOR INTERNAL
LENGTH       = INCHES (IN)
MASS         = LBF-S**2/IN
TIME         = SECONDS (SEC)
TEMPERATURE = FAHRENHEIT
TOFFSET      = 460.0
FORCE        = LBF
HEAT         = IN-LBF
PRESSURE     = PSI (LBF/IN**2)
ENERGY       = IN-LBF
POWER        = IN-LBF/SEC
INPUT  UNITS ARE ALSO SET TO BIN
1
FRACTURE_MECHANICS_1--Static Structural (A5)
***** ANSYS ANALYSIS DEFINITION (PREP7) *****
```

********** Nodes for the whole assembly **********
********** Elements for Body 1 "Boss-Extrude9" **********
********** Elements for Body 2 "Sweep1" **********
********** Elements for Body 4 "Boss-Extrude7" **********
********** Elements for Body 5 "Boss-Extrude10[1]" **********
********** Elements for Body 6 "Boss-Extrude10[2]" **********
********** Elements for Body 7 "Boss-Extrude13" **********
********** Elements for Body 8 "Boss-Extrude11" **********
********** Elements for Body 9 "Boss-Extrude12" **********
********** Elements for Body 10 "Split Line2" **********
********** Elements for Body 11 "Boss-Extrude8" **********
********** Send User Defined Coordinate System(s) **********
********** Set Reference Temperature **********
********** Send Materials **********
********** Create Face-Face MPC Contacts for "Crack" **********
Real Contact Set For Above Contact Is 13 & 12
********** Start Creating Assist Nodes For Crack Calculation **********
********** Done Creating Assist Nodes For Crack Calculation **********
********** Fixed Supports **********
******* Constant Zero Displacement X *******
********** Define Force Using Surface Effect Elements **********
***** ROUTINE COMPLETED ***** CP = 3.588
--- Number of total nodes = 153066
--- Number of contact elements = 1108
--- Number of spring elements = 0
--- Number of bearing elements = 0
--- Number of solid elements = 75163
--- Number of total elements = 76271
*GET _WALLBSOL FROM ACTI ITEM=TIME WALL VALUE= 14.5636111
***** ANSYS SOLUTION ROUTINE *****
PERFORM A STATIC ANALYSIS
THIS WILL BE A NEW ANALYSIS
NEW SOLUTION CONTROL OPTION IS ACTIVATED,
THE FOLLOWING COMMANDS ARE RESET TO NEW DEFAULTS:
AUTOTS, DELTIM, NSUB, CNVTOL, LNSRCH, PRED, NROPT,
TINTP, CUTCONTROL, OPNCONTROL, MONITOR, NEQIT, SSTIF, KBC.
CONTACT TIME PREDICTIONS ARE BASED ON ELEMENT KEYOPT(7) SPECIFIED
USE SPARSE MATRIX DIRECT SOLVER
CONTACT INFORMATION PRINTOUT LEVEL 1
********** Start Sending CINT Commands For All Cracks **********
PARAMETER _IASSISTNODE = 153188.0000
PARAMETER _SIFS = 1.000000000
START CRACK INTEGRATION DATA SET 1
SET CINT TYPE TO SIFS
COMPONENT NS_CRACK_FRONT
DESIGNATES CRACK EXTENSION NODES FOR SET 1
SET NUMBER OF CONTOURS FOR CRACK INTEGRATION SET 1 TO 20
ASSIGN CRACK SURFACE NORMAL FOR SET 1
TO COORDINATE SYSTEM 12 Y DIRECTION
PARAMETER _JINT = 2.000000000

START CRACK INTEGRATION DATA SET 2
SET CINT TYPE TO JINT
COMPONENT NS_CRACK_FRONT
DESIGNATES CRACK EXTENSION NODES FOR SET 2
SET NUMBER OF CONTOURS FOR CRACK INTEGRATION SET 2 TO 20
ASSIGN CRACK SURFACE NORMAL FOR SET 2
TO COORDINATE SYSTEM 12 Y DIRECTION
********** Done Sending CINT Commands For All Cracks **********
NLDIAG: Nonlinear diagnostics CONT option is set to ON.
Writing frequency : each ITERATION.
DEFINE RESTART CONTROL FOR LOADSTEP LAST
AT FREQUENCY OF LAST AND NUMBER FOR OVERWRITE IS 0
WRITE MULTIFRAME RESTART FILES EVEN
WHEN IT IS A LINEAR STATIC ANALYSIS
DELETE RESTART FILES OF ENDSTEP
****
********** SOLVE FOR LS 1 **********
SELECT FOR ITEM=TYPE COMPONENT=
IN RANGE 14 TO 14 STEP 1
66 ELEMENTS (OF 76271 DEFINED) SELECTED BY ESEL COMMAND.
SELECT ALL NODES HAVING ANY ELEMENT IN ELEMENT SET.
174 NODES (OF 153066 DEFINED) SELECTED FROM
66 SELECTED ELEMENTS BY NSLE COMMAND.
SPECIFIED SURFACE LOAD PRES FOR ALL SELECTED ELEMENTS LKEY = 1 KVAL = 1
SET ACCORDING TO TABLE PARAMETER = _LOADVARI84X
SPECIFIED SURFACE LOAD PRES FOR ALL SELECTED ELEMENTS LKEY = 2 KVAL = 1
SET ACCORDING TO TABLE PARAMETER = _LOADVARI84Y
SPECIFIED SURFACE LOAD PRES FOR ALL SELECTED ELEMENTS LKEY = 3 KVAL = 1
SET ACCORDING TO TABLE PARAMETER = _LOADVARI84Z
ALL SELECT FOR ITEM=NODE COMPONENT=
IN RANGE 1 TO 153188 STEP 1
153066 NODES (OF 153066 DEFINED) SELECTED BY NSEL COMMAND.
ALL SELECT FOR ITEM=ELEM COMPONENT=
IN RANGE 1 TO 76482 STEP 1
76271 ELEMENTS (OF 76271 DEFINED) SELECTED BY ESEL COMMAND.
PRINTOUT RESUMED BY /GOP
USE AUTOMATIC TIME STEPPING THIS LOAD STEP
USE 10 SUBSTEPS INITIALLY THIS LOAD STEP FOR ALL DEGREES OF FREEDOM
FOR AUTOMATIC TIME STEPPING:
USE 10 SUBSTEPS AS A MAXIMUM
USE 10 SUBSTEPS AS A MINIMUM

TIME= 1.0000
ERASE THE CURRENT DATABASE OUTPUT CONTROL TABLE.
WRITE ALL ITEMS TO THE DATABASE WITH A FREQUENCY OF NONE
FOR ALL APPLICABLE ENTITIES
WRITE NSOL ITEMS TO THE DATABASE WITH A FREQUENCY OF ALL
FOR ALL APPLICABLE ENTITIES
WRITE RSOL ITEMS TO THE DATABASE WITH A FREQUENCY OF ALL
FOR ALL APPLICABLE ENTITIES

WRITE NLOA ITEMS TO THE DATABASE WITH A FREQUENCY OF ALL
FOR ALL APPLICABLE ENTITIES
WRITE STRS ITEMS TO THE DATABASE WITH A FREQUENCY OF ALL
FOR ALL APPLICABLE ENTITIES
WRITE EPEL ITEMS TO THE DATABASE WITH A FREQUENCY OF ALL
FOR ALL APPLICABLE ENTITIES
WRITE EPPL ITEMS TO THE DATABASE WITH A FREQUENCY OF ALL
FOR ALL APPLICABLE ENTITIES
WRITE MISC ITEMS TO THE DATABASE WITH A FREQUENCY OF ALL
FOR ALL APPLICABLE ENTITIES
WRITE CINT ITEMS TO THE DATABASE WITH A FREQUENCY OF ALL
FOR ALL APPLICABLE ENTITIES
NONLINEAR STABILIZATION CONTROL:
KEY=OFF
*GET ANSINTER_ FROM ACTI ITEM=INT VALUE= 0.00000000

*IF ANSINTER_ (= 0.00000) NE
0 (= 0.00000) THEN
*ENDIF
***** ANSYS SOLVE COMMAND *****

*** WARNING *** CP = 3.916 TIME= 14:33:49
Element shape checking is currently inactive. Issue SHPP,ON or
SHPP,WARN to reactivate, if desired.
*** WARNING *** CP = 3.978 TIME= 14:33:49
SOLID186 wedges are recommended only in regions of relatively low stress gradients.
*** NOTE *** CP = 4.103 TIME= 14:33:50
The model data was checked and warning messages were found.
Please review output or errors file (D:\!1Share\THESIS
MODELS_ProjectScratch\ScrCF58\file.err) for these warning messages.
*** SELECTION OF ELEMENT TECHNOLOGIES FOR APPLICABLE ELEMENTS ***
--- GIVE SUGGESTIONS AND RESET THE KEY OPTIONS ---
ELEMENT TYPE 1 IS SOLID187. IT IS NOT ASSOCIATED WITH FULLY INCOMPRESSIBLE
HYPERELASTIC MATERIALS. NO SUGGESTION IS AVAILABLE AND NO RESETTING IS
NEEDED.

ELEMENT TYPE 2 IS SOLID187. IT IS NOT ASSOCIATED WITH FULLY INCOMPRESSIBLE
HYPERELASTIC MATERIALS. NO SUGGESTION IS AVAILABLE AND NO RESETTING IS
NEEDED.

ELEMENT TYPE 3 IS SOLID186. KEYOPT(2)=0 IS SUGGESTED AND HAS BEEN RESET.
KEYOPT(1-12)= 0 0 0 0 0 0 0 0 0 0 0 0

ELEMENT TYPE 4 IS SOLID187. IT IS NOT ASSOCIATED WITH FULLY INCOMPRESSIBLE
HYPERELASTIC MATERIALS. NO SUGGESTION IS AVAILABLE AND NO RESETTING IS
NEEDED.

ELEMENT TYPE 5 IS SOLID187. IT IS NOT ASSOCIATED WITH FULLY INCOMPRESSIBLE
HYPERELASTIC MATERIALS. NO SUGGESTION IS AVAILABLE AND NO RESETTING IS
NEEDED.

ELEMENT TYPE 6 IS SOLID187. IT IS NOT ASSOCIATED WITH FULLY INCOMPRESSIBLE HYPERELASTIC MATERIALS. NO SUGGESTION IS AVAILABLE AND NO RESETTING IS NEEDED.

ELEMENT TYPE 7 IS SOLID187. IT IS NOT ASSOCIATED WITH FULLY INCOMPRESSIBLE HYPERELASTIC MATERIALS. NO SUGGESTION IS AVAILABLE AND NO RESETTING IS NEEDED.

ELEMENT TYPE 8 IS SOLID187. IT IS NOT ASSOCIATED WITH FULLY INCOMPRESSIBLE HYPERELASTIC MATERIALS. NO SUGGESTION IS AVAILABLE AND NO RESETTING IS NEEDED.

ELEMENT TYPE 9 IS SOLID187. IT IS NOT ASSOCIATED WITH FULLY INCOMPRESSIBLE HYPERELASTIC MATERIALS. NO SUGGESTION IS AVAILABLE AND NO RESETTING IS NEEDED.

ELEMENT TYPE 10 IS SOLID187. IT IS NOT ASSOCIATED WITH FULLY INCOMPRESSIBLE HYPERELASTIC MATERIALS. NO SUGGESTION IS AVAILABLE AND NO RESETTING IS NEEDED.

ELEMENT TYPE 11 IS SOLID187. IT IS NOT ASSOCIATED WITH FULLY INCOMPRESSIBLE HYPERELASTIC MATERIALS. NO SUGGESTION IS AVAILABLE AND NO RESETTING IS NEEDED

1

***** ANSYS - ENGINEERING ANALYSIS SYSTEM RELEASE 14.5 *****

ANSYS Structural

00352168 VERSION=WINDOWS x64 14:33:50 JUN 18, 2014 CP= 4.165

FRACTURE_MECHANICS_1--Static Structural (A5)

S O L U T I O N O P T I O N S

PROBLEM DIMENSIONALITY. 3-D
DEGREES OF FREEDOM. . . . . UX UY UZ
ANALYSIS TYPE . . . . . .STATIC (STEADY-STATE)
OFFSET TEMPERATURE FROM ABSOLUTE ZERO 459.67
EQUATION SOLVER OPTION. . . . . .SPARSE
GLOBALLY ASSEMBLED MATRIX . . . . . .SYMMETRIC
MAKE COMPONENTS FOR CRACK DATA SET 1
MAKE COMPONENTS FOR CRACK DATA SET 2

L O A D S T E P O P T I O N S

LOAD STEP NUMBER. 1
TIME AT END OF THE LOAD STEP. 1.0000
AUTOMATIC TIME STEPPING . . . . . ON
INITIAL NUMBER OF SUBSTEPS 10
MAXIMUM NUMBER OF SUBSTEPS 10
MINIMUM NUMBER OF SUBSTEPS 10
STEP CHANGE BOUNDARY CONDITIONS . . . . . NO
PRINT OUTPUT CONTROLS . . . . . .NO PRINTOUT

DATABASE OUTPUT CONTROLS

ITEM FREQUENCY COMPONENT

Appendix E. Field Failure Photos

Figure D1. View of a typical field failure (inner surface of rib)

Figure D2. View of a typical field failure (outer surface of rib)

Figure D3. View of a typical field failure (inner surface of rib)

Figure D4. View of a typical field failure (outer surface of rib).

This is to certify that we have examined this copy of the thesis by

George E. Selburg Jr.

and have found that it is complete and satisfactory in all respects.

The thesis has been approved by:

_____

Dr. Raymond A. Fournelle

Thesis Director, Department of Mechanical Engineering

_____

Dr. James A. Rice, Committee Member

_____

Dr. Joseph Domblesky, Committee Member

Approved on: _____